EVALUATING THE IMPACT OF E-LIQUIDS ON SMALL EXTRACELLULAR VESICLES RELEASED FROM THREE-DIMENSIONAL CELL CULTURE OF HUMAN LUNG CELLS

Alex Theresa Couchman

Master of Philosophy

School of Science, Engineering, and Environment

University of Salford

2024

Supervisor: Dr Arijit Mukhopadhyay

Co-Supervisor: Dr Pika Miklavc

Table of Contents

List of Tables

List of Figures

Acknowledgements

I'd first like to thank Dr Arijit Mukhopadhyay and Dr Pika Miklavc for the opportunity, and for their continued support and expertise throughout the project.

I'd also like to thank my peers in the lab. Sowmya and Toby for their expertise, advice, and encouragement. Joe for the motivational speeches. Jess for being the best lab partner I could have asked for, and for being a true friend. Muna, Grace, and Rumana for their support any time I needed it.

Finally, my friends and family. I'm incredibly grateful for their constant support and encouragement in everything I do.

Abbreviations

2D – Two Dimensional

3D – Three Dimensional

ASH - Action on Smoking and Health

BCA – Bicinchoninic Acid

BEST - Biomarkers, EndpointS, and other Tools

BSA – Bovine Serum Albumin

CDNA – Complementary DNA

CMO – Cell Mask Orange

CO2 – Carbon Dioxide

DMEM – Dulbecco's Modified Eagle Medium

DNA – Deoxyribose Nucleic Acid

ECM – Extracellular Matrix

EGFR - Epidermal Growth Factor Receptor

ESCRT - Endosomal Sorting Complex Required for Transport

EV – Extracellular Vesicles

EVALI - E-Cigarette or Vaping Product Use-Associated Lung Injury

fNTA – Fluorescence Nanoparticle Tracking Analysis

hEGF – Human Epidermal Growth Factor

ILV – Intraluminal Vesicles

KRAS - Kirsten Rat Sarcoma Viral Oncogene Homolog

LRG1 - Leucine-Rich α-2-Glycoprotein

MiRNA – MicroRNA

MRNA – Messenger RNA

MVB – Multivesicular Body

NSCLC – Non-Small Cell Lung Cancer

nSmase2 - Neutral Sphingomyelinas 2

NTA – Nanoparticle Tracking Analysis

ONS – Office of National Statistics

PBS – Phosphate Buffered Saline

PCR – Polymerase Chain Reaction

Poly-HEMA - poly(2-hydroxyethyl methacrylate)

qPCR – Quantitative PCR

RISC – RNA Induced Silencing Complex

RNA – Ribose Nucleic Acid

RNS – Reactive Negative Species

ROS – Reactive Oxygen Species

RPMI – Rosewell Park Memorial Institute

SCLC – Small Cell Lung Cancer

SEC – Size Exclusion Chromatography

sEV – Small Extracellular Vesicles

TEM – Transmission Electron Microscopy

WHO – World Health Organization

Abstract

Small Extracellular Vesicles (sEVs), membrane-bound vesicles used in cellular communication can be used as a source of biomarkers for lung damage and disease, to minimise need for invasive test procedures. E-cigarette use has grown in recent years, but little is known about how e-liquids impact on sEVs, and therefore how they might cause dysregulation in sEV cargo. Previous studies using two-dimensional cultures of human lung cells have identified that sEVs may be impacted by the addition of e-liquids.

This study used a three-dimensional culture protocol for human lung cells, to more accurately model a physiological environment, compared to a two-dimensional monolayer of cells.

Cultures were treated with flavoured e-liquids, with and without nicotine, and the sEVs released were isolated using size exclusion chromatography. These vesicles were characterised using transmission electron microscopy, nanoparticle tracking analysis, fluorescence nanoparticle tracking analysis, and western blotting techniques to confirm morphology and protein marker presence. Total RNA was isolated, and expression of target microRNA was evaluated using qPCR.

Characterisation techniques confirmed that this project was successful in isolating sEVs from three-dimensional cultures, with vesicles exhibiting the correct “cup-shaped” morphology, 50-200 nm size range, and CD9 and CD63 tetraspanin protein markers to be classified. sEVs derived from e-liquid treated cultures did not exhibit significant differences in size or concentration compared to untreated cultures. Total RNA was successfully isolated from all samples, and expression of microRNAs miR-410-5p and miR-21-5p in sEVs derived from A549 cultures showed variation between treated and untreated samples. This indicates that the e-liquid treatments had an impact on microRNA expression in sEVs, as suggested by previous literature.

The results of this study demonstrate that e-liquids did have an impact on the cargo of sEVs in the microRNA tested, and therefore that sEVs derived from three-dimensional cell culture could be a useful tool in establishing the impacts of e-liquids on potential biomarkers for lung disease.

Chapter 1

Introduction

Introduction

1.1. Extracellular Vesicles

1.1.1 Background

The term extracellular vesicles (EVs) is a general term referring to the particles released from cells. Previously thought to be solely a method of waste disposal for cells, studies have shown that extracellular vesicles also carry out more complicated roles, such as cell to cell communication through the transfer of nucleic acids, proteins, and lipids. Additionally, EVs are released by a wide variety of cell types such as epithelial cells, endothelial cells, dendric cells and stem cells (Yáñez-Mó et al., 2015).

The classifications of extracellular vesicles have changed over the years, and a variety of terms have been used for the particles. As these particles were not originally as well defined and may have had other origins and sizes, much of the previous studies produced using this term are subsequently open to misinterpretation. To better define different particles released by cells, the international society for extracellular vesicles (ISEV) created a guideline: “Minimal Information for the Studies of Extracellular Vesicles” (MISEV) (Théry et. al., 2018). These guidelines were originally released in 2014 and have been updated multiple times since then, to ensure that they stay current (Lötvall et al., 2014; Witwer et al., 2021).

1.1.2 Classification and Biogenesis

Extracellular vesicles can be categorized by their size and origin in the cell. According to MISEV guidelines, medium and large EVs are above 200 nm and are formed from the plasma membrane. Small EVs (sEVs) originate in the endosome and are generated when the multivesicular body (MVB) buds inwards and forms vesicles, then called intraluminal vesicles (ILVs). SEVs are classified as the vesicles released when multivesicular bodies fuse with the plasma membrane of the parent cell (Théry et. al., 2018).

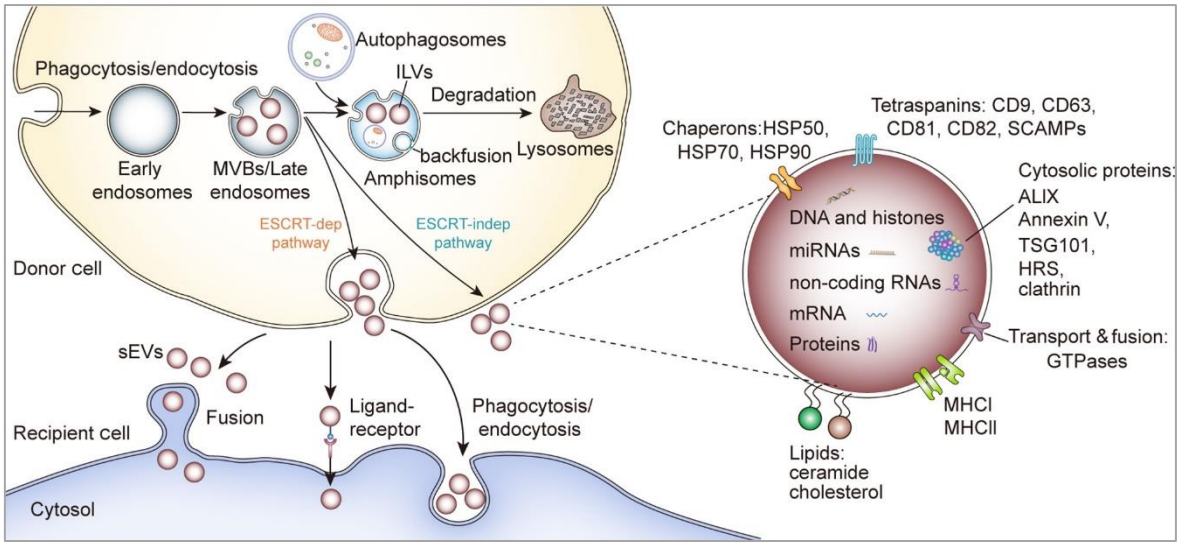

Figure 1.1 The pathways for the production and uptake of small extracellular vesicles. This figure demonstrates the ESCRT-dependent and ESCRT-independent pathways for sEV formation; the uptake of sEVs by recipient cells via fusion, receptors or phagocytosis; and the known nucleotide and protein components of sEVs. Gao et. al., 2021

There are two main pathways that that produce sEVs; the endosomal sorting complex required for transport (ESCRT) – dependent pathway, and the ESCRT-independent pathway. In the ESCRT-dependent pathway the ESCRT complex is responsible for the formation of the MVB, whereas in the ESCRT-independent pathway, the MVB is formed by neutral sphingomyelinas 2 (nSmase2) (Hessvik and Llorente, 2018). There are some differences in the size range used for sEVs in different studies, with some taking sEVs to be below 200 nm and some to be below 150 nm, because of this some studies may not be as comparable (Kotrbova et al., 2019) (Théry et al., 2018) (Gao et al., 2021). Membranes of sEVs contain tetraspanin proteins such as CD9, CD63, and CD81, which may be used to differentiate sEVs from other particles (Kowal et al., 2016). Other markers that may be used to identify sEVs are Alix and Tsg101 (Théry et al., 2018). Evidence suggests that the tetraspanin proteins used as identifying markers for sEVs play more complex roles in cell targeting, cargo selection, cell uptake, and EV biogenesis (Andreu and Yáñez-Mó, 2014; Willms et al., 2018).

Other subclasses of EVs may occur within the same size range as sEVs; such as microvesicles and apoptotic bodies. Microvesicles have a size range of 100-1000 nm and are thought to be produced via plasma membrane shedding and by pinching off from membrane protrusions. The presence of markers ARF6 and Annexin A1 can be used to

identify microvesicles. Apoptotic vesicles are formed from apoptotic cells and may occur in the size range of 100-1000 nm and are sometimes mistaken for, or grouped with, apoptotic bodies which are in the size range of 1000-5000 nm. Phosphatidylserine may be used to differentiate these from other EVs (Fu et. al., 2023; Liu et al., 2018; Hochreiter-Hufford et al., 2013).

1.1.3 Mechanism of Communication

The contents of sEVs include microRNA (miRNA), mRNA, proteins and lipids from the cell of origin and are thought to aid in cell-to-cell communication. Much of the communication via sEVs occurs through the uptake of sEVs into the cell. This may occur through several processes, namely the endocytosis pathway, membrane fusion, phagocytosis, and micropinocytosis. The endocytosis pathway is the most frequent mechanism for sEV uptake and can be split into clathrin-dependent and clathrin-independent pathways (Tian et al., 2014). While the mechanisms of communication via sEVs are thought to be an important component in regulating processes within the body, studies have shown that this process can also spread disease and encourage tumour growth (Hood, San, and Wickline, 2011).

1.1.4 Therapeutic Use of sEVs

As sEVs can play a significant role in the dissemination of diseases, many therapeutic advances have focussed on inhibiting the release and uptake of sEVs (Chiba et al., 2018; Greenberg et al., 2022). Methods to inhibit the formation or release of sEVs commonly focus on the ESCRT-dependent or ESCRT-independent pathways. Studies have shown that inhibition of ESCRT may be achieved using manumycin A and tipifarnib, resulting in decreased production of sEVs (Datta et al., 2017; Greenberg et al., 2022). GW4869 has been shown to inhibit nSmase2, again decreasing the rate of sEV production (Kosaka et al., 2013). By inhibiting the production of sEVs, less cargo is transferred from diseased cells to normal cells, slowing the progression of disease (Greenberg et al., 2022).

Preventing the uptake of sEVs may also slow the progression of disease, by preventing the transfer of information and cargo from diseased cell to healthy cell. For clatherin-dependent uptake pathways, dynasore, a dynamin inhibitor has been shown to inhibit the uptake of sEVs into cells (Chiba et al., 2018). As there is not yet a reliable method to selectively inhibit sEVs forming unhealthy cells, while allowing the uptake of healthy sEVs important for pathological functions, this method is not currently a viable therapeutic strategy (McKelvey et al., 2015).

1.1.5 The Use of sEVs in Diagnosis

As sEVs are found circulating in body fluids such as saliva, urine, and blood, retrieval is less invasive than methods such as tissue biopsy (Chiam et al., 2020). Whilst sEVs are considered a source of biomarkers, they themselves have been suggested a potential biomarkers too. Biomarkers, discussed later in **1.3**, provide an alternative diagnostic method which is minimally invasive (FDA-NIH Biomarker Working Group, 2016). Li et. al. (2011) found that the presence of leucine-rich α-2-glycoprotein (LRG1) on sEVs could be promising as a biomarker of non-small cell lung cancer (NSCLC) if present in urine samples. Lipids have also been suggested as biomarkers for some diseases, however a current lack of research means there is not significant evidence for this method for diagnosis (Gao et al., 2021). Cargo such as miRNA has shown promise as potential biomarkers (Chiam et al., 2020).

1.2 MicroRNA

1.2.1 Background of MicroRNA

MicroRNA are classified as short, non-coding RNA strands of approximately 19 to 25 nucleotides long (Bartel, 2004). First discovered in 1993 in the nematode *Caenorhabditis elegans* (*C. elegans*), MiRNA was thought to be involved in the translation of lin-4 (Bartel, 2004; Lee, Feinbaum, and Ambros, 1993). A second miRNA was found in *c. elegans* in 2000. This was named let-7 and found to regulate the developmental timing in *c. elegans* larvae (Roush and Slack, 2008). In the same year let-7 was found to also be present in

humans, the first miRNA to be confirmed as such, and had functions linked to gene expression (Bartel, 2004). Further research in the field has led to the discovery of many miRNA molecules. MiRbase.org, a database for miRNA sequences, describes 2654 mature sequences in the human genome, with 1917 annotated hairpin precursors also available in the database (Kozomara, Birgaoanu, and Griffiths-Jones., 2019; miRbase.org, 2019).

1.2.2 MiRNA Biogenesis

The biogenesis of miRNA begins in the nucleus of the cell (**Figure 1.2**).

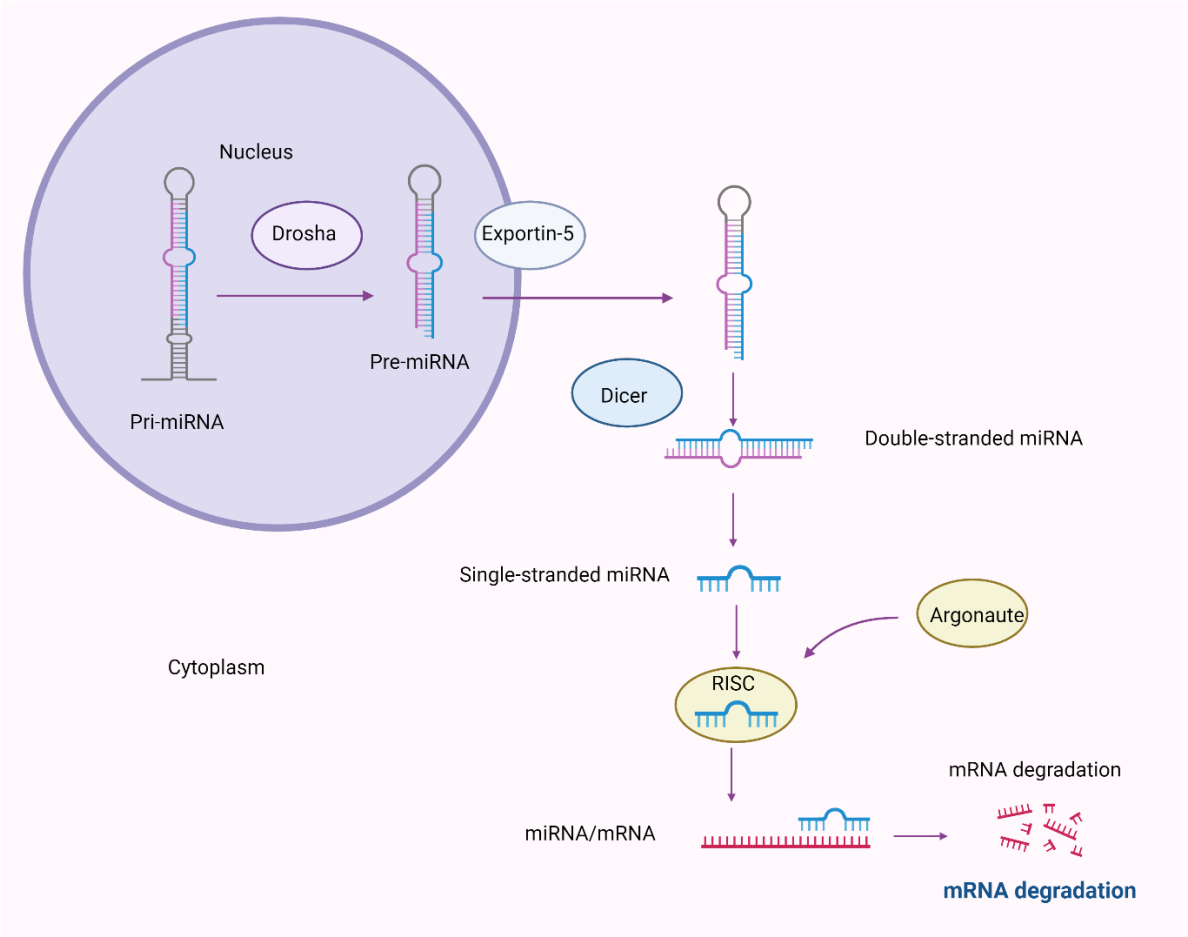

Figure 1.2 Biogenesis of miRNA in the cell. MiRNA formed in the nucleus is cleaved by the enzyme Drosha, and exported out of the nucleus by Exportin-5. Undergoing further cleaving by Dicer, the mature miRNA forms the RISC with the Argonaute complex, to target mRNA and regulate translation. Created with BioRender.com

The primary miRNA (pri-miRNA) is a stem loop structure that is transcribed in the nucleus, before being cleaved by the enzyme Drosha. Exprotin-5 then exports the resulting precursor miRNA (pre-miRNA) to the cytoplasm of the cell. The enzyme Dicer cleaves the pre-miRNA at the loop, leaving a small double stranded RNA molecule. Following association with the Argonaute protein, one or both strands become mature miRNA and form the 'RNA Induced Silencing Complex' (RISC) (Meister et al., 2004) (Michlewski & Cáceres, 2019). RISC may regulate gene expression using one of two methods. The first of these methods prevents the translation of messenger RNA (mRNA) by cleaving the mRNA. This will only occur when there is sufficient complementarity between the mRNA and the miRNA in the complex. The second method of expression regulation prevents mRNA translation by imprecise binding of the miRNA and the mRNA strand (Bartel, 2004; Lan et al., 2023). Here, the RISC delivers mRNA to the processing body (P body), where the mRNA is degraded following the processes of deadenylation and decapping (Iwakawa and Tomari, 2022).

1.2.3 Cellular phenotype could impact expression of microRNA

The differences in miRNA expression in sEVs can be attributed to the ability of cells to selectively sort miRNA into EVs prior to their release. The mechanisms responsible for sorting miRNA into cells vary and include RNA-binding proteins and membranous proteins. Different disease states have also been shown to influence the miRNA content of sEVs (Groot and Lee, 2020).

Some mechanisms of miRNA sorting have been found to alter disease states and progression. In cancer, studies have found that nearby healthy cells secrete tumour-suppressing miRNA to be carried to nearby cancer cells. The cell surface protein Syndecan-1 has been shown to have functions in cancer cell signalling and the suppression of cancers. A study comparing the miRNA expression of A549 cells with syndecan-1 and with syndecan-1 deleted cells found that many miRNA had different expression levels, including an 184-fold upregulation in miR-485-3p, an miRNA previously shown to supress cancer growth. The same study found that A549 cells cultured with

sEVs from syndecan-1 expressing cells showed decreased proliferation when compared to A549 cells cultures with sEVs from cells without syndecan-1 (Parimon et al., 2018).

The mechanism of miRNA sorting in cancer cells may also be responsible for the progression of cancers. Some tumour-derived sEVs have been found to contain the Dicer enzyme, the enzyme involved in the conversion of precursor miRNA to mature miRNA. A study by Melo et. al. (2014) treated healthy mammary cells with sEVs from cancerous MDA-MB-231 cells, which was suggested to induce proliferation and have the potential to convert healthy cells to tumour-forming cells. Healthy cells were also treated with sEVs with Dicer deleted, which was found to decrease the growth of healthy cells. While the study stated that there may be many obstacles that would stop this process in-vivo, the results suggest a potential answer to the role of miRNA sorting in disease progression.

With over 2500 miRNA identified in humans and a variety of functions, it's unsurprising that many have been found to impact different mechanisms involved in cancers. These mechanisms include apoptosis, metastatic colonisation, and cell proliferation. Dependent on the environment, some miRNA are capable of acting as both a tumour suppressor and an oncogene (Svoronos et al., 2016; Zhang et al., 2019).

Key to many early miRNA studies, the Let-7 family of miRNA have been found to act as a tumour suppressor, with reduced levels of these miRNA often leading to increased tumour growth. Low levels if Let-7 detection is often linked to a poor prognosis for the patient (Trang et al., 2010; Lee et al., 2016).

1.3 Biomarkers

Biomarkers have the potential to be key in the development of non-invasive testing, in addition to other areas such as therapeutics and vaccinations. The complexity and heterogeneity of biomarkers, however, means that there is much research to be undertaken to explore this potential (LeBleu and Kalluri, 2019). Biomarkers are a measurable characteristic that indicate biological and pathological processes, or biological responses to exposure to substances or changes in the environment (FDA-NIH Biomarker Working Group, 2016). According to the American Thoracic Society, useful

biomarkers must have influence on clinical decisions that lead to improved patient care, to an extent that the benefits outweigh any potential risks from false results. Biomarkers should minimise expense and harm to patients, without causing delay to therapeutic care (Mazzone et al., 2017).

1.3.1 Identification of Alternative Potential Tools for Diagnosis and Monitoring

Expression profiles of many miRNA have been shown to differ greatly between different diseases; the upregulation of a particular miRNA may be associated with a good clinical outcome in one disease, but indicate disease progression in another. The expression levels of some miRNA may also be an indicator of several diseases, and not be specific enough to be used as a biomarker. MiR-21 has been frequently studied as a biomarker for many diseases, with its upregulation being associated with pancreatic cancer, prostate cancer, Crohn's disease, and pneumonia, amongst many others, while the downregulation of mir-21 can indicate increased necrosis (Zahm et al., 2011; Abd-El-Fattah et al., 2013; Liu et al., 2014; Abue et al., 2015; Porzycki et al., 2018).

Several studies have noted that the levels of miRNA and expression profiles can differ significantly depending on the sample type. Mompeón et. al (2020) found that the expression of miR-133a and miR-26a were upregulated significantly in serum, but not in plasma, while miR—499a was upregulated in plasma, but not in serum. The same study noted that miR-21 levels were increased in serum, but decreased in plasma.

1.4 Three-Dimensional Cell Culture

1.4.1 Challenges in Two-Dimensional Cell Culture

2D cell cultures have been used for over a hundred years to study cellular reactions to toxic substances, medical treatments, and different environments (Duval et. al., 2017). While 2D cultures have the advantage of being simpler and low cost, there are also disadvantages. The monolayer, adherent growth of the cells limits the structural organisation of the cells, and the subsequent cell-to-cell interaction (Kapałczyńska et al.,

2018). 2D culture methods are unable to mimic interactions between cells and the extracellular matrix (ECM) environment found *in vivo*, a key feature in many cellular mechanisms (Thippabhotla, Zhong, and He, 2019). Such limitations indicate the need for a more applicable method.

1.4.2 Improvements and Challenges in Three-Dimensional Cell Culture

Recent developments in the field have led to increased use of 3D cell cultures in research settings. There are different types of 3D cell culture methods available; techniques using scaffolds and scaffold- free techniques. Scaffold based techniques utilise support from hydrogel, which may be natural or synthetic, or hard polymer (Jongpaiboonkit et al., 2008; Rudinger et al., 2015). In scaffold-free cell culture, low or non-adherent plates, hanging drop, or magnetic levitation techniques are among those that may be used (Foty, 2011; Haisler et al., 2013; Breslin and O'Driscoll, 2016). While scaffold-based techniques such as hydrogels can provide an environment similar to the extracellular matrix (ECM), scaffold free spheroids have also been shown to reliably secrete the proteins necessary such as collagen and fibronectin (Nenderman et al., 1984; Valdoz et al., 2021).

3D cell culture methods offer a more accurate representation of cells in-vivo, with more cell-to-cell communication, accurate shape and structure in comparison to 2D (Breslin and O'Driscoll, 2016). 3D cells demonstrate a realistic proliferation pace, whereas 2D cells often proliferate at a far more rapid pace than cells in-vivo. Multicellular 3D cultures often contain multiple layers, unlike the monolayer structure in 2D cultures, and 3D cells are better differentiated. The multicellular formation of spheroids often leads to nutrients being divided unevenly between cells, and the core of spheroids often becomes inactive due to lack of oxygen and nutrients from the surrounding media (Barisam, 2018). This gives an opportunity in cancer research, as the core of these cells comes to represent the necrotic core found in tumour cells (Däster et. al., 2017).

3D models are more applicable to substance treatment and resistance research than their 2D counterparts (Habanjar et al., 2021). When studying resistance to the anti-cancer

drugs epirubicin, cisplatin, and docetaxel, Muguruma et. al. (2020) found higher resistance to the three drugs in different cell lines grown using a scaffold-free 3D culture on ultra-low adherence plates, when compared to 2D cultures of the same cell lines. Other studies have also reported findings of lower drug sensitivity in 3D cultures. A study using poly(2-hydroxyethyl methacrylate) (poly-HEMA) coated plates to culture 3 HER2-positive breast cancer cell lines found that the 3D cultures grown also showed greater resistance the chemotherapy drug docetaxel, as well as the HER-targeted drug neratinib, than the 2D cultures of the same cell lines. Cellular ATP measured from each culture did reveal that the cell viability of each cell line was lower in the 3D models, than their 2D counterparts (Breslin and O'Driscoll, 2016). Imamura et. al. (2015) reported greater drug resistance in some 3D cell lines, but similar results to 2D in others, suggesting that the lower sensitivity to treatment is not applicable to every cell line. This study also noted that different cell lines behaved differently when added to adherent spheroid plates, with 3 of the 6 breast cancer cell lines used forming dense aggregates by the day after seeding, while the other 3 took more time, and formed smaller, looser aggregates. The denser aggregates were the cell lines to produce results of greater drug resistance. The little resistance to drugs found in 2D cultures often suggest that a substance may have more of an impact to the cell than it would in-vivo. Drug metabolism in 3D cultures has also been found to be more efficient than in 2D cultures, where drugs are often poorly metabolised. The increased comparability of results between 3D and in vivo could allow for a more accurate starting point when looking to move forward in research (Langhans, 2018).

Despite the clear advantages to the use of 3D cultures, there are challenges in the field that may prevent some from using the methods available. Some have commented that experiments performed using 3D culture are difficult to replicate, and data found can be more difficult to replicate (Langhans, 2018). Cells in 3D are more difficult to accurately image, with simple 'XY' images used for 2D cultures not showing a full image of the cell (Booij et al., 2019). Performing flow cytometry on a 3D culture for cell counting or to detect cell characteristics requires the multicellular structures to be disrupted into single cells. This requires the use of an enzyme such as Trypsin and disruption by the user, which renders the cells unusable for future experiments (Gong et al., 2019).

3D cell cultures have previously been suggested to secrete extracellular vesicles similar to those found in-vivo (Thippabhotla, Zhong, and He, 2019). Upon evaluating the small RNA profiles from EVs released from 2D and 3D cultures compared to human plasma samples, Thippabhotla et. al (2019) found that the RNA profile from EVs released from 3D cultures shared a 96% similarity to the patient sample, whereas the 2D culture shared 80% similarity. This could provide an excellent opportunity to identify much needed potential biomarkers in diseases, more accurately than can be found in 2D cultures.

1.5 Background and Model of Study

1.5.1 The Use of 3D Lung Epithelial Cells as a Model to study the use of a 3D cell culture model in sEV and miRNA research

Previous work by Chinta (2022) at the University of Salford, used 2D cultures of A549 and Beas 2B human lung epithelial cells to study the impacts of e-liquids on the sEV and miRNA released from the cells following treatments. As 3D cultures have been suggested to be an improvement on 2D cultures as a model for reactions *in vivo*, then developing protocols for 3D culture work could aid in developing applicable research in the biomarker field. Scaffold-free 3D models have been shown to be a more reliably reproducible and lower cost method. Previous studies have successfully utilised poly-HEMA coated plates as a cost-effective alternative to ultra-low adhesive plates (Breslin and O'Driscoll, 2016; Djomehri et. al., 2019). This study attempts to effectively optimise these protocols for A549 and BEAS-2B cells, and further sEV isolation from these cultures.

The human respiratory system is often divided into two parts, the proximal conducting airways, and the distal respiratory airways. The proximal conducting airways consist of the nasal passage, the trachea, and the bronchi, and are responsible for conducting the passage of inhaled and exhaled gas to and from the distal respiratory airways. The respiratory bronchioles and the alveoli form the distal respiratory airways, and are responsible for the exchange of gases between the inhaled air and the bloodstream (Harkema, Nikula, and Haschek, 2018). The respiratory system is lined with a heterogenous system of epithelial cells, which encounter the air inhaled, along with any toxic substances that are inhaled with it (Davis and Wypych, 2021). It is due to this that

epithelial cells are frequently regarded as “the first line of defence” for lung damage (Gaurav, 2019). The A549 cells are derived from a non-small cell lung carcinoma found in alveolar basal cells of a 58 year old male (Giard et al., 1973). The cells are epithelial cells recommended for use in cancer, immune-oncology, and toxicology research (ATCC, 2022). The BEAS-2B cells were derived from the normal human bronchial epithelium tissue extracted during the autopsy of a non-cancerous individual (ATCC, 2022).

Both cancerous and non-cancerous individuals may be impacted by the effects of e-liquids due to the varying populations of users and reasoning for their uses (Action on Smoking and Health (ASH), 2022) (Office of National Statistics (ONS), 2022). Characterized by the unregulated proliferation of mutated cells, cancer is the leading cause of death globally. Cancers can be characterized by groups; carcinomas, sarcomas, leukaemias or lymphomas; by their cell type; and by their location in the body. There are many causes of cancer, with common causes being inherited risk and exposure to toxic substances (Cooper, 2019; Bray et al., 2021; Sung et al., 2021).

Cancers are caused by changes at various molecular levels; genetic, epigenetic, and protein. These changes can cause the activation of growth promoting pathways, leading to the proliferation of cells. The activation of this pathway can be caused by the activation of genes for proteins that promote growth such as epidermal growth factor receptor (EGFR), Kirsten rat sarcoma viral oncogene homolog (KRAS), and v-raf murine sarcoma viral oncogene homolog B1 (BRAF) (Yan et. al., 2022). These genes are also known as oncogenes. Pathways usually responsible for the inhibition of cancerous cell growth, often called tumour suppressor pathways, can also become inhibited. This occurs when tumour suppressor genes involved in these pathways such as TP53 are inactivated (Levine, Momand, and Finley, 1991; Wang et al., 2023).

Studies have shown that approximately 72% of lung cancer cases in the UK can be attributed to the smoking of tobacco products (Brown et al., 2018). Despite historical evidence of the risks of tobacco smoking products accumulating over the last 200 years, evidence was largely ignored until 1950, when studies finding evidence of correlation between lung cancer sufferers and the use of smoking products were released (Peto et al., 2000). One study found that of the lung carcinoma patients interviewed, 26% of 649 men and 14.6% of 60 women interviewed confirmed that their smoking habits were 25 or

cigarettes per day. In comparison, just 0.3% of men and 31.7% of women patients were non-smokers (Doll and Hill, 1950). As the 1950 study results were from a smaller study, Doll and Hill released a further study to validate the results, using a larger group and evaluating other possible causes of lung carcinoma (1952). Progress in cigarette research has led to the identification of over 70 carcinogens commonly found in tobacco cigarettes, including polycyclic aromatic hydrocarbons, benzenes, and nitrosamines, among many others (IARC, 2004). Following metabolic activation many these chemicals have the potential to cause DNA adducts, which if left unrepaired by enzymes present in the body can drive mutations in oncogenes such as KRAS, and tumour suppressor genes such as P53 (Stratton et al., 2009; Hwa Yun et al., 2020). Mutations in these genes are likely to lead to carcinogenesis, particularly in the lungs when tobacco smoke is inhaled (Gealy et al., 1999).

There are two main types of primary lung cancers; small cell lung cancer (SCLC) and non-small cell lung cancer (NSCLC). NSCLC is the more common of the two, accounting for approximately 85% of lung cancers. Within this category of lung cancers are large cell carcinomas, squamous cell carcinomas, and adenocarcinomas. Adenocarcinoma are the most common, accounting for 40% of all lung cancers, and involve gland cells such as goblet cells. This cancer type grows in the peripheral lung tissue. Squamous cell carcinoma (20% of total lung cancers) grows in the tissue along major airways, and large cell carcinoma, representing less than 3% of all lung cancers, can grow proximally or in peripheral lung tissue, and involves large tumours (Zheng, 2016). SCLC is less common, accounting for the remaining 15% of lung cancers, but noted to have particularly aggressive tumours. Approximately 70% of patients with this type present at metastatic stage and have poor prognosis (Lu et al., 2019; Hiddinga et al., 2021).

With 48,549 new cases in the UK from 2016 to 2018, and 35,000 deaths in the same period, lung cancer is the leading cause of cancer related deaths in the UK, accounting for 21% (Cancer Research UK, 2018). Globally, there are approximately 2.2 million cases of lung cancer annually (Sung et al., 2021). While the incidence numbers for lung cancer are undoubtably high, incidence of lung cancer has declined in the last few decades (Siegel et al., 2023). Improved treatment options have led to an increase in lung cancer survival

rates. In 1973 the 5 year survival rate for lung cancer was approximately 10.7%, this figure has improved but remains less than 21% (Lu et al., 2019).

Screening for lung cancer, diagnosis and treatment are associated with increased health anxiety and distress for patients (Gareen et al., 2014; Morrison et al. 2017). There are multiple methods currently used to aid in the diagnosis of lung cancer. Radiological imaging such as x-rays may be used to look for signs such as hilar enlargement, pulmonary opacity at the site of the tumour, and plural effusion. As x-rays cannot distinguish between malignant and benign masses, any found may be viewed in more detail using a enhanced contrast CT (Panunzio and Sartori, 2020). Clinical diagnosis often requires a tissue biopsy to confirm the diagnosis and determine the stage of the cancer. As some of the methods are particularly invasive and distressing for patients, there is a need for less invasive options for diagnosis (Brocken et al., 2015).

While the risk of lung cancer remains higher in former smokers than in non-smokers, smoking cessation has been proven to reduce the risk of developing the disease (Tindle et al., 2018). Various studies have found links between the use of tobacco and nicotine products and dysregulation of miRNA. The expression levels of miR-99b, miR-192, and miR-218 in individuals have all been dysregulated using more traditional smoking products. Following smoking cessation, some miRNA expression levels were found to return to that of a non-smoker, while others continued to be dysregulated (Wang et al., 2015; Du et al., 2018).

As many now recognise the risks of cigarette smoking, alternatives have become increasingly popular to aid smoking cessation (Wieczorek et al., 2020). Having originally been manufactured in 2003, electronic cigarettes (e-cigarettes or ‘vapes’) are much newer than their manual counterparts (Schraufnagel et al., 2014). Initially invented by a pharmacist named Hon Lik, the device was created to be a safer form of nicotine inhalation, following the death of his father to lung cancer (Sullivan and Alexander, 2022; Gordon et al., 2022). There are different types of e-cigarettes available on the market, all containing a heating element, a cartridge, an atomizer, and a battery. The e-cigarettes also contain some of the large variety of e-liquids available. The e-liquids within the e-cigarette are vaporised by the heating mechanism, and the vapours, sometimes containing nicotine, are inhaled by the user (Sundar et al., 2016). The use of e-cigarettes

as a tool in smoking cessation was advised in NICE guidelines as a safer alternative, studies have found that when used as aid in the cessation of smoking, electronic cigarettes are among the most successful methods. When compared to other common methods in the UK, electronic cigarettes containing nicotine were suggested to be effective in the absence of traditional smoking methods (Hartmann-Boyce et al., 2018; NICE, 2023).

A study in the UK on smoking found that 7.7% of participants used e-cigarettes in 2021, compared to 3.7% in 2014 (ONS, 2022).

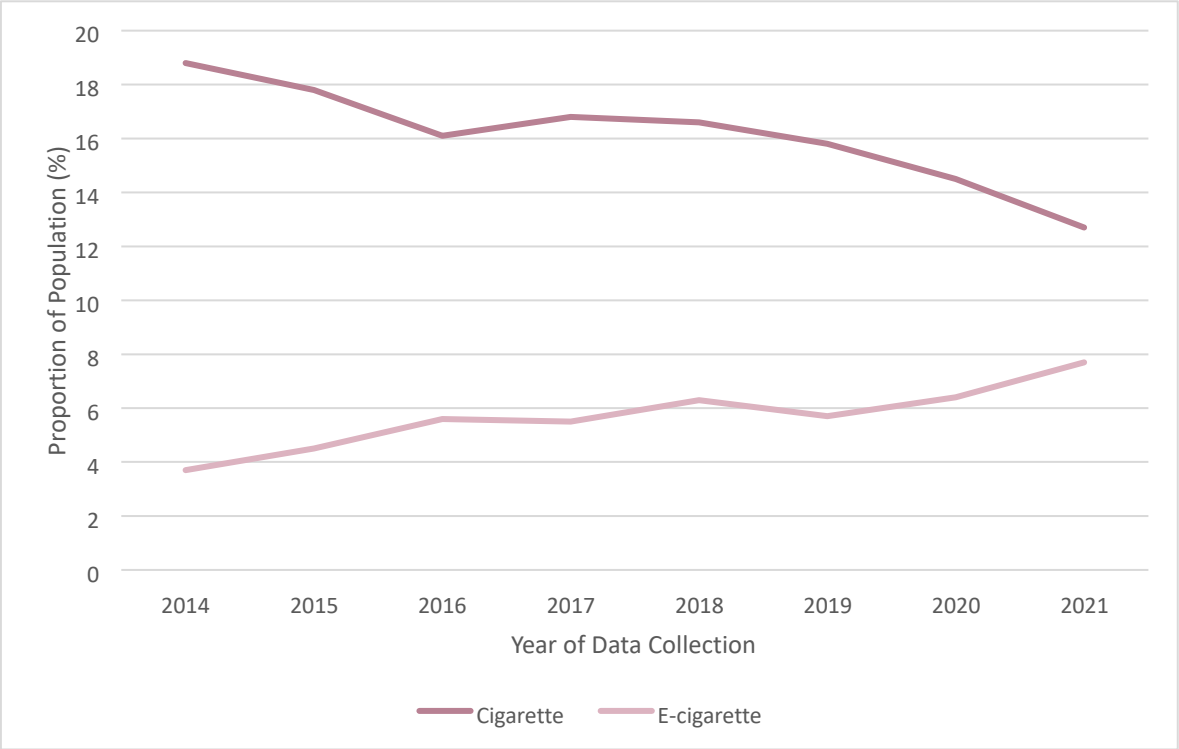

Figure 1.3 The proportion of the UK population who stated they used cigarettes or e-cigarettes in the annual surveys from the Office of National Statistics. Graph produced from datasets available from the 2022 ONS report.

The use of cigarettes continues to decline, while e-cigarette use increases, albeit inconsistently as demonstrated in **figure 1.3** (ONS, 2022). When asked for reason for their use of e-cigarettes, 50.6% of e-cigarette users were previous or current cigarette users who used e-cigarettes to help them quit (ONS, 2020).

A 2022 survey by the organisation Action on Smoking and Health (ASH) found that 8.6% of 11–18-year-olds in England participated in regular or occasional 'vaping', up from the 4% reported on 2021 and 4.8% reported in 2020. The same survey found that 6% of the target group were regular or occasional smokers, again up from previous years. The use of vaping products were found to be similar across socio-economic groups, contrasting with the previous year's data suggesting that the prevalence of vaping in young people was higher in more advantaged groups. The survey also suggested a shift in the type of vaping product used by young people. Previous years had found that the most popular device for vaping was a tank, a refillable and rechargeable device. Most recent data suggests a contrast with this, with 52.8% of users now using disposable vapes. The most popular reasons for smoking in young people were found to be to "give it a try" and "liking the flavours", the most popular flavours being fruit flavours. Among young people who had previously smoked cigarettes, quitting was a common reason (ASH, 2022).

While e-liquid use is often stated to be much safer than actual cigarettes, studies have found that their use is not as safe as first thought. E-cigarette or vaping product use-associated lung injury (EVALI) has been documented in the US, Canada, and Europe (Wieczorek et al., 2020; Shinbashi & Rubin, 2020). There were 2800 cases documented in the US from autumn of 2019 to February 2020, with e-liquid users found to have significant damage the lungs, with chest pain, shortness of breath, and tachycardia. In some cases, EVALI has proven fatal (Shinbashi & Rubin, 2020). The clinical diagnosis of EVALI requires the patient to have used an e-cigarette or vape within 90 days prior to the initial presentation of symptoms. A radiograph or chest CT should show pulmonary infiltrates, and there should not be other possible causes, such as infection, present (Zulfiqar, Sankari, and Rahman, 2022).

The exact cause of EVALI is unclear, with multiple causes under investigation. One potential cause is vitamin E acetate, with a study of 51 EVALI patients finding vitamin E acetate in the bronchoalveolar lavage fluid samples of 48 patients (Zulfiqar, Sankari, and Rahman, 2022). Vitamin E acetate is not usually associated with adverse health effects and is used as an ingredient in some dietary supplements (Reboul, 2017). The safety of inhaling vitamin E acetate is unknown, and Wu and O' Shea (2020) suggested that the heating of vitamin E acetate by the e-cigarette could allow for the release of ketene gas

through pyrolysis. Ketene is thought to be toxic to the pulmonary system (Matsumoto et al., 2020; Wu and O'Shea, 2020).

Lung damage from e-cigarettes could also be due to the wide variety of chemical flavourings used by many brands, with over 7000 different flavours available online in a study in 2014 (Zhu et al., 2014). Lack of knowledge of chemical composition, and variety in voltage and temperature of e-cigarette devices, can make evaluating the effects of a toxicological profile complex (Kaur et al., 2018). The concentration of flavourings can vary greatly, with one 2014 study finding that the concentration of flavourings varied from 2.3-43 mg/ml. The study used gas chromatography to show that both glycerol and propylene glycol were present in the samples, as they are stated to be in most e-liquids but found evidence to suggest that one of the seven manufacturers may have been replacing the two compounds with ethylene glycol. Allergens and prohibited compounds such as cinnamic aldehyde, coumarin, and benzyl alcohol among others were also identified in some e-liquids. The same study found that 7 of the 10 of the flavoured e-liquids analysed that had claimed to be nicotine free, yet actually contained nicotine levels ranging from 0.1 – 15 μg/ml. This study analysed just 28 of the thousands of e-liquid flavours available, and just those purchased in Germany, so the variety in concentrations in both flavourings and nicotine may be greater still (Hutzler et al, 2014). The results of this study could suggest that while there are now regulations in place to cover e-cigarettes, harmful components still appear in commercially available e-liquids and could be the causing further damage to those who use them.

Suryadinata and Wirjatmadi (2021) found that exposing rats to e-cigarette smoke for 2 minutes daily over a 4 week period triggered an inflammatory process, degraded the type 2 collagen found in the lung tissue, and caused an increase in free radicals present, which could lead to oxidative stress. A study by Lerner et al. (2015) also found that the use of e-cigarettes can cause oxidative stress. The severity of the damage caused depended on the type of e-liquid used. Free radicals contain reactive oxygen species (ROS) and reactive nitrogen species (RNS). When inhaled, free radicals would usually be neutralised by antioxidants such as catalase or glutathione peroxidase. When an excess of free radicals is present, the body is unable to completely neutralise the free radicals (Goel et al., 2017). This in turn leads to oxidative stress, and damage to cellular structure as lipids and

proteins, and DNA may be degraded. Oxidative stress has been linked to a wide range of diseases, including cancer, COPD, Alzheimer's, and cardiovascular diseases (Pizzino et al., 2017).

The use of e-liquids has been linked to a dysregulation in miRNA. Solleti et.al. (2017) found an increase in the expression of miR-126-5p and suggested that this could be due to increased oxidative stress to the user's lung cells. Singh et.al. (2020) assessed miRNA levels from plasma sEVs in cigarette smokers, waterpipe smokers, e-cigarette users, and dual smokers. The study found that hsa-miR-365a-3p, hsa-miR-365b-3p, hsa-miR-1299 and hsa-miR-193b-3p, miRNA associated with cancers and cardiovascular complications were downregulated in e-cigarette users. All four smoker groups had down regulated levels of hsa-let-7a, hsa-let-miR-21-5p, hsa-let-7i-5p, hsa-let-7f-5p, hsa-miR-143-3p, and hsa-miR-30a-5p.

1.5.2 Potential of MiRNA in diagnosis of lung damage and disease

As miRNA levels have been found to be dysregulated in lung cancer patients and e-liquid users, miRNA expression levels in circulating sEVs could be used as biomarkers for diagnosis (Matsuzaki & Ochiya, 2017). Due to the protective membrane of the sEVs, miRNA found within are protected from degradation. The isolation of miRNA from sEVs for testing has been promising in cancer diagnosis as tumour cells have been found to release more EVs than their non-cancerous counterparts (Reclusa et al., 2017; Kinoshita et al., 2017). The variety of miRNA found to be dysregulated in lung damage has lead to different miRNA being suggested for diagnostic purposes. In Lung cancers these include Let-7i-3p and miR-154-5p; tumour suppressors found to be downregulated in lung cancer patients; and miR-494, a tumour promotor found to be over expressed in lung cancer (Huang et al., 2014; Zhang et al., 2019).

MiRNA for this project were selected from the large profile of miRNA found to be expressed in sEVs produced by 2D lung cells (Chinta, 2022). MiR-410-5p is found on chromosome 14 in humans, and is featured in previous studies of cancers of the lung, breast, liver and prostate, among others (Altuvia et. al., 2005; Wang et. al., 2016; Wu et. Al., 2018). A study by Wu et. al. (2018) suggested that miR-410 could downregulate the

protein Endoplasmic reticulum lipid raft-associated 2 (ERLIN2), which is associated with the proliferation of some human breast cancer cells such as MCF-7. Overexpression of miR-410 was found to slow cell progression and migration of MCF-7, acting as a tumour suppressor. Results of a study by Yuan et. al. (2020) suggested a complex involvement of miR-410 in NSCLC, as a results of miR-410 targeting the phosphatase and tensin homolog (PTEN); a tumour suppressor gene. By downregulating the expression of PTEN, the intracellular signalling pathways of phosphatidylinositol 3-kinase (PI3K)/Akt and mTOR become overactivated. This could lead to tumorigenesis, and was also suggested to increase cell resistance to radiotherapy.

As previously noted in **1.3.1** MiR-21 has been associated with a large number of diseases and injuries, and while many have suggested its use as a biomarker, others have suggested that its lack of specificity could prove challenging (Abue et al., 2015; Porzycki et al., 2018; Jenike and Halushka, 2021). Nevertheless, as a largely studied miRNA, it was decided that its identification would be useful to evaluate preliminary results in this study.

Circulating miRNA extracted from plasma and serum has previously been shown to remain stable when incubated at room temperature for up to 24 hours, or subjected to up to eight freeze-thaw cycles. This stability increases its potential for clinical use as a circulating biomarker (Mitchell et al., 2008). Despite its stability in these conditions, optimal storage for longer term has been shown to be at -80°C, and freeze-thaw cycles have been shown to affect quality of sample and should be avoided (Grasedieck et al., 2012; Matias-Garcia et al., 2020).

1.6 Research Aims

As many instances of lung cancer are in current or former smokers, and e-liquids are a common tool for smoking cessation, many patients with lung cancer may also use or have previously used e-liquids (Brown et al., 2018; Wieczorek et al., 2020; NICE, 2023). Evidence of the impacts of the use of e-liquids in relation to diseases such as cancers is insufficient, and needs to be further explored (Banks et al., 2022). As the use of e-liquids has shifted to also being used by those who have never smoked tobacco, and try simply

for the flavourings, those impacted by the effects of e-liquids would not only be previous or current smokers (ASH, 2022). Therefore, the use of healthy cells in research concerning e-liquids would not only be useful as a comparative to cancerous cells, but could provide valid insight for potential biomarkers in healthier populations.

Therefore, there is much to learn regarding the use of e-liquids and the impact they may have on potential circulating biomarkers such as sEVs and miRNA, both in cancerous patients, and those in the population who would be considered clinically healthy. Many of the studies in this area use 2D cultures, which allow for higher throughput studies than many of the clinical studies available due to restrictions and availability of sample collection, but do not represent conditions in-vivo accurately. 3D culture presents an opportunity to conduct higher throughput studies while maintaining a closer environment to in-vivo than its 2D counterpart. This study aims to establish a 3D culture method for A549 and BEAS-2B cells that could be used to evaluate the small extracellular vesicles released and the miRNA found in these small extracellular vesicles. By meeting this aim, further research could be conducted into the effects of e-liquids and nicotine on the production of sEVs and expression levels of miRNA. These results could contribute to future research into much needed minimally invasive diagnostics and monitoring tools for lung diseases.

Chapter 2

Research Methods

Methods

2.1 Scaffold-free spheroid cell culture

2.1.1 Cell Culture and Treatment

Initially, two-dimensional cell cultures were used to maintain the cell lines. Cultures were set up using commercially purchased cell lines, A549 adenocarcinoma basal epithelial lung cells (ATCC CRM-CCL-185) and BEAS-2B normal epithelial lung cells (ATCC CRL-9609). Under sterile conditions cells were passaged into RPMI + glycolycine medium (Roswell Park Memorial Institute, Labtech, UK), with 10% FBS (Gibco, UK) as a growth factor and 1% penicillin streptomycin to reduce risks of contamination. Cells were incubated at 37°C with 5% CO2. Cells were passaged at 80% confluency for optimal growth.

Three-dimensional cultures were set up using non-adherent flasks, created by adding 12 grams of poly(2-hydroxyethyl methacrylate) (poly-HEMA) (Sigma-Aldrich) to 1 litre of 95% ethanol. This is left 6 hours to dissolve, before 20 ml was added to T175 flasks and kept at 40°C for 12 hours. During the 12 hours the ethanol evaporated, and the poly-HEMA attached to the surface of the flask, preventing future cells from attaching. For 3D cultures DMEM/F12 media without phenol red (Gibco, UK) was used, with 1% penicillin streptomycin and a 2% addition of B-27 (Gibco, UK) supplement and human EGF growth hormone. The B-27 and hEGF were mixed prior at a 100:1 ratio.

Multiple cultures of each cell type were set up, allowing for untreated control cultures and cultures treated with e-liquids. E-liquids used were produced by the brand Jucee. Of the products available, the flavours Strawberry and Apple were selected, both with 18mg/ml Nicotine content and Nicotine-free. The molarity of nicotine was calculated, and solutions of 1mM nicotine were made by diluting e-liquid with nicotine in plain DMEM media. The same volume of e-liquid without nicotine was also diluted in plain DMEM media. Solutions were further diluted, and 1ml of 100 µM nicotine concentration was added to the e-liquid with nicotine cultures, with the same volume of e-liquid without nicotine being used in nicotine-free cultures. These e-liquid solutions will henceforth be denoted with the abbreviations in **table 2.1.**

Table 2.1 Abbreviations used for e-liquid solutions used for cell culture treatments

E-liquid	Abbreviation
Strawberry flavoured e-liquid containing nicotine	St+Nic
Strawberry flavoured e-liquid not containing nicotine	St-Nic
Apple flavoured e-liquid containing nicotine	App+Nic
Apple flavoured e-liquid not containing nicotine	App-Nic

Cells were added to a flask with 20 ml total media, with 2 million cells total seeded for each individual sample. Following 72 hours of treatment at 37°C and 5% CO2, the surrounding media was collected and sEVs isolated.

2.2 Small Extracellular Vesicles

2.2.1 Isolation of Small Extracellular Vesicles

For the extraction of sEVs, media containing cells was removed from 3D flasks and centrifuged at 300 *x g* for 5 minutes to separate the cells from the surrounding media. The supernatant above the cell pellet was removed and centrifuged at 1000 *x g* for 10 minutes. The supernatant was again removed and centrifuged at 2000 *x g* for 10 minutes. Following this a 200 nm filter and 10 ml syringe was used to add the supernatant to a new flask, to separate any remaining larger particles from the EVs.

Further methodology was adapted from the Cell Guidance Exo-Spin Protocol, which uses the principle of size exclusion chromatography (SEC), a method recommended by MISEV guidelines for the isolation of extracellular vesicles (Théry et. al., 2018). The media was centrifuged at 10,600 *x g* for 48 minutes, before the Cell Exo-Spin Buffer (Cell Guidance, Cambridge, UK) was added at a 2:1 ratio and the mixture was incubated overnight at 4°C, to precipitate EVs. Following incubation, the mixture was centrifuged for a further 96 minutes at 10,600 *x g*. The supernatant was then removed from the falcon, leaving approximately 500 µl. This was centrifuged for a further 10 minutes at 10,600 *x g*, before removing remaining media. The remaining pellet of precipitated EVs would be concentrated via these steps, to be used in exo-spin columns for size exclusion chromatography, allowing smaller EVs to be isolated.

Each remaining pellet was resuspended using 100 µl of PBS. Exo-Spin columns (Cell Guidance, Cambridge, UK) were prepared using methods described by Cell Guidance, and samples were added to the top of the column, and allowed to enter the column matrix. Once sample had entered the column, PBS was added, allowing sEVs separated by size exclusion chromatography to flow through to the awaiting Eppendorf. To prevent protein degradation, 1 µl of protease inhibitor was added per 100 µl of sample. Sample was kept at -80°C.

2.2.2 Transmission Electron Microscopy

To aid in the confirmation of size and shape of the particles found in EV samples, and to differentiate EVs from other particles present, 10 µl of sample was sent to the University of Liverpool to be imaged using Transmission Electron Microscopy (TEM).

In short, the sample was suspended on a carbon coated grid and washed with PBS, before fixation using 1% glutaraldehyde in PBS at room temperature, to preserve the sEVs. Sample was washed further with ddH2O and stained with 1% uranyl acetate, followed by further staining with a 1:9 ratio of 4% uranyl acetate and 2% methyl cellulose, performed on ice. Samples were dried prior to imaging TEM imaging was performed using a FEI 120kV Tecnai G2 Spirit BioTWIN.

2.2.3 Nanoparticle Tracking Analysis

Nanoparticle tracking analysis (NTA) was performed using a Zetaview nanoparticle tracking analyzer (Particle Matrix, Germany). NTA aids in the characterisation of nanoparticles by calculating the number and size of particles between 10 nm and 1000 nm by detecting the light scattered. The machine was prepared according to instructions from Analytik, and sEV samples for analysis were prepared at a 1:1000 dilution in PBS. Samples were added and particles were illuminated by laser. The video sequence taken by the Zetaview was analysed by the program and the Brownian motion of the particles was determined to calculate size. The program provided raw data of the number of particles, concentration, and the size distribution within the sample. Using Excel 365, mean

concentrations of particles were used in unpaired t-tests to evaluate if there were significant differences in concentrations of different sample types.

2.2.4 Fluorescence Nanoparticle Tracking Analysis

In addition to basic NTA, the Zetaview can be used to detect the presence of fluorescently conjugated antibodies that tag proteins on nanoparticles. A filter in the Zetaview blocks the scattered light used in NTA, permitting the 520 nm wavelength reflecting from fluorescently tagged particles to be detected. This can aid in differentiating between EVs and sEVs, by identifying the concentrations of the sample that contains tetraspanin proteins CD9, CD63, and CD81.

Sample dilutions in PBS were calculated following NTA to allow for 150-200 particles per frame in order to accurately detect the fluorescently tagged particles. Cell mask orange (CMO) (Invitrogen, UK) a lipophilic membrane dye, was diluted to 1:250 in PBS. Fluorescent antibodies for CD9 (PE/Dazzle™ 594 Antibody), CD63(PE/Dazzle™ 594 Antibody), and CD81 (PE/Dazzle™ 594 Antibody)(Biolegend UK) were diluted to 1:2.5 in PBS. Samples for fNTA were prepared at 9 µl of sEV sample to each 1 µl of CMO dye or antibody and incubated in the dark for 1 hour.

Following incubation, the particle count and particle size were measured using the Zetaview with the 520 nm filter and scatter setting. Readings were taken in triplicate and analysed using Excel 365. Results were normalised and compared using CMO readings, which should detect 100% of lipid bound particles present in the sample. Results for tetraspanin CD markers were then used calculate the percentage of positive particles when compared to the CMO.

2.2.5 BCA Protein Assay

To ensure adequate protein content in samples, the Pierce™ BCA Protein Assay Kit (Thermo Scientific, Catalogue no. 23225 and 23227) was used. In accordance to the manufacturers protocol, samples were prepared as denoted in **Table 2.2**.

Table 2.2. Dilutions used for BSA Standards

Dilution for standard microplate procedure (working range = 20-2000 µg/mL)			
Vial	Diluent Volume (µL)	BSA Volume and Source (µL)	Final Concentration of BSA (µg/mL)
A	0	300 of stock	2000
B	125	375 of stock	1500
C	325	325 of stock	1000
D	175	175 of vial B	750
E	325	325 of vial C	500
F	325	325 of vial E	250
G	325	325 of vial F	125
H	400	100 of vial G	25
I	400	0	0 (blank)

The working reagents was prepared at 50:1 of working reagents A and B, with sufficient volume of 200 µL for each well used. In a 96 well plate, 20 µL of each standard was used. Samples were added to create 1:20 and 1:10 dilutions with the working reagent. 200 µl of working reagent was added to each well and covered. The plate was mixed well on a plate shaker for 30 seconds, before being incubated at 37°C for 30 minutes. Absorbance was then measured on a Varioskan plate reader at a wavelength of 562 nm.

Absorbance of standards were normalised using the blank result and plotted into a standard curve. This curve and the known protein concentration of the standards were then used to calculate the protein concentration of each sample.

2.2.6 Western Blot

2.2.6.1 Solutions

Solutions required for western blot analysis were prepared in advance of the western blot. 10x Running Buffer was made at 250 mM Tris, 1.92 M Glycine, 1% (w/v) SDS; 1x Transfer Buffer was made to 25 mM Tris, 192 M Glycine, 20% (v/v) Methanol; 1x wash buffer was 0.1% tween in PBS; and blocking buffer was 5% BSA in PBS.

2.2.6.2 Sample preparation

For each sample 25 µl of sample (5 µl of cell lysate) was added to an Eppendorf tube with an equal amount of RIPA (Sigma-Aldrich) and agitated at 4°C for 30 minutes. Following this, 40 µl of PBS was added to the cell lysate tube, before 12.5 µl of LDS sample buffer (Nu-PAGE) was added to all tubes. These were then incubated at 70°C for 10 minutes.

2.2.6.3 Hand-Cast Gel

Prior to the western blot, hand cast gels were made up of resolving gel and stacking gel. First, resolving gel was prepared using the following.

Table 2.3 Preparation of Resolving Gel

Resolving Gel (12%)	10 ml Total
ddH20	3.3 ml
Acrylamide 30%	4.00 ml
Tris-HCL [1.5M] pH 8.8	2.34 ml
SDS [10%]	100 µl
APS [10%]	100 µl
TEMED	4 µl

The resolving gel was allowed to set before the stacking gel was prepared.

Table 2.4 Preparation of Stacking Gel

Stacking Gel	2 ml Total
ddH20	1.4 ml
Acrylamide 30%	330 µl
Tris-HCL [1.5M] pH 6.8	250 µl
SDS [10%]	20 µl
APS [10%]	20 µl
TEMED	2 µl

A comb was added to the stacking gel before it was allow to set to create wells for sample.

2.2.6.4 SDS-PAGE Running and Transfer

Gels were secured in a tank and 1x running buffer was added to the tank. The gel was carefully loaded with 250 kDa protein ladder (Thermo Scientific), samples and cell lysate. Attaching the lid to the tank, the gel was run at 0.2 A per gel, at 100 V for 30 minutes to allow samples to pass through the stacking gel, followed by 150 V for an hour, monitoring the gel to ensure the sample didn't run off the gel.

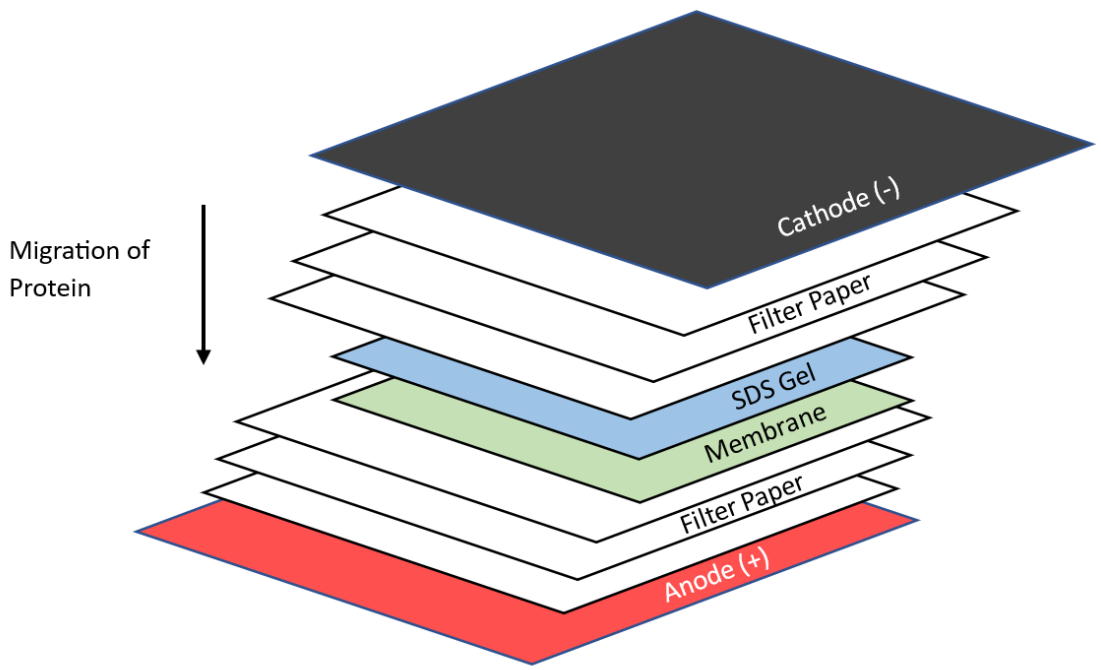

Figure 2.1 The Western Blot Sandwich used to transfer protein from gel to membrane. Figure created in Microsoft Word

Following the gel run, a blotting sandwich was assembled starting at the positive anode; 3 pieces of blotting paper, a blotting membrane, the gel, and three pieces of blotting paper at the end facing the negative cathode. Ensuring each component is appropriately covered in transfer buffer, the sandwich was clamped shut and inserted into the transfer tank with an appropriate volume of transfer buffer. The tank was run on ice for an hour at 100 V while the protein migrated from the gel to the blotting membrane. Once this run was complete the membrane was washed with 1x wash buffer 3 times for 10 minutes, at no point allowing the membrane to dry out. The membrane was then incubated in 5% BSA (Sigma-Aldrich) on a rocker for an hour at room temperature to block.

2.2.6.5 Antibody Incubation

Prior to probing with the primary antibody, the membrane was washed 3 times for ten minutes using 1x wash buffer. Following this, the membrane was added to a 1:2000 dilution of antibodies in 2.5% BSA blocking solution, with PBS and 0.1% Tween. For this project the antibodies for CD9, CD63, and Calnexin (Thermo Fischer). The membrane was incubated overnight at 4°C.

Following overnight incubation, membranes were washed 3 times for 10 minutes with 1x wash buffer, before being incubated in 1:5000 secondary anti-mouse HRP conjugate antibody (Cell signalling, UK) for an hour at room temperature. Following this the membrane was washed 3 times for 10 minutes with 1x wash buffer.

2.2.6.6 Imaging

For imaging the membrane was incubated in 1:1 enhancer to luminol ELC reagents (Thermo Fischer) for 1 minute, before being imaged in an imaging box. Membranes were initially imaged and viewed using a G-Box and GeneSys software, and later viewed using a Li-Cor Odessey XF.

2.3 MicroRNA

2.3.1 Small RNA isolation

Fifty µl of sEV sample was added to a collection tube with 1 µl of proteinase k, this was pipetted up and down and vortexed for 60 seconds to mix well. This mixture was then incubated at 37°C for 30 minutes. Following this, 0.5 µl of protease inhibitor was added and vortexed, before incubating the sample on ice for 10 minutes. Following this, 1 µl of RNAse A was added. This was again vortexed and incubated for 30 minutes at 37°C. To stop this reaction, 700 µl of QIAzol lysis reagent was added immediately following the incubation period and vortexed. This was incubated for 20 minutes at room temperature. Following incubation, 90 µl of chloroform was added to the sample and shaken vigorously for 15 seconds. The sample was incubated for a further 2 minutes at room temperature, before centrifugation at 12,000 *x g* for 15 minutes at 4°C. Following centrifugation, the clear aqueous phase separated to the top of the tube was carefully transferred to a new tube, and 1.5x the sample volume of 100% ethanol was added and mixed by pipetting. 700 µl of this mixture was added to the RNeasy MinElute spin column, and centrifuged at 8000 *x g* for 15 seconds at room temperature. Flow through was discarded and any additional sample was added and this step was repeated. Following this, 700 µl of RWT buffer was added to the column, and centrifuged at 8000 *x g* for 15 seconds at room

temperature. Flow through was again discarded and 500 µl of RPE buffer was added to the column, and again centrifuged at 8000 *x g* for 15 seconds at room temperature. This flow through was discarded, and the column was placed above a new collection tube. This was centrifuged at full speed with the column lid open, in order to dry out the membrane, and the flow through was discarded. The column was again placed above a new collection tube, and 14 µl of RNAse-free water was carefully added to the centre of the membrane. This was centrifuged at full speed for 1 minute, and the RNA eluted.

The isolated small RNA was quantified using a Qubit MiRNA assay (Thermo Fischer). A mastermix of 199 µl and 1 µl of Qubit reagent per sample was prepared to form a Qubit Working Solution (Thermo Fischer). Two standards were also used for calibration. Standard 1 has a concentration of 0 ng/µl and standard 2 has a concentration of 10 ng/µl. These are each prepared with 190 µl of working solution and 10 µl of standard in a sample tube. 2 µl of samples to be quantified are added to sample tubes with 198 µl of the working solution. All tubes were vortexed for 30 seconds and incubated at room temperature for 2 minutes. The Fluorometer 3.0 was standardised using standards 1 and 2, before small RNA concentrations for each sample were measured.

Small RNA samples were stored at -80°C.

2.3.2 cDNA conversion

For cDNA conversion, a QuantiMir kit was used (System Biosciences). Quantimir RT kit protocols state that 10 pg – 10 ng of RNA in 5 µl of Total RNA should be used for cDNA conversion. Following optimisation, 3 ng of RNA in 5 µl was used. Qiagen miRNeasy Spike-in Control kit was used for an internal spike-in control of *C. elegans* to normalise sample, with 1.5 µl was added to each sample. In the first step to form a polyA tail, the microRNA/c. elegans sample was added to the tube with 2 µl of 5x polyA buffer, 1 µl of 25 mM MnCl2, 1.5 µl of 5nM ATP, and 0.5 µl of polyA polymerase. This was incubated for 30 minutes at 37°C in the thermocycler.

Following this incubation, 5 µl of Oligo dT Adaptor was added to each sample tube and heated at 60°C for 5 minutes to anneal to the sample, and then cooled to room temperature for 2 minutes.

Once the sample is at room temperature, 4 µl of 5x RT buffer, 2 µl of dNTP mix, 1.5 µl of 0.1M DTT, 1.5 µl of RNase-free H2O, and 1 µl of reverse transcriptase was added to the sample tubes. This was incubated at 42°C for 1 hour to reverse transcribe the RNA to cDNA, before being heated to 95°C for 10 minutes.

The final cDNA samples were stored at -20°C

2.3.3 Quantitative PCR with SYBR Green

As there is no housekeeping gene available for miRNA work, samples were prepared with primers for the Cel-Mir-39 spike-in as a control, to ensure accuracy of pipetting work. RNase-free water was also added to an additional set of samples in place of cDNA, to act as a negative control. This was run alongside samples with forward primers for specific miRNA. All forward primer sequences were identified using miRbase (http://www.mirbase.org) and obtained from Eurofins Genomics.

Table 2.5 Forward primer sequences required for amplification of MiRNA

MiRNA	Forward Primer Sequence
Cel-mir-39-3p	5'-TCACCGGGTGTAAATCAGCTTG-3'
MiR-410-5p	5'-AGG TTG TCT GTG ATG AGT TCG -3'
MiR-21-5p	5'-TAG CTT ATC AGA CTG ATG TTG A -3'
MiR-382-5p	5'-GAA GTT GTT CGT GGT GGA TTC G-3'
MiR-541-5p	5'-AAA GGA TTC TGC TGT CGG TCC CAC T-3'

Primers in **Table 2.5** were used in sample preparation for qPCR following the QuantiMir RT kit protocol, **Table 2.6**. 2x SYBR Green qPCR Mastermix buffer was purchased from Bio-line, and is utilised as it binds to the double-stranded DNA produced in qPCR and fluoresces, with fluorescence increasing as the quantity of DNA increases.

Table 2.6 QuantiMir Samples for qPCR

2X SYBR Green qPCR Mastermix buffer	15 µl
Universal Reverse Primer (10 µM)	0.5 µl
MiRNA Specific Forward Primer (10 µM)	1 µl
cDNA (Diluted 1:10)	1 µl
RNase-free water	12.5 µl

Rotor-Gene-Q (Qiagen) was used for PCR amplification. The qPCR cycle begins with heating samples to 50°C for two minutes for activation, then heating to 95°C for 10 minutes for initial denaturation. Following this the steps of heating to 95°C for 15 seconds followed by cooling to 60°C for 1 minute were cycled 40 times. The qPCR data was read at 60°C 15 seconds on the green channel.

Using qPCR data for miRNA results in triplicate, a relative fold change for the CT values between untreated samples and treated samples, which were normalised using the Cel-Mir-39 results. Relative fold change was calculated by first establishing a mean CT value for results, and then calculating ΔCT by subtracting the target miRNA results from the Cel-Mir-39 results. ΔΔCT values were calculated by subtracting the untreated (control) result from the treated result. Final relative fold change results were calculated using the formula = 2^-(ΔΔCT) (Livak and Schmittgen, 2001). Relative fold change in expression of miRNA was then analysed by comparing the result to the control value of 1, where results of 0.5 to 1.5 would be considered as not differentially expressed, and anything outside of these results would be considered to show upregulated or downregulated expression.

2.4 Statistical tests

NTA results were compared using unpaired, 2-tailed student's t-tests to establish if differences in concentrations found between samples were statistically significant, using triplicate means of 3 NTA readings.

Relative fold change of CT values found in qPCR were established using 2^-(ΔΔCT) (Livak and Schmittgen, 2001).

Chapter 3

Results

Results

3.1 Three-Dimensional Spheroid Culture methods were optimised to establish an appropriate cell seeding density

Initial 3D cell cultures were trialled using techniques described in methods by Shaw et al. (2012) and Amaral et al. (2017), to evaluate which techniques formed the most effective protocol. The ethanol/polymer mix used was found to be effective, although the volume initially used was found to be too high, with 8ml per T75 flask found to be optimal. Simultaneous to the preparation of the flasks, A549 cancerous alveolar cells and BEAS-2B healthy bronchial cells were grown up to confluency as 2D cultures in adherence flasks. Prior to transfer to the non-adherence flasks prepared, cells were counted using a haemocytometer.

During initial development of 3D culture protocol, different quantities of cells were trialled. Microscope images of A549 spheroids formed by a starting quantity of 2 million cells are shown below.

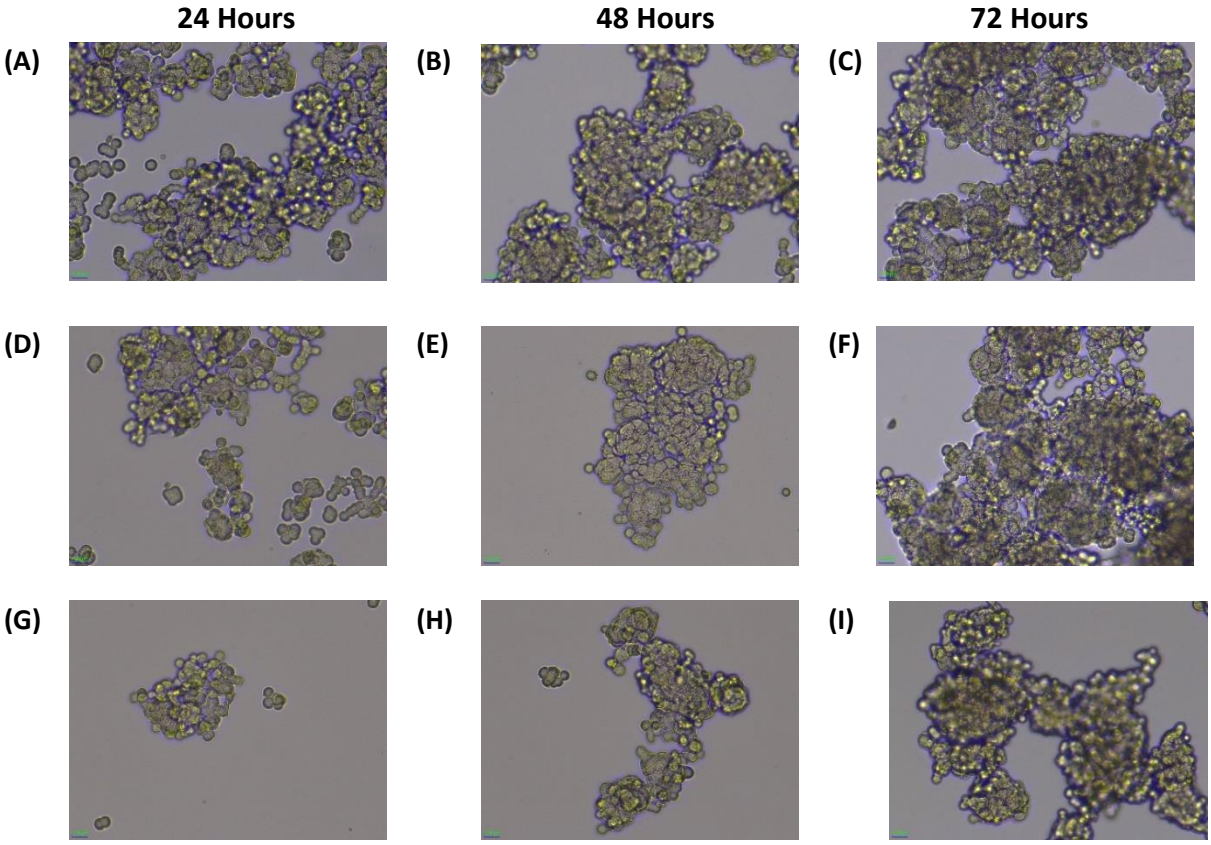

Figure 3.1. A549 spheroids in variable seeding densities in low adherence flasks at three time points. Images (A), (B), and (C) show cells at a seeding density of 2 million at 24 hours (A), 48 hours (B), and 72 hours (C). Images (D), (E), and (F) show cells at a seeding density of 1 million at 24 hours (D), 48 hours (E), and 72 hours (F). Images (G), (H), and (I) show cells at a seeding density of 500,000 at 24 hours (G), 48 hours (H), and 72 hours (I). Each image was taken at x10 magnification, with a 100 µm size bar.

A549 cells formed spheroids when seeded on non-adherent flasks in DMEM with B27/hEGF. A549 spheroids formed non-uniform aggregates of varying sizes, particularly when seeded in larger quantities. To allow for space for spheroids to form and sufficient EV production, 2 million A549 cells were initially seeded in 20 ml of media. This quantity of cells were found to form large aggregates immediately (**figure 3.1 (A**)), and appeared to proliferate quickly. Other quantities of A549 cells were trialled, starting with 1 million cells. The second starting cell count attempted was 1 million cells, again seeded in the low adherence flasks prepared in DMEM and B27/hEGF. While the 1 million cells per low adherence flask initially formed much smaller aggregates than the 2 million cells, the cells were also found to form large aggregates over the 72 hour period (**figure 3.1 (F)**) that would be required for e-liquid treatment and EV production. Seeded using the same

method as the previous quantities, 500,000 cells per flask were found to form much smaller aggregates and had more room between the aggregates. This could indicate a larger percentage of the cell surface is available to the surrounding media and nutrients.

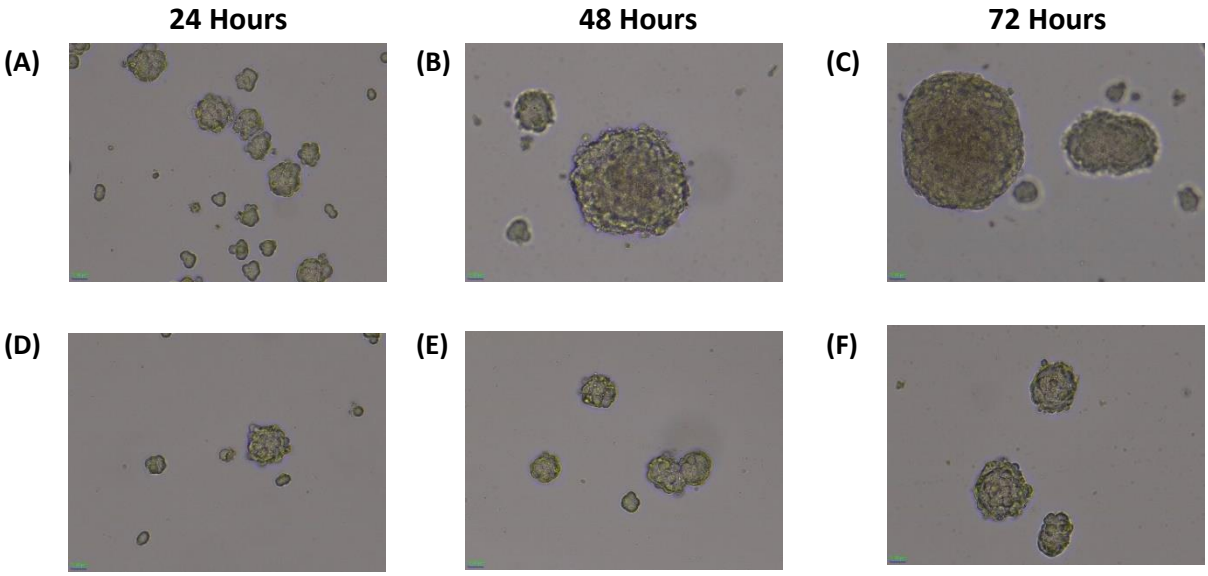

Figure 3.2. BEAS-2B spheroids in Variable seeding densities in low adherence flasks at three time points. Images (A), (B), and (C) show cells at a seeding density of 2 million at 24 hours (A), 48 hours (B), and 72 hours (C). Images (D), (E), and (F) show cells at a seeding density of 500,000 at 24 hours (D), 48 hours (E), and 72 hours (F). Each image was taken at x10 magnification, with a 100 µm size bar.

BEAS-2B were found to form spheroids well in non-adherent flasks both at a starting quantity of 2 million cells. As seen in the **figure 3.2 (C)**, higher quantities of beas2b such as 2 million in 20ml allowed for large, rounded spheroids to form over the 72 hour period, which remained separate from the other spheroids. At 500,000, smaller round spheroids formed, which were more spaced out. These spheroids remained smaller over the 72 hour period as can be seen in **figure 3.2 (F)**, and did not appear to develop as significantly as the BEAS-2B spheroids from the 2 million cell starting quantity.

3.2 Characterising Small Extracellular Vesicles by TEM, NTA, fNTA, and Western Blot

Following the development of a 3D culture protocol, cells were grown and treated at 500,000 cells per flask, with 4 flasks total for each sample. Cultures of A549 and BEAS-2B were grown with different treatments; untreated; treated with St+Nic; treated with St-

Nic; treated with apple flavoured e-liquid with nicotine; and treated with apple flavoured e-liquid without nicotine. Size exclusion chromatography, using the Cell Guidance Exo-Spin columns, was used to isolate sEVs from each sample. Multiple methods were used to characterise the particles found in each sample, in accordance with MISEV guidelines (Théry et. al., 2018). These methods included Transmission Electron Microscopy, Nanoparticle Tracking analysis, Fluorescence Nanoparticle Tracking analysis, and Western Blot.

3.2.1 Transmission Electron Microscopy showed particles of the correct size and morphology for small extracellular vesicles.

Untreated samples from both A549 and BEAS-2B cell lines were imaged using TEM to evaluate to size and shape of particles in the samples. These images were produced at the University of Liverpool, and multiple images were taken of each sample, to allow review of any variation in size and morphology that could be present.

(A) **(B)**

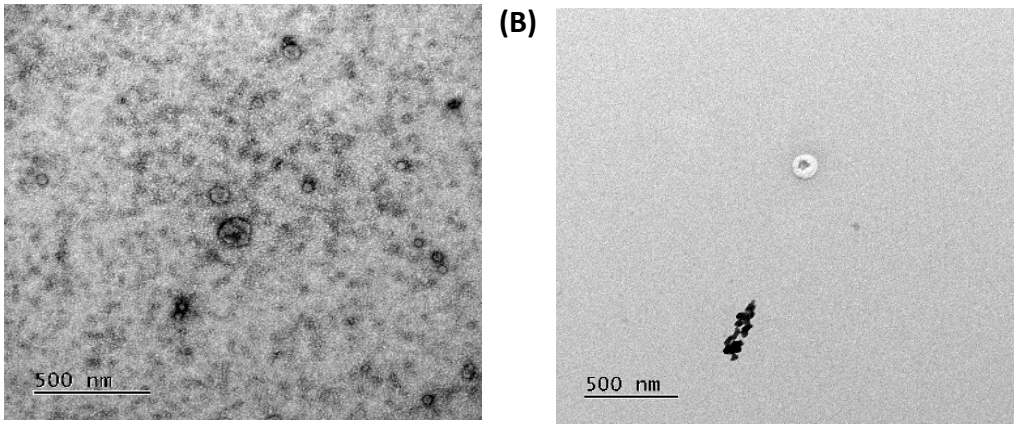

Figure 3.3 Representative of images produced from transmission electron microscopy Particles found in sEV sample from (A) untreated 3D A549 and (B) untreated 3D BEAS-2B cultures.

Particles found in the A549 sEV samples in **figure 3.3 (A)** were seen to be rounded and under 200 nm, with some under 150 nm in size. Some particles, visible also exhibited a “cup-shape”. Some particles in additional images taken, visible in the appendices,

exhibited a less uniform shape, though was the correct size for sEVs. Like the A549 EV sample, the sample from BEAS-2B were found to be rounded with a size range under 200 nm. The desired “cup-shape” was seen in some particles **figure 3.3 (B).**

3.2.2 Size distribution and concentration of particles was demonstrated using Nanoparticle Tracking Analysis

NTA measurements were taken soon after completing day 2 of sEV isolation to help ensure accuracy of results. Measurements were used to find size distribution of particles within samples, diluted to 1:1000 in PBS.

(A)

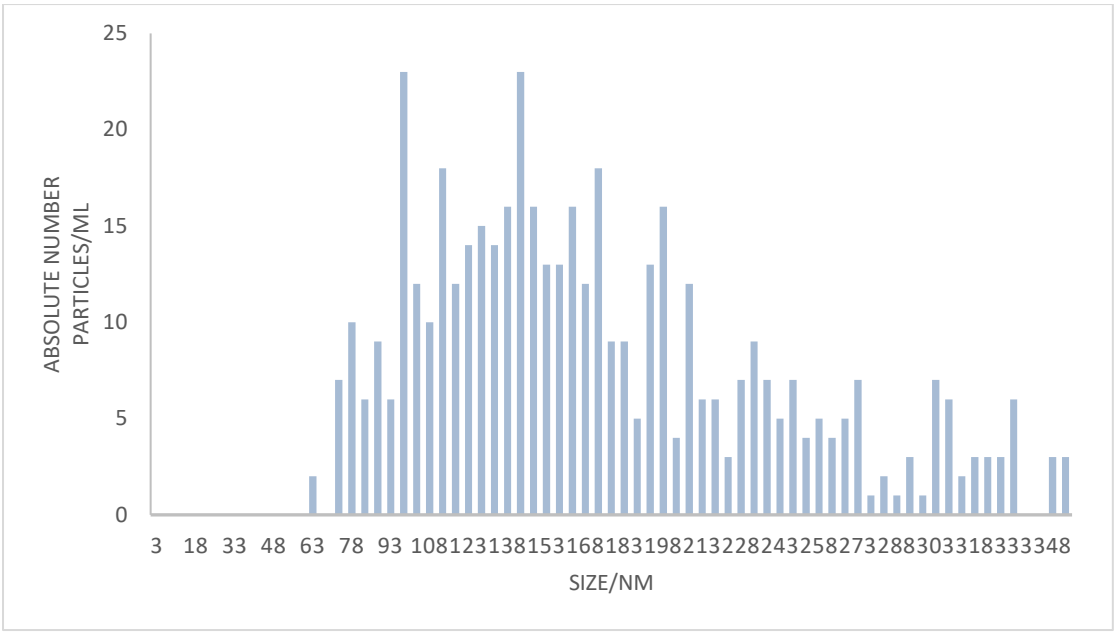

(B)

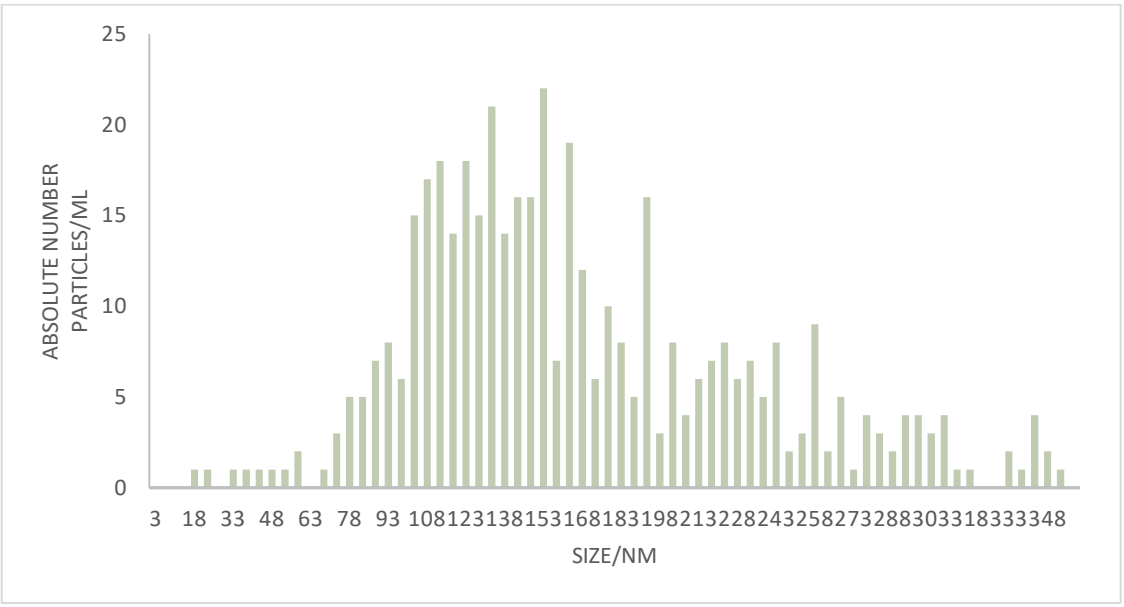

Figure 3.4 Visual representative of results for NTA for size range of A) A549 sEVs and B) BEAS-2B. Results obtained from the Zetaview Nanoparticle Tracking Analyzer demonstrating size distribution of sEVs isolated from **A)** untreated 3D cultures of A549 and B) untreated 3D cultures of BEAS-2B. Sample was diluted at 1:1000 in PBS prior to measurement.

Size of particles in the A549 sEV sample varied between 63 nm and 348 nm as shown in **figure 3.4 (A)**. Much of the particles found were under the expected size of 200 nm. **Figure 3.4 (B)** shows that SEVs isolated from untreated BEAS-2B varied in size from 18 nm to 348 nm. Again, much of the sample measured below the expected 200 nm. Some

larger particles were seen from readings for both samples, which could be larger EVs or aggregates.

In addition to size distribution, the concentration of particles found in the sample was also measured. SEV sample produced as part of this project was also used as part of other research projects in the laboratory. Raw data produced from NTA for these projects was collected alongside data produced in this project to find the mean concentrations for A549 samples.

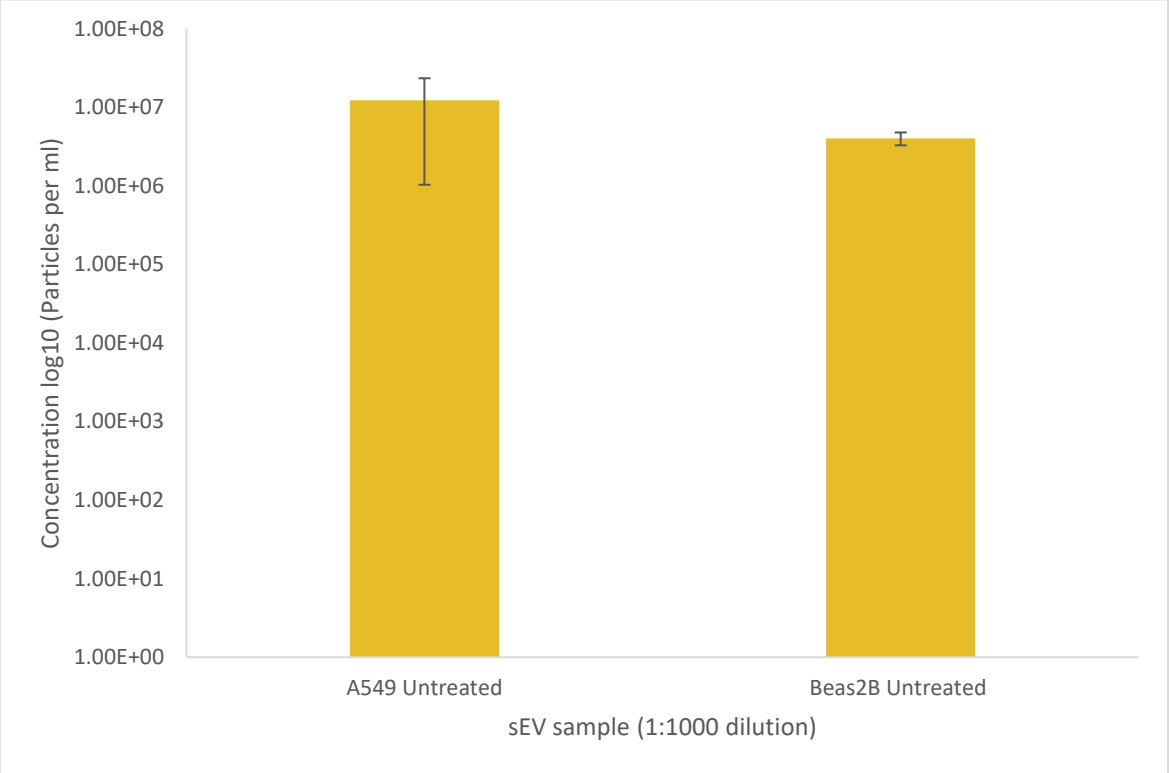

Figure 3.5 The mean concentrations of sEVs isolated from untreated 3D cell cultures of A549 and BEAS-2B. Samples were added in 1:1000 dilutions in PBS, measured using a Zetaview Particle Tracking Analyzer. Mean concentrations were calculated from readings from 3 samples, with error bars produced from SD.

Mean concentrations of sEVs from untreated A549 and untreated BEAS-2B, demonstrated in **figure 3.5**, were 1.22 x10^7 and 4.03 x10^6 respectively. The standard deviation was found to be higher in the A549 sample than in the BEAS-2B sample. Using an unpaired Student's t-test, no significant difference was found between the two data sets.

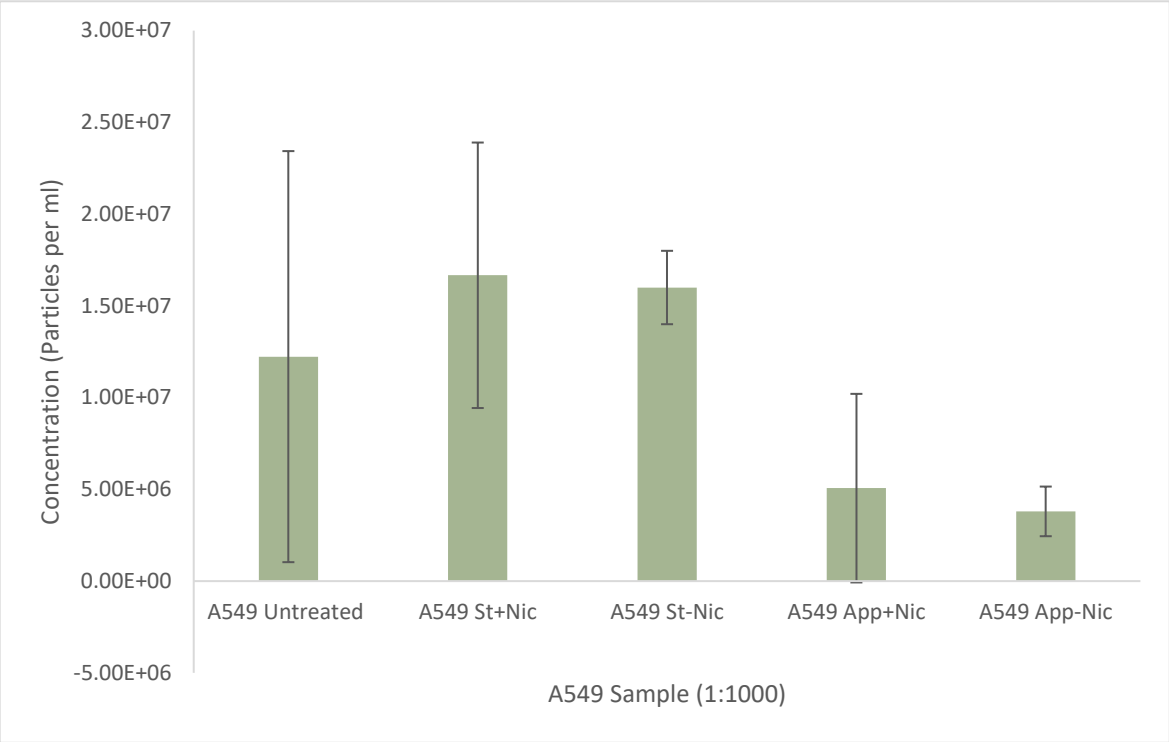

Figure 3.6 Bar chart demonstrating the mean concentrations and standard deviations of A549 sEV samples. Mean particle concentration of three samples using Zetaview Particle Tracking Analyzer were untreated, strawberry flavoured e-liquid with nicotine, strawberry flavoured e-liquid without nicotine, apple e-liquid with nicotine, and App-Nic. Error bars representative of SD.

The mean concentrations of A549 derived sEV samples shown in **figure 3.6**. A549 samples treated with St+Nic had a mean concentration of 1.67x10^7, St-Nic had a mean concentration of 1.60x10^7, App+Nic had a mean concentration of 5.07x10^6, and App-Nic had a mean concentration of 3.80x10^6. The differences between these results were statistically insignificant to each other, and to the untreated A549 sEV sample when compared using an unpaired Student' t-test. Standard deviations for these results were larger for untreated samples and samples treated with e-liquids containing nicotine.

3.2.3 Fluorescence Nanoparticle Tracking Analysis

Following NTA, samples were diluted for fNTA to allow for 150-200 particles per sample.

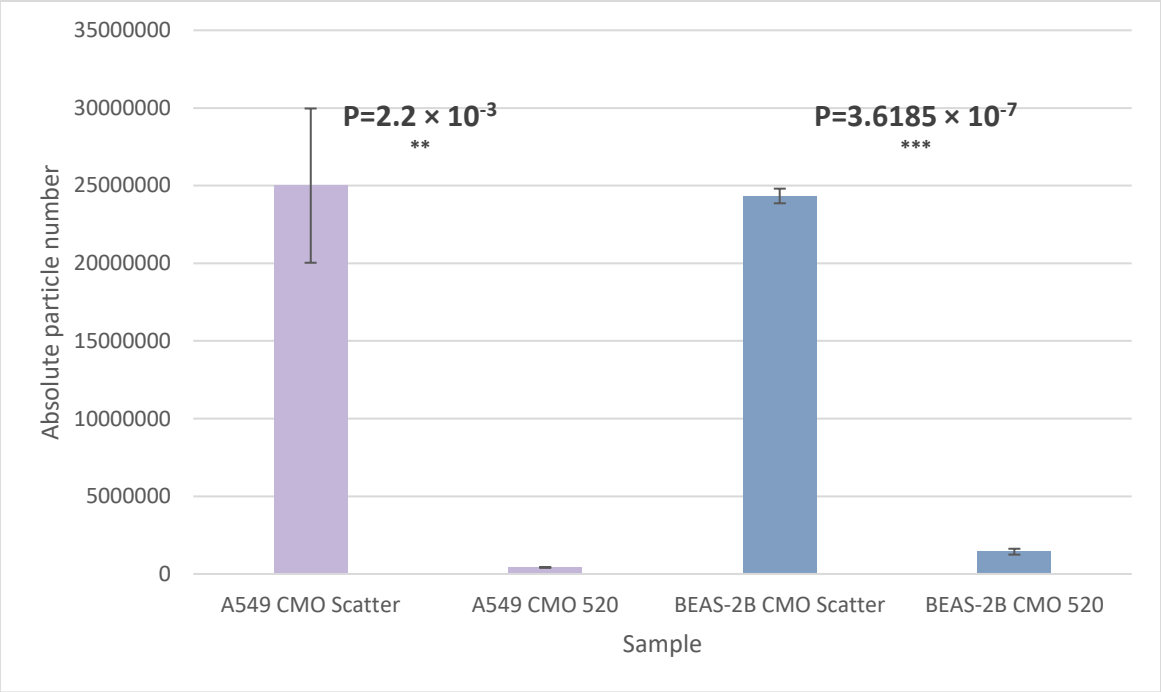

Figure 3.7 Comparison of scatter results and 520 nm results of potential sEVs derived from untreated 3D A549 and BEAS-2B cultures. Results shown from A549 incubated with CMO dye and BEAS-2B incubated with CMO dye. Scatter results were measured using the Zetaview Particle Tracking Analyzer on scatter mode, with CMO and CD9 reading taken with the same equipment with the filter used to block scattered light and permit only that which is reflected at a 520 nm wavelength from fluorescent particles. Results shown are mean of three samples, with SD represented by error bars. Unpaired students t-test was used to compare samples from each cell line when measured with scatter settings and at a 520nm wavelength. Significant differences calculated by unpaired student's t-test are indicated with * ($P \leq 0.05$), ** ($P \leq 0.01$), *** ($P \leq 0.0001$).

Comparison of scatter and fluorescence concentrations (seen in **figure 3.7**) using an unpaired student's t-test showed that scatter results for each sample were significantly higher than the corresponding fluorescently labelled vesicles detected. Vesicles derived from BEAS-2B cultures also showed lower concentration of CMO labelled vesicles than CD marker probed vesicles, suggesting that the CMO readings may not be accurate. As tetraspanin proteins are present on lipid bound membranes, all vesicles successfully probed with CD markers should also be dyed by CMO. This result could indicate an under

estimation of CMO, or could indicate that the sample is heterogenous, and contains more than just the sEVs isolated from cell culture media.

As part of another project, sample from this project was used to detect CD9 levels in sEVs isolated from A549. Concentrations of fluorescently labelled particles detected under the filter were taken, with CMO taken to be 100% of particles with a lipid bilayer.

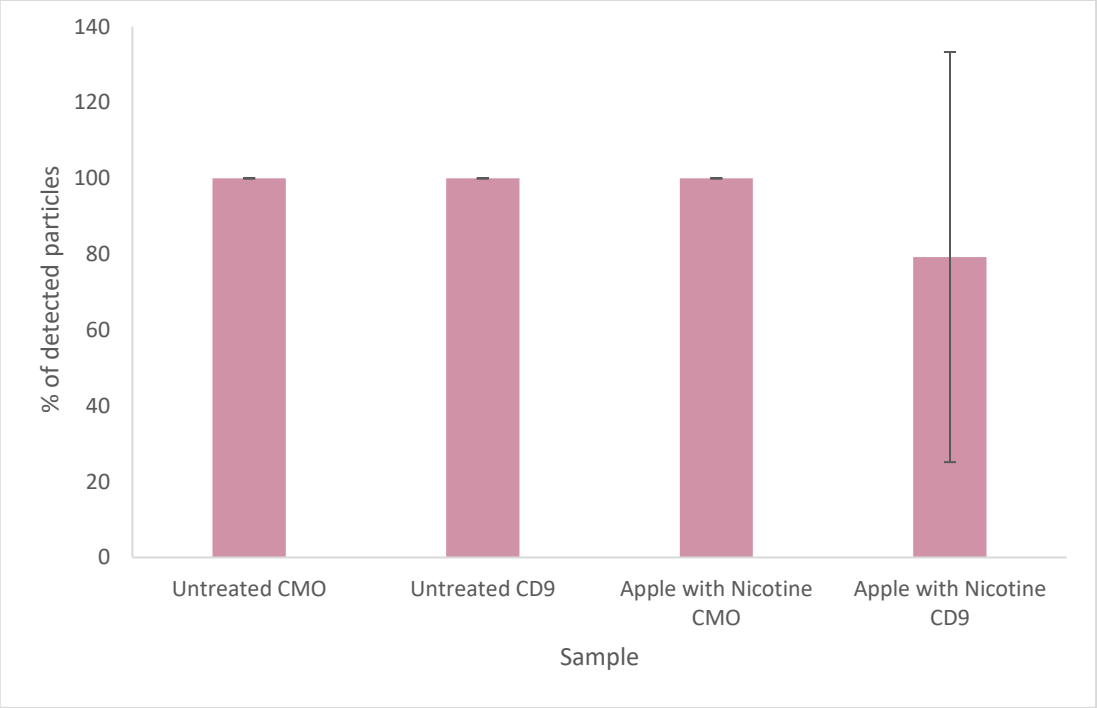

Figure 3.8 Detected untreated and apple e-liquid with nicotine treated A549 sEVs, detected with CMO and CD9 antibodies. Vesicle concentrations measured using the 520nm filter on the Zetaview Nanoparticle Tracking Analyzer. Percentages of CD9 positive vesicles shown were normalised by taking the CMO positive particles as 100% of lipid bound particles present in the sample, to evaluate the percentage of lipid bound particles that could be sEVs.

Untreated A549 sEV samples and A549 sEV samples treated with apple e-liquid containing nicotine produced a positive for CMO. Following normalisation to the CMO counterpart, 100% of untreated samples were positive for the sEV marker CD9, as demonstrated in **figure 3.8**. Results in **figure 3.8** also show that 79.23% of sEV sample from cells treated with apple e-liquid containing nicotine was positive for CD9, however this result had a high standard deviation not seen in the other samples. The detection of CD9 in the sample indicates the presence of sEVs in the samples.

Sample containing sEVs isolated from the untreated BEAS-2B were diluted according to NTA results, and fluorescently tagged for CMO and sEV markers CD9, CD81, and CD63.

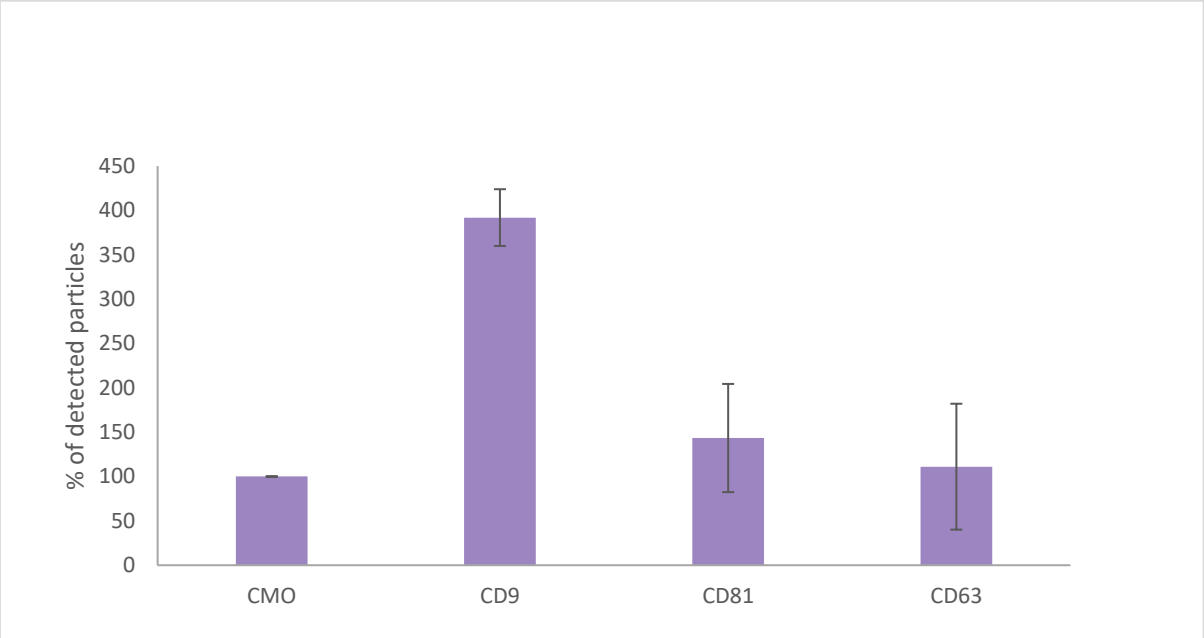

Figure 3.9 percentages of detected particles from untreated BEAS-2B tagged with CD9, CD81, and CD63, taking detected CMO as 100%. CMO was used to measure the total lipid bound particles found in the sample. Vesicles incubated with CMO dye read as lower concentrations than samples probed with fluorescently conjugated antibody, leading to higher percentages calculated when sample was normalised against CMO readings. Readings were taken from 3 samples.

Positive results were found for all three tetraspanin markers CD9, CD81, and CD63, with the most common marker being CD9, as demonstrated in **figure 3.9**. CMO in the BEAS-2B samples registered as being the lowest value. Due to the expected function of CMO, this result was unexpected, as all lipid bound particles should be detected using the dye. While tetraspanin markers were detected, the percentage of CD markers would be lower had CMO results been as expected. The positive results for the presence of tetraspanin proteins indicates the presence of sEVs in the BEAS-2B proteins.

3.2.4 Tetraspanin protein marker CD9 and negative control Calnexin were successfully identified in Western Blot

Tetraspanin protein CD9 was used as a positive marker to further confirm the presence of EVs in the samples produced from A549 and BEAS-2B cultures.

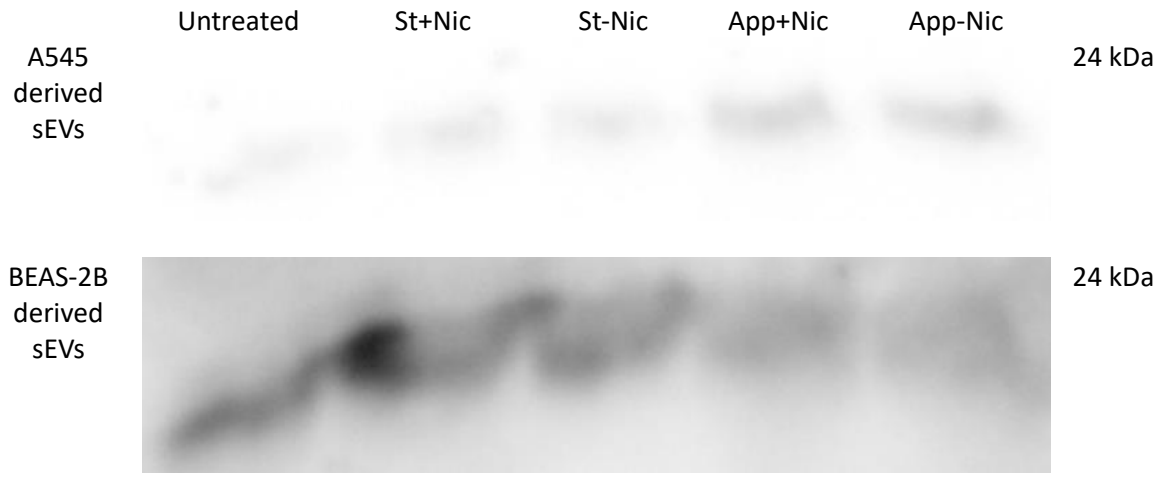

Figure 3.10. sEV samples isolated from 3D A549 and BEAS-2B used in western blots, and incubated with antibody for tetraspanin protein CD9. Samples obtained from untreated, strawberry flavoured e-liquid with nicotine treated, strawberry flavoured e-liquid without nicotine treated, apple e-liquid with nicotine treated, and apple e-liquid without nicotine treated cultures. Full blot images can be seen in **figure A.7** and **A.9** in the appendices.

Positive results for CD9 in A549 and BEAS-2B SEVs untreated, treated with St+Nic, treated with St-Nic, treated with App+Nic, and treated with App-Nic are present in **figure 3.10**. The blots incubated with CD9 antibodies showed a positive band at approximately 24kDa. This positive result indicated the presence of sEVs in all 5 samples from derived from each cell line. Further investigation using antibodies for CD63 were unsuccessful, the positive smeared bands at 30-60 kDa were unreliable. These blots are viable in **figure A.7** and **figure A.9**.

The intracellular endoplasmic reticulum marker protein calnexin was used as a negative control in the western blot for both sets of samples.

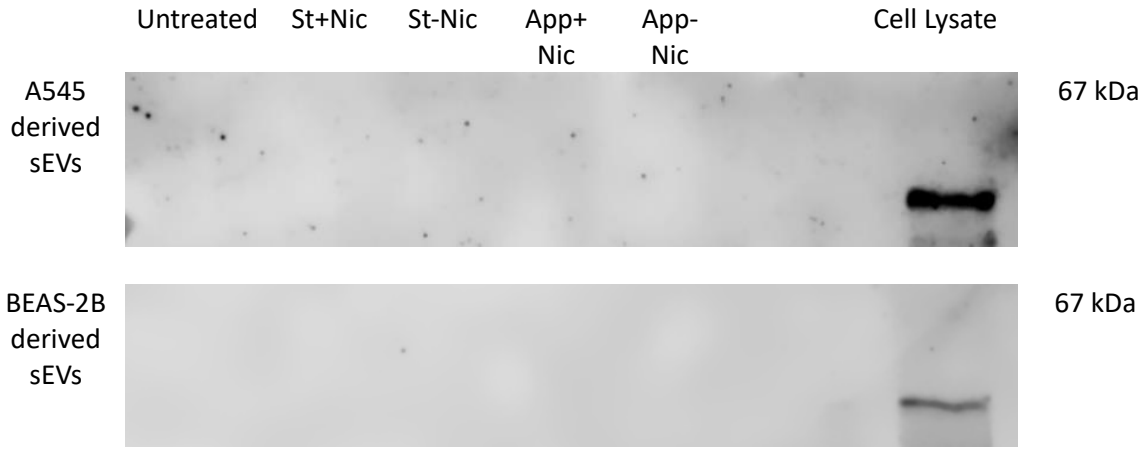

Figure 3.11 sEV samples isolated from 3D A549 and BEAS-2B ran in western blot and incubated with calnexin. Samples were isolated from untreated, strawberry flavoured e-liquid with nicotine treated, strawberry flavoured e-liquid without nicotine treated, apple e-liquid with nicotine treated, and apple e-liquid without nicotine treated 3D cultures. Full blot **figure A.11** and **A.12** in the appendices.

Figure 3.11 shows negative results for calnexin in the EV lanes; untreated, treated with St+Nic, treated with St-Nic, treated with App+Nic, and treated with App-Nic; with a positive result in the cell lysate lane at approximately 67kDa. This result helps confirm that the sEV sample was not contaminated with the cells the sample originated from, increasing confidence in the previous tetraspanin western blot results. Due to degradation of cell lysate sample additional bands do appear in the cell lysate lane (visible in full blot image found in the appendix), as a result this would not be considered with as much certainty as blots in **figure 3.10.**

3.3 Isolation and Expression of MicroRNA

3.3.1 Isolation

Concentrations of small RNA found in each sample was measured using a qubit, to confirm that there was enough small RNA in each sample to convert to cDNA.

Table 3.1 Concentrations of total RNA measured in ng/µl, isolated from sEV samples from A549 and Beas2B cell lines.

	Total RNA Concentration (ng/µl)	
Treatment	A549	BEAS-2B
Untreated	0.36	0.40
St+Nic	1.55	0.45
St-Nic	1.88	2.43
App+Nic	0.97	1.36
App-Nic	0.29	1.53

The concentration of total RNA isolated from sEV samples was measured to ng/µl. Results found were varied, and concentrations found do not appear to correlate with cell type or treatment type, further evaluated in **Figure 3.12**.

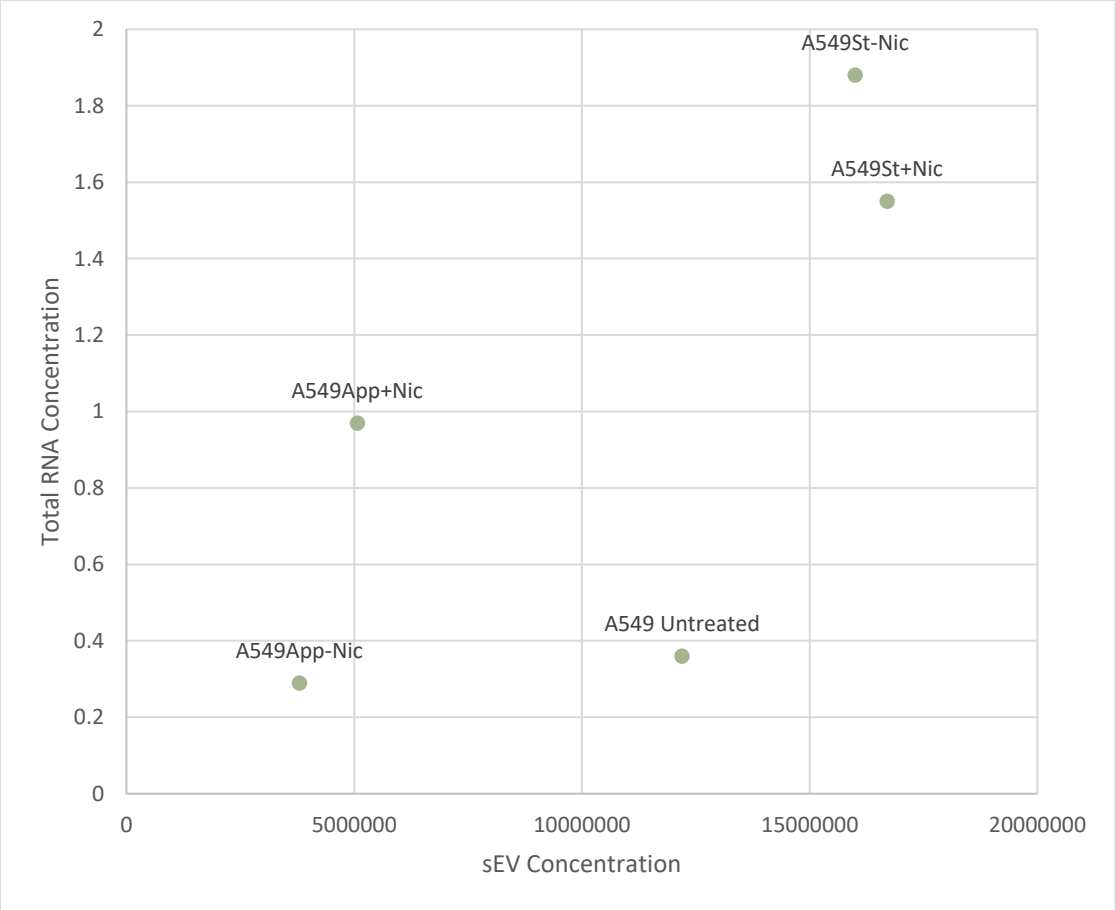

Figure 3.12 A scatter plot demonstrating the concentration of sEVs found in samples from all 5 A549 culture types plotted against the concentration of total RNA measured from those samples.

Concentrations of small RNA were plotted against the concentrations of the sEV samples to visualise correlation between the two. Corelation was not seen between the two factors in these samples. However, as total RNA was isolated from each sample, and 3 ng of total RNA was required from each 14 µl total sample, it was possible to convert to cDNA for further analysis.

3.3.2 Expression of MiR-410-5p and MiR-21-5p were measured using SYBR green real-time quantitative PCR

Following successful cDNA conversion, samples were tested for target microRNA using RT-qPCR. An MiRNA profile produced by Chinta (2022) in an unpublished doctoral thesis was used to select initial target miRNA, that were known to be dysregulated in lung diseases.

Table 3.2 Representative table of calculations used to obtain relative fold change of miR-410-5p

	Mean CT of Cel-miR-39	Mean CT of miR-410-5p	ΔCT	ΔΔ CT	2^-(ΔΔCT)
Untreated	33.25	33.37	0.12	0	
Treated with St+Nic	35.93	33.09	-2.84	-2.96333	7.80
Treated with St-Nic	34.73	32.55	-2.18	-2.3	4.92
Treated with App+Nic	31.84	32.47	0.633	0.51	0.70
Treated with App-Nic	29.58	33.1	3.52	3.40	0.09

A representative of the calculations used to obtain relative fold change of miRNA is shown in **table 3.2**, using values used to calculate the relative fold change of miR-410-5p in the sEVs derived from treated cultures of A549 compared to the sEVs derived from untreated cultures of A549. ΔCT values were established by normalising results against the CT values of cel-mir-39, while ΔΔ CT were established by comparing the treated results against the untreated result.

Expression fold change of mir-410-5p and miR-21-5p in treated A549 samples in comparison to untreated A549 samples can be seen **figure 3.13 (A) and (B)** respectively.

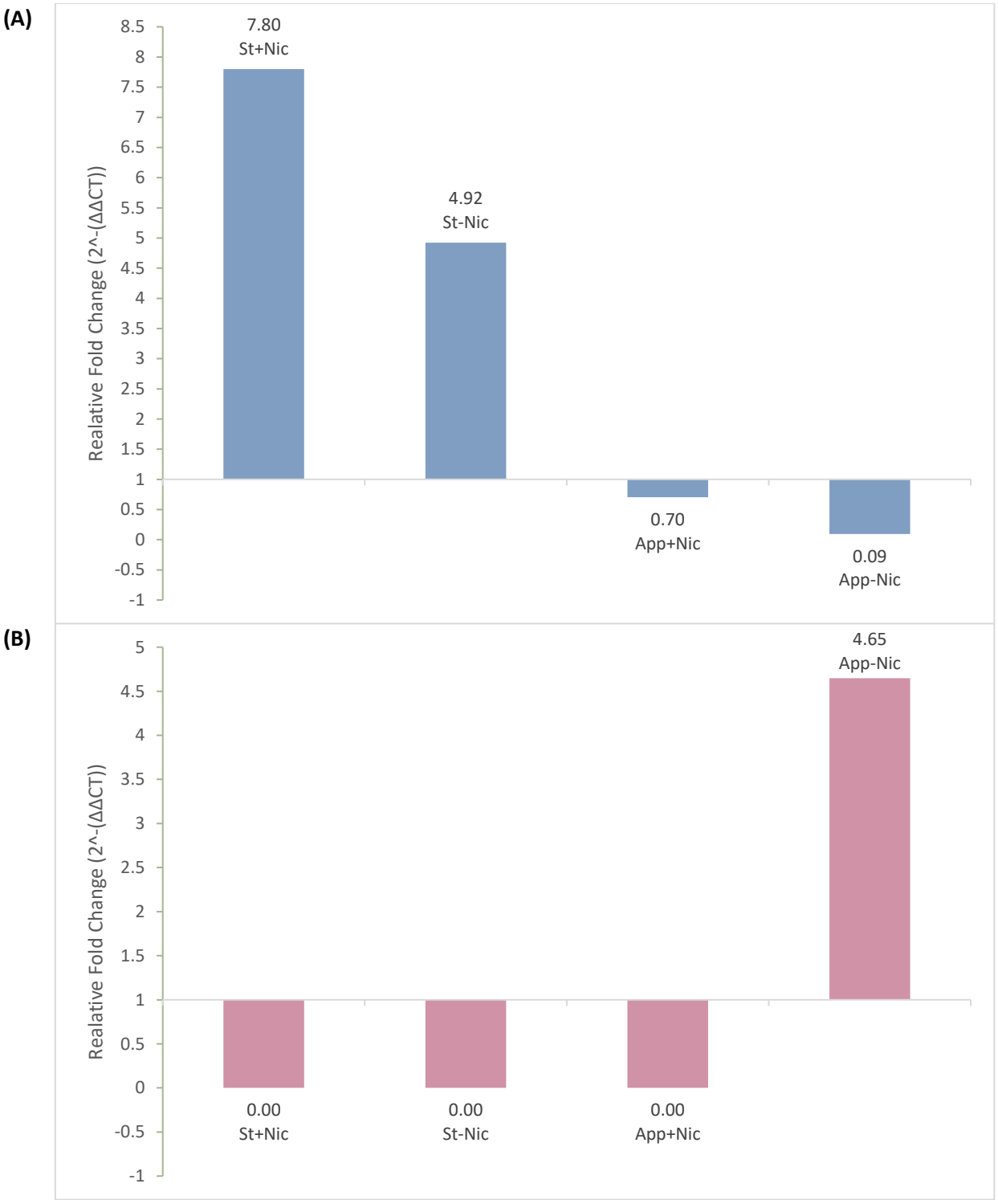

Figure 3.13 Relative fold change of (A) miR-410-5p miRNA and (B) miR-21-5p extracted from sEVs produced by 3D A549 cells treated with e-liquids compared to sEVs produced by untreated 3D A549 cells. Results were normalised using expression of Cel-miR-39-3p, and analysis was produced from triplicate results. With relative fold change from untreated 3D A549 sEV samples, results between 0.5 and 1.5 were not considered differentially expressed.

The target miRNA miR-410-5p was successfully found in each of the A549 samples, with varying expression levels as demonstrated in **figure 3.13 (A)**. When expression fold

changes were calculated from untreated expression levels, miRNA isolated from sEVs produced by cultures produced by strawberry e-liquid treated cultures showed upregulation in both cases, with samples treated with e-liquid containing nicotine showing higher expression at 7.80 than samples treated with e-liquid without nicotine at 4.92. MiRNA from samples treated with Apple flavoured e-liquids showed lower expression, however samples treated with apple containing nicotine would not be considered to be differentially expressed at 0.70, with samples treated with App-Nic would be considered downregulated at 0.09.

As demonstrated in **figure 3.13 (B)**, no reliable expression of miR-21-5p was found for samples treated with St+Nic, St-Nic, or apple flavoured e-liquid with nicotine. Samples treated with App-Nic showed an upregulated expression of miR-21-5p at a relative fold change of 4.65, when compared to the A549 untreated sample.

Previous work in the laboratory by Chinta (2022) found differential expression of miR-410-5p in sEV samples isolated from 2D cultures using the same sEV treatments, shown with a heatmap in **figure 3.14**.

	Relative Fold Change of MiR-410-5p Expression from Untreated Sample	
E-liquid Treatment	**2D A549 sEV Sample**	**3D A549 sEV Sample**
St+Nic	2.58	7.80
St-Nic	1.76	4.92
App+Nic	1.09	0.70
App-Nic	2.14	0.09

Figure 3.14 Heatmap of Relative Fold Change in MiR-410-5p Expression from Untreated to Treated sEV Samples From 2D and 3D cultures. Expression of miR- 410-5p was measured using qPCR on sEV samples extracted from untreated, strawberry flavoured e-liquid with nicotine treated, strawberry flavoured e-liquid without nicotine treated, apple e-liquid with nicotine treated, and apple e-liquid without nicotine cultures. This project produced results for sEV samples from 3D cell cultures, while previous work in the laboratory by Chinta (2022) produced results for sEV samples from 2D cultures. The relative fold change was calculated against expression in untreated samples, and normalised using expression of cel-mir-39-3p. Red indicates upregulated expression of >1.5, green indicates downregulated expression of <0.6, and black indicates no differential expression ranging 0.6-1.5

Relative fold change values varied between 2D and 3D samples, however upregulation of miR-410-5p expression was consistent in strawberry flavoured e-liquid treatments, both with and without nicotine content. Samples from cultures treated with apple flavoured e-liquid with nicotine both demonstrate no differential expression of the miRNA. Contrasting results were found between sEV samples form 2D and 3D cultures treated with App-Nic, samples from 2D cultures showed an upregulation of miR-420-5p at a relative fold change of 2.14. SEV samples from 3D cultures that had undergone the same treatment showed a downregulation *of miR-410-5p*, at a relative fold change of 0.09.

The sample produced as part of this project was used as part of two MSc projects for further analysis. Expression of miR-382-5p and miR-541-5p were tested for in the samples produce from A549 cultures. Results produced in these projects showed expression of these miRNA, but the CT values produced were inconsistent at times, and were not used to calculate relative fold change, however a table demonstrating detected miRNA is available in **Table A1.** Expression of miR-410-5p and miR-382-5p was expressed in all 3D A549 derived sEV samples. Untreated and App-Nic 3D A549 derived sEV samples showed expression of miR-21-5p, while all samples except the sEV sample derived from App+Nic treated culture showed expression of miR-541-5p.

Chapter 4

Discussion and Conclusions

Discussion

4.1 Summary of Project Aims

This project looked at the impact of E-liquids on small extracellular vesicles released from the three-dimensional cell culture, and the miRNA expressed in these vesicles. It aimed to establish a spheroid culture method suitable for A549 cells, derived from the alveolar basal cells of an individual with NSCLC, and BEAS-2B cells, derived from non-cancerous human bronchial epithelium tissue. Upon establishing this method, the project further aimed to investigate how treatment with e-liquids would impact the sEVs released from the cells. Finally, the project aimed to study how the treatment may impact the miRNA cargo found in sEVs. This project aimed to add to the wider body of knowledge surrounding sEVs and miRNA, as these may one day be utilised in diagnostic tests, amongst other clinical applications.

4.2 Different cell lines form different spheroid aggregates.

This project investigated 3D cultures and found that cancerous and non-cancerous cell lines grew in distinct patterns, with both models secreting EVs. While 2D cell cultures were the gold standard for research for many years, recent developments have led to the increased use of 3D cell cultures in research (Thippabhotla, Zhong, and He, 2019). 3D cultures show more accurate growth and metabolic rates, and are known to have drug metabolism and drug resistance more akin to *in vivo* than 2D cultures (Langhans, 2018). These factors make these cultures better models for studies such as these, where the effects of toxic substances are to be investigated.

The ethanol/poly-HEMA mix was found to be an effective method for preventing the adherence of cells to the flask, encouraging 3-dimensional formation, which corresponds to previous literature (Shaw et al., 2012). While the polymer did not always set smoothly, for the most part it was smooth and did not appear to impact the formation of 3D cells, which appeared consistent in all flasks. This suboptimal coating of polymer has previously been noted to occur when preparing low or non-adherent plates (Garcia-Alegria et. al., 2021).

This study observed that A549 spheroids formed large aggregates when cells were added on day 1 at two million and one million cells per 20 ml of media. While the aggregation of cells has been suggested to potentially mimic in-vivo more accurately due to cell-cell interactions, it was unknown if such large aggregates would impact the uptake of e-liquids and the production of sEVs in this project (Habanjar et. al., 2021). Studies have previously noted that the multicellular formation of spheroids can lead to uneven uptake of nutrients from surrounding media (Däster et. al., 2017). It would therefore be reasonable to hypothesise that this could impact e-liquid uptake in the same way, although further study would be required to confirm this. The A549 aggregates found here align with previous studies, that have noted that A549 cells in suspension have previously been found to form larger aggregates than BEAS2B cells (Kim et. al., 2017). To investigate the large aggregates often formed by this cell line, Min et. al. (2021) examined protrusions found on the cell surface of A549 spheroids. They identified that these protrusions interacted via the actin cytoskeleton and displayed exploratory coalescence. Investigation into the gene expression found that upregulation of aquaporin 3 contributed to this aggregation, and downregulating this gene prevented the aggregates from forming. Contrastingly, previous study by Choe et. al. (2018), did not appear to have experienced the same larger aggregates, despite their methods suggesting that cultures with seeding volumes of 8 x10^5 cells in 10cm plates were split into 2D and 3D cultures following 48 hours. The study used A549 cells seeded on poly-HEMA coated plates and produced microscope images 72 hours after seeding, in addition to florescence microscopy and SEM images. These images showed similar protruding cells on the aggregate surface to those seen in this study, but the aggregates were smaller and more separate.

In this study BEAS-2B spheroids grew in smaller, more uniform shapes, and did not appear to aggregate outside of these. The spheroids seen for BEAS-2B were similar to those previously seen in studies such as those by Baarsma et al. (2022). The smaller nature of the BEAS-2B aggregates in comparison to A549 could be down to the high proliferating nature of cancerous cells, which would allow A549 cells to grow and divide faster than BEAS-2B cells, giving A549 more opportunity to form the larger aggregates seen (Sung et. al., 2021).

In order to count the number of cells present in spheroid cultures, attempts were made to separate spheroids using the enzyme trypsin and manual separation using a needle, as recommended by Shaw et. al. (2012). This was unsuccessful, as many spheroids would not completely separate using this method, with aggregates visible under the microscope when cell counting was attempted. The multilayer structure of spheroids has previously been stated to prevent equal exposure to nutrients from the media, particularly the core cells which often receive less oxygen and growth factors (Barisam, 2018; Costa et. al., 2016). The same could apply to the exposure to the trypsin used, which could explain the remaining aggregates following attempts to separate. As a result of this, cells from spheroids could not be accurately counted or reused. The multilayer structure described by Barisam et al. (2018) could also impact the number of total cells exposed to e-liquid treatments.

Further study would be required to evaluate how results from large A549 aggregates would be comparable to cells such as BEAS-2B, which only formed smaller spherical aggregates. Therefore, a smaller confluency at a starting 500,000 cells per 20 ml of media was used for each cell line, to isolate EVs for further work in order to achieve more comparable spheroid structures. To allow for a sufficient sEV yield for characterisation, a total of 2 million cells was isolated from for each sample. These cell numbers were significantly lower than the number of cells possible to seed in 2D cultures, with the normal capacity of the T75 flasks estimated to be over 8 million (Thermo Fisher, 2023). Many previous spheroid studies using commercial ultra-low products or poly-HEMA methods utilise plates such as 96-well plates with lower cell numbers and media volume, rather than the T-75 flasks utilised in this study (Breslin and O'Driscoll, 2016; Choe et al., 2018). When investigating HCC1954 cells Breslin and O'Driscoll (2016) seeded at a density of 3 × 103 cells/150 µL, while Choe et al. (2018) seeded at 1000 cells per well in 100 µL. These studies showed round, uniform spheroids. As sEV populations are thought to be heterogenous and characterisation such as western blot requires sufficient protein content to be accurate, a larger yield of sEVs allows for more accurate analysis of sEV and sEV cargo (Fathi et al., 2023). Quantification of total RNA performed in this project by Qubit analysis showed low RNA content in some samples, with around 10 µL of the available 14 µL required for the optimised amount of 3 ng required for cDNA conversion.

Lower available concentration of RNA would've made analysis of miRNA cargo difficult in this project. Low yields of EV derived RNA are known challenge in the field (Jenjaroenpun et al, 2013; De Souza et al, 2022). The use of smaller well plates for projects such as those performed previously would not be efficient, due to the bulking of EV sample that would be required for sufficient yield for characterisation in this project. The 2 million total starting quantity of cells per sample used in this project was the maximum it was possible to use for the sEV isolation method at one time, due to the observed large aggregates at higher confluency and limitations in the amount of sample media that may be added to the exo-spin columns needed for sEV isolation (Cell Guidance, Cambridge, UK).

Outside of the time constraints of this project, further work could be completed to establish how the aggregates formed by A549 cells would affect the results produced by EV samples, if the cell-to-cell interactions between cells in large aggregates would better mimic condition in vivo, and how to then make the two cell culture types more comparable. Further work could also be done to establish a method for counting cells in spheroid form, and to establish how the physiology of individual cells from established 3D cultures differs from newly suspended cells, for purposes of reusing untreated cells in the laboratory. Other methods of 3D culture that allowed for media to be collected, such as scaffold-free magnetism techniques and hydrogel scaffolds, could also be trialled (Jongpaiboonkit et al., 2008; Haisler et al., 2013; Rudinger et al., 2015). Like scaffold free spheroid cultures, other 3D culture methods have a range of advantages and disadvantages that could impact results found (Temple et. al., 2022). While the poly-HEMA methods used in this study have previously been suggested to be more cost effective and reproducible than some scaffolded methods available, trialling other methods could provide a solution to the challenges in aggregate size and EV yield experienced in this study (Breslin and O'Driscoll, 2016; Temple et. al., 2022).

This study could further benefit from expanding the range of cell types used, to provide comparison to the two used, and establish which factors may impact results. Other cancerous lung epithelial lines include H2126, isolated from the NSCLC of a 65-year-old male; and H1975, isolated from the NSCLC of a female non-smoker (ATCC, 2023; ATCC, 2023). An alternative non-cancerous bronchial epithelial cell line could be HBEC3-KT, isolated from a 65-year-old female (ATCC, 2022). The information available regarding the

individuals from which cell lines originate can vary. The use more recent clinical samples, or samples with more in-depth characteristics could also improve the reliability of results and analysis, as information profiles for each sample could be used to evaluate if specific characteristics impacted factors such as spheroid aggregation.

4.3 Characterisation methods showed varying degrees of success for small extracellular vesicles

One of the aims of this study was to evaluate the impacts of e-liquids on the small extracellular vesicles released from the 3D culture of human lung cells. Before any analysis can begin, the presence of sEVs must be confirmed, to confirm that analysis is specific to sEVs and sEV cargo. According to MISEV 2018, multiple methods of characterisation should be used to confirm presence of sEVs within a sample. These methods may be used to confirm a size of 50-200 nm, a cup-shaped appearance, and the presence of appropriate surface markers. Confirmation of appropriate cargo, such as miRNA may also be used (Théry et. al., 2018).

In accordance with MISEV guidelines, techniques utilised in this study were TEM, NTA, fNTA, and Western Blot (Théry et. al., 2018). The TEM technique is useful in studies such as this to establish whether the particles are in the desired size range of 50-200 nm, and if they exhibit the correct “cup-shaped” morphology for sEVs (Théry et. al., 2018). NTA tracks scattered light of particles moving in Brownian motion to establish size and concentration, so can also be used to establish if particles are within the desired size range (Bai et al., 2017). FNTA detects fluorescently tagged proteins on the sEV surface to confirm presence of surface protein markers. Protein markers can also be detected using western blot, which may also be used to establish if there is any cell contamination, using proteins not found in sEVs such as calnexin as a control (Théry et. al., 2018).

Morphological characteristics such as size and shape can be evaluated using techniques such as TEM, with NTA used to further confirm size range of particles. Images taken by TEM of untreated samples from A549 and BEAS2B cell lines showed particles in the correct size range for sEVs of 50-200 nm, and particles showed the correct cup-shaped structure consistent with sEVs (Théry et. al., 2018). Particles demonstrating unregular shape (visible in the appendices) may indicate some degradation of sample or other

particle types such as microvesicles or apoptotic vesicles, which may present within the same size range (Dou et. al., 2020). Size ranges measured in NTA confirmed that many particles in the sample measured within the 50-200 nm size range, in line with observations from TEM and increasing evidence of the presence of sEVs (Théry et. al., 2018). Some particles measured outside of the desired size could be due to aggregation of sample or larger EVs (Dou et. al., 2020). As NTA can only detect concentration and size within a sample, it cannot differentiate between EVs and potential contaminants such as proteins or lipids. This leads to a requirement to further confirm the presence of EVs by the presence of known surface protein (Bai et al., 2017; Théry et. al., 2018).

Both fNTA and Western Blot results show presence of tetraspanin sEV markers CD9 and CD63, in line with MISEV guidelines (Théry et. al., 2018). These tetraspanin proteins have previously been shown to be present on the surface of sEVs and can help differentiate from other EVs of similar size (Kowal et.al., 2016). Results for fNTA show presence of CD9 in all A549 samples, and presence of CD9, CD63 and CD81 in BEAS-2B samples. Unexpected readings for the CMO used in the BEAS-2B samples meant that percentages of positive particles compared to all lipid-membrane bound particles could not be established. Comparison of scatter results to those measured under the 520 nm filter in the same sample showed significant differences, with scatter being significantly higher. This suggests that the majority of the vesicles did not show fluorescence from the CMO membrane dye or antibody probes. This could indicate that many of the particles measured in scatter were not lipid bound particles, but could be down to other elements of the sample such as PBS salts. Another explanation could be degradation or permeability of the membrane, preventing membrane dyes from labelling the vesicles (Kilgore, Dolman, and Davidson, 2014). Excessive photobleaching or insufficient fluorescent labelling of particles could also prevent vesicles from being detected under the 520 nm filter (Harrison, Gardener, and Sargent, 2013).

Western blot results showed positive results in treated and untreated samples from both A549 and BEAS-2B cell lines for CD9, however bands were not as clear or defined as would be ideal, suggesting that further optimisation would be required. CD63 did show smearing at the appropriate weight, but bands were unclear and would need to be more defined to consider these results. The negative control of calnexin, recommended for use

in MISEV 2018, only showed in the control cell lysate lane (Théry et al., 2018). This result is less reliable than others due to the possible degradation of the cell lysate sample in both blots, resulting in some smearing in the cell lysate lane, however the positive band is present in both blots. Untreated and treated sEV samples showed no results for calnexin, suggesting that the isolation method used was successful in producing samples free from cell contamination. Troubleshooting was required for western blot experiments due to differences of contrast seen between protein marker, sEV samples and cell lysate, as seen in full blot figures in the appendices. Further work to establish a more suitable protocol could allow for more suitable images to be produced. Guidelines also recommend the use of a cytosolic protein marker to confirm the presence of sEVs (Théry et al., 2018). Time constraints of this project did not allow for this, but further work would help confirm the sEV presence with more certainty. Other further work to increase confidence in these results could be performed with other positive markers such as CD81, CD82, and Tsg101 (Théry et al., 2018).

Freeze thaw cycles are known to cause degradation in biological samples such as sEV samples and proteins (Kueltzo et al., 2008; Sivanantham and Yin, 2022). While efforts were made to avoid excessive freeze-thaw to samples during this project, time constraints and recommended storage of -80°C for sEV samples may have caused some degradation in sample prior to fNTA and western blot experiments (Sivanantham and Yin, 2022).

Concentrations of sEVs in the samples measured in NTA showed no significant differences. This contrasts with previous research that suggests that cancerous cells produce more sEVs than healthy cells. Hikita et.al. (2019) found evidence that suggested that the membrane associated tyrine kinase c-Src, activated during carcinogenesis, could interact with the protein Alix. This interaction was found to activate the ESCRT-dependent pathway, increasing formation of ILVs, and subsequently sEVs. A small study of 17 participants found that the endothelial and platelet derived EVs drastically increased 4 hours following inhalation of e-liquid vapour for 30 minutes, suggesting that he use of e-cigarettes increased the production of EVs (Mobarrez et. al. 2020). This was not something indicated in the NTA results measured here. Further research could be done to validate concentration of sEVs produced from the 3D cultures, as well as to establish if

differences in sEV concentrations become significantly different over different incubation periods.

A further method to validate results and tackle the limitations of the characterisation methods used in this study could be the use of flow cytometry. While flow cytometry is not available everywhere, it does give further opportunity to measure size range of samples to validate NTA, and can detect the presence or absence of fluorescent antibodies to validate fNTA and western blot (Maia et al., 2020).

As recommended by MISEV guidelines, multiple methods of characterisation were used to confirm the presence of sEVs (Théry et. al., 2018). Results from all methods of characterisation used in this project indicated positive results for sEVs in the samples, suggesting success in isolating sEVs from 3D cell culture media. Previous studies have suggested that the secretion of EVs from 3D cell cultures is more accurate to that demonstrated in-vivo than in 2D cultures (Thippabhotla, Zhong, He, 2019). The sEVs isolated in this project should therefore be more accurate to those produced in-vivo, and a good model to use to identify sEV biomarkers such as miRNA. Further work could be done to validate results found using NTA, as no significant differences were found in cancerous and non-cancerous cell lines, as well as samples treated with e-liquids, conflicting with prior studies.

4.4 MicroRNA expression changed following the introduction of e-liquids to spheroid cultures

This study found that small RNA was consistently expressed in sEVs from 3D cell culture of A549 and BEAS-2B cell lines. Concentration of total RNA in each sample varied, and did not correspond to the variety in concentrations of sEVs. This could be explained by the heterogeneity of sEV populations and their cargo as described by Wang et al. (2021). Regardless, the amount of total RNA available for cDNA conversion was sufficient for further analysis in accordance to Quantimir protocols and optimisation.

Circulating miRNA has proven to have great potential in diagnostics and monitoring of diseases, due to the dysregulation of many miRNA in diseases, the ease of retrieval from patients in comparison to more invasive methods such as biopsy, and the relative stability

of miRNA once retrieved (Matsuzaki & Ochiya, 2017; Li et. al., 2011; Matias-Garcia et. al., 2020).

When tested for expression of miRNA mir-410-5p, samples from A549 cultures were all found to express the miRNA, with varying levels of expression. This is promising result for the recommendation of sEVs from 3D culture as a research tool, as it proves that this study was successful in isolating miRNA in its small RNA sample, and these methods could be a useful tool in further study. Mir-410 has previously been suggested to induce cell proliferation in NSCLC, and has been noted to be over expressed in NSCLC cells and tissues (Li et al., 2015). The relative fold change of miRNA expression from sEVs released from treated cultures and untreated cultures was compared, with cultures treated with strawberry flavoured e-liquids showing upregulated sEV mir-410-5p expression compared to the untreated culture. Cultures treated with apple flavoured e-liquids showed lower expression of mir-410-5p from the sEVs produced, though results from App+Nic would not be considered to be differentially expressed. A previous study from this laboratory by Chinta (2022) evaluated sEV miRNA from treated 2D cell cultures, using the same brand of e-liquid as this study. The results of this study correlated with the upregulation of sEV mir-410-5p in cultures treated with strawberry e-liquid, although the upregulation found in this study was much higher. Results found by Chinta also showed that Apple flavoured e-liquid treatment did not show a differential change in mir-410-5p, however the results of these two studies showed differing results from cultures treated with apple flavoured e-liquid, with this study finding downregulation compared to the upregulation found in the study by Chinta (Chinta, 2022).

Interestingly, results of mir-410-5p expression in this study were higher in sEVs from cultures treated with e-liquids with nicotine, than their counterparts treated with e-liquids without nicotine. This could indicate that nicotine had an entirely separate effect on the expression of the target miRNA. Outside of this project, additional work to test the effects of nicotine on the sEV miRNA from 3D cultures could be carried out to explore this, and establish if mir-410-5p expression is increased when cultures are treated with nicotine.

The miRNA miR-21 is commonly suggested as a diagnostic biomarker, despite the challenges or misinterpretation that could be caused by the lack of specificity of the

miRNA to diseases (Abue et al., 2015; Porzycki et al., 2018). MiR-21 is often overexpressed in cancers, and has been linked to cell proliferation (Volinia et al., 2010; Bai et al., 2022). This study measured the expression of miR-21 from A549 sEVs as part of the initial expression profile, with samples treated with App-Nic showing upregulation from the untreated sample. Other treated samples did not show expression of miR-21. Previous study using 2D cultures by Chinta found expression of miR-21 in all treated samples, and lower expression of miR-21 in the sample from cultures treated with App-Nic which was not statistically significant (Chinta, 2022). Previous study by Singh et al. (2020) suggested that expression of mir-21-5p was downregulated in samples from e-cigarette users. However, the sample size of this study is unknown, and previous study has identified that other factors such as age can impact the expression of mir-21 (Ameling et al., 2015).

A lack of further literature concerning e-liquids and miRNA mir-21 and mir-410 leads to a need for further study to draw more reliable conclusions.

Additional work was carried out in MSc projects linked to this project using miR-382 and miR-541. The studies found expression of miR-382 in all A549 derived sEV samples, and expression of miR-541 in all A549 derived sEV samples except the sample except the sample treated with the apple flavoured e-liquid containing nicotine. In Previous work by Chinta (2022), all samples showed expression of miR-382 as was found in samples produced in this study. Expression of miR-541 was found in all samples except the sample from cultures treated with strawberry treated e-liquid without nicotine. Further work could be done to validate the miRNA results found in this study and establish reliable expression levels of miRNA.

The differential expression seen between samples treated with e-liquids and untreated samples suggest that the use of e-liquids did cause differences in the miRNA expressed in the sEVs produced in the different 3D cultures. This correlates with previous research that found that the use of these products do effect the levels of expression, and help indicate that the use of 3D culture could be a valuable tool in researching the miRNA cargo of sEVs (Chinta, 2022; Singh et al. 2020).

4.5 Future work and recommendations

Further work could be done to analyse the miRNA that has been proven to be successfully extracted during his study. By creating a profile of miRNA expression levels, miRNA could be evaluated for differences in expression levels between sEVs derived from cancerous and non-cancerous cells treated with different types of e-liquids. This in turn could be used to identify target miRNA for further research in biomarkers for lung damage such as lung cancer and EVALI. Previous studies have evaluated the expression of over 130 miRNA in lung cancer (Malik et. al., 2019). This establishes that there is much potential work to do to explore how many of these are impacted by the use of e-liquids.

Following identification of target miRNA, further work could be carried out to investigate their use as biomarkers in a clinical setting. There are many challenges to overcome in this area, including specificity of miRNA to diseases, and the heterogeneity of miRNA profiles between different physiological profiles (Abue et. al., 2015; Porzycki et. al., 2018; Asare et. al., 2022). A study by Ameling et al. (2015) identified 7 miRNA that were sex related, 12 that were associated to the individuals age, and 19 that were associated with BMI. This indicates that variations in expression of miRNA would have to be evaluated in a range of individuals in order to establish reliable biomarkers. Sample type can also have an impact on whether some miRNA are upregulated or down regulated, as shown by Mompeón et. al (2020). Evaluating target miRNA identified for biomarkers in different sample types could help further establish which could be used as biomarkers, or what sample type is recommended in clinical use.

Consideration should also be given to the impacts of e-liquid use on expression levels of biomarkers for other diseases. The research field of circulating biomarkers is ever-growing, with potential miRNA biomarkers being suggested for a range of diseases, some going to clinical trial (Clinicaltrial.gov NCT04772495, 2021; Clinicaltrials.gov NCT06258824, 2024). As evidence in this study and others suggests that e-liquids can impact a range of miRNA expression levels, these impacts should be considered when testing for biomarker expression levels in the increasing number of e-cigarette users (ONS, 2022). Failure to consider impacts such as these could potentially result in false test results, leading to an increase in diagnosis times, distress in patients, and delays in key treatments (Brocken et. al., 2015). The 3D culture and sEV isolation methods trialled in

this study showed promise, and should be more accurate to in-vivo than 2D models typically used in the lab (Thippabhotla, Zhong, and He, 2019). These methods could be repeated using other cell types treated with e-liquids, to help establish considerations needed for e-cigarette users who could receive biomarker testing. Previous study has also identified that alcohol can impact the expression levels miRNA (Tseng et. al., 2019). In the UK 57% of the population aged 16 and over drink alcohol (ONS, 2018). With such a high proportion of the population potentially impacted, methods used in this study could also be used to investigate how miRNA expression profiles for different diseases could be impacted by alcohol consumption.

Other challenges in the research of the impact of e-liquids in particular is the variety of e-liquids available, the inconsistency of e-liquid contents, and the potential for the contents listed to be untrue in some cases (Hutzler et.al, 2014; Kaur et al., 2018). Wider study with a larger variety of e-liquids than those used in this study, could be used to validate any results found and establish how sEVs and miRNA from 3D cultures are affected by other e-liquid types. This in turn could be used as a method to establish how any target miRNA identified as potential biomarkers are impacted by the use of these e-liquids.

While the use of 3D cultures is proven to be a better model to in vivo than 2D culture in many areas, organoid cultures and patient tissue samples may provide a better insight again into the production and expression of sEVs in vivo, particularly following treatments (Fatehullah, Tan, and Barker, 2016; Handa et al., 2021). These methods do have their own limitations, such as cost, availability, and additional ethical concerns, but could be used to validate the results found in this study and other preliminary study (*Human Tissue Act*, 2004; Huang et. al., 2021).

4.6 Limitations of study methodology

The viability of cells treated with e-liquids was not evaluated in this study due to failure in initial attempts to adequately separate spheroids, and the volume of media found to be needed for spheroid cultures. Previous investigation by Chinta (2022) suggested that e-liquids did have an impact on cell viability of A549 and BEAS-2B cells. Interestingly, apple flavoured e-liquids were suggested to increase cell viability in both cell lines, whereas impacts of strawberry e-liquid varied between treatment length and nicotine content. It

was unclear which component could be causing this variation, and further investigation would be warranted. To investigate this in spheroid cultures, future work to establish a suitable method cell counting in spheroids or for the use of MTT assays could allow for this to occur and give further indication of the impact of these e-liquids.

Another limitation of this study was the methods of e-liquid treatment to cells. In-vivo, those who use e-cigarettes would inhale the vapours of e-liquids created by the heating mechanism in the e-cigarette (Sundar et. al., 2016). The mechanisms of inhaling substance from an e-cigarette would be difficult to mimic in cell culture. The heating element of an e-cigarette could have additional risks to cells, such as the release of ketene from vitamin-e acetate which is known to be toxic (Wu and O' Shea, 2020).

Many e-cigarette users use the products frequently, and for a much longer period of time, than the cells were exposed to the e-liquids for in this study, with 4.9% of responders to an ONS smoking survey reporting that they used e-cigarettes daily (ONS, 2022). It would have been interesting to establish if different lengths of treatment would have had an impact on the sEVs produced, and subsequently the miRNA expression levels from these cells. Studies to investigate this could be carried out over a number of days or weeks, and cultures could receive multiple doses, to mimic repeated use of e-cigarettes. As further work is required to understand cell viability under treatment with e-liquids, this and work to optimise dosage would have to be carried out to establish a protocol (Chinta, 2022).

Delays caused by the Covid-19 pandemic prevented the completion of work initially planned for this study. Further work into the expression levels of miRNA found in all samples would provide better insight into useful biomarkers for diagnostics and monitoring of lung diseases.

4.7 Conclusions

The first aim of this study was to evaluate the use of three-dimensional cell culture and the small extracellular vesicles released, to establish if this could be a useful tool for identifying biomarkers that could one day be used to develop non-invasive testing methods for lung disease and damage. The aim was to evaluate how the sEVs released from these cultures was impacted following treatment with e-liquids. As instances of lung damage potentially related the use of e-liquids and these products are becoming

increasingly popular, establishing how these change the release of small extracellular vesicles in cell culture, and the microRNA found within, is an important step to help identify novel biomarkers to monitor lung disease and damage (Chiam et al., 2020; Zulfiqar, Sankari, and Rahman, 2022; ONS, 2022).

Previous research has shown that while there many challenges to be considered for the use of sEVs and miRNA as biomarkers, they have the potential to be an incredibly useful tool that could greatly improve on current methods for diagnosis of lung damage and disease. There is much to still find regarding the extent of possible damage caused by e-liquids, but as their popularity is ever-increasing in healthy individuals, those who have used them as a tool for smoking cessation to avoid the complex health issues caused by traditional smoking, and those who have already been diagnosed with the often smoking related lung cancer, finding suitable methods to identify suitable biomarkers is an important step to improving diagnosis and increasing recovery chances.

This study was able to establish a method for producing 3D culture of A549 and BEAS-2B cells, suitable for isolating small extracellular vesicles produced. Further work could be carried out to establish if other forms of 3D culture would more accurately mimic in-vivo conditions, particularly for treatment for toxic substances. Results of this study established that sEVs were produced by 3D cultures of A549 and BEAS-2B, and treatment with e-liquids with and without nicotine did not appear to have significant impact on size or concentration of sEVs produced. Small RNA was successfully isolated from all samples, with expression of miR-410-5p found in all A549 samples. These samples showed variation in expression, with differential expression established between 3 of the 4 samples from treated 3D A549 cultures and the untreated 3D A549 culture. Expression levels of miR-21 found in A549 samples need further validation, as does results produced from miR-382 and miR-541. These results present the possibility of future research to establish how expression levels of other miRNA change between samples. Establishing how miRNA levels vary between sEVs derived from healthy and cancerous cells, and following usage of the increasingly popular e-liquids, could provide the key to discovering much needed minimally invasive diagnostic methods for lung damage and disease, as well as to indicate e-liquid specific damage.

While work still needs to be done to validate some of the results in this study and analyse additional miRNA content, the initial findings suggest that the use of e-liquids does impact the miRNA cargo of sEVs, and that 3D cultures as a method to study these impacts could be a valuable tool to contribute to the establishment of effective biomarkers.

References

Abd-El-Fattah, A. A., Sadik, N. A. H., Shaker, O. G., & Aboulftouh, M. L. (2013). Differential microRNAs expression in serum of patients with lung cancer, pulmonary tuberculosis, and pneumonia. *Cell biochemistry and biophysics*, *67*, 875-884.

Abue, M., Yokoyama, M., Shibuya, R., Tamai, K., Yamaguchi, K., Sato, I., ... & Satoh, K. (2015). Circulating miR-483-3p and miR-21 is highly expressed in plasma of pancreatic cancer. *International journal of oncology*, *46*(2), 539-547.

Action on Smoking and Health (ASH). (2022). Use of e-cigarettes (vapes) among young people in Great Britain. https://ash.org.uk/uploads/Use-of-e-cigarettes-among-young-people-in-Great-Britain-2022.pdf

Altuvia, Y., Landgraf, P., Lithwick, G., Elefant, N., Pfeffer, S., Aravin, A., Brownstein, M. J., Tuschl, T., & Margalit, H. (2005). Clustering and conservation patterns of human microRNAs. *Nucleic acids research*, *33*(8), 2697–2706. https://doi.org/10.1093/nar/gki567

Amaral, R. L., Miranda, M., Marcato, P. D., & Swiech, K. (2017). Comparative analysis of 3D bladder tumor spheroids obtained by forced floating and hanging drop methods for drug screening. *Frontiers in physiology*, *8*, 605.

Ameling, S., Kacprowski, T., Chilukoti, R.K., Malsch, C., Liebscher, V., Suhre, K., Pietzner, M., Friedrich, N., Homuth, G., Hammer, E. and Völker, U., 2015. Associations of circulating plasma microRNAs with age, body mass index and sex in a population-based study. *BMC medical genomics*, *8*(1), pp.1-9.

American Type Culture Collection. (2022). A549 Product Sheet. https://www.atcc.org/api/pdf/product-sheet?id=CCL-185

American Type Culture Collection. (2022). HBEC3-KT Product Sheet. https://www.atcc.org/products/crl-4051

American Type Culture Collection. (2022). Non-Small Cell Lung Cancer p53 Hotspot Mutation Cell Panel. https://www.atcc.org/products/tcp-2030

American Type Culture Collection. (2023). NCI-H1975 [H-1975, H1975] Product Sheet. https://www.atcc.org/products/crl-5908

American Type Culture Collection. (2023). NCI-H2126 [H2126] Product Sheet. https://www.atcc.org/products/ccl-256

American Type Culture Collection. (N.D.). BEAS-2B Product Sheet

Andreu, Z., & Yáñez-Mó, M. (2014). Tetraspanins in extracellular vesicle formation and function. *Frontiers in immunology*, *5*, 442.

Asare, A., Yao, H., Lara, O. D., Wang, Y., Zhang, L., & Sood, A. K. (2022). Race-associated molecular changes in gynecologic malignancies. *Cancer Research Communications*, *2*(2), 99-109.

Baarsma, H. A., Van der Veen, C. H. T. J., Lobee, D., Mones, N., Oosterhout, E., Cattani-Cavalieri, I., & Schmidt, M. (2022). Epithelial 3D-spheroids as a tool to study air pollutant-induced lung pathology. *SLAS discovery : advancing life sciences R & D*, *27*(3), 185–190.

Bai, J., Shi, Z., Wang, S., Pan, H., & Zhang, T. (2022). MiR-21 and let-7 cooperation in the regulation of lung cancer. *Frontiers in Oncology*, *12*, 950043.

Bai, K., Barnett, G. V., Kar, S. R., & Das, T. K. (2017). Interference from proteins and surfactants on particle size distributions measured by nanoparticle tracking analysis (NTA). *Pharmaceutical research*, *34*, 800-808.

Banks, E., Yazidjoglou, A., Brown, S., Nguyen, M., Martin, M., Beckwith, K., ... & Joshy, G. (2022). Electronic cigarettes and health outcomes: systematic review of global evidence.

Barisam, M., Saidi, M. S., Kashaninejad, N., & Nguyen, N. T. (2018). Prediction of necrotic core and hypoxic zone of multicellular spheroids in a microbioreactor with a U-shaped barrier. *Micromachines*, *9*(3), 94.

Bartel D. P. (2004). MicroRNAs: genomics, biogenesis, mechanism, and function. *Cell*, *116*(2), 281–297. https://doi.org/10.1016/s0092-8674(04)00045-5

Booij, T. H., Price, L. S., & Danen, E. H. (2019). 3D cell-based assays for drug screens: challenges in imaging, image analysis, and high-content analysis. *SLAS Discovery: Advancing Life Sciences R&D*, *24*(6), 615-627.

Bray, F., Laversanne, M., Weiderpass, E., & Soerjomataram, I. (2021). The ever-increasing importance of cancer as a leading cause of premature death worldwide. *Cancer*.

Breslin, S., & O'Driscoll, L. (2016). The relevance of using 3D cell cultures, in addition to 2D monolayer cultures, when evaluating breast cancer drug sensitivity and resistance. *Oncotarget*, *7*(29), 45745–45756. https://doi.org/10.18632/oncotarget.9935

Brocken, P., van der Heijden, E. H., Oud, K. T., Bootsma, G., Groen, H. J., Donders, A. R. T., ... & Prins, J. B. (2015). Distress in suspected lung cancer patients following rapid and standard diagnostic programs: a prospective observational study. *Psycho-Oncology*, *24*(4), 433-441.

Brown, K. F., Rumgay, H., Dunlop, C., Ryan, M., Quartly, F., Cox, A., Deas, A., Elliss-Brookes, L., Gavin, A., Hounsome, L., Huws, D., Ormiston-Smith, N., Shelton, J., White, C., & Parkin, D. M. (2018). The fraction of cancer attributable to modifiable risk factors in England, Wales, Scotland, Northern Ireland, and the United Kingdom in 2015. British journal of cancer, 118(8), 1130–1141.

Cancer Research UK. (2018). Cancer Statistics. https://www.cancerresearchuk.org/health-professional/cancer-statistics/statistics-by-cancer-type/lung-cancer/mortality. Accessed March 2023

Chiam, K., Mayne, G. C., Wang, T., Watson, D. I., Irvine, T. S., Bright, T., Smith, L. T., Ball, I. A., Bowen, J. M., Keefe, D. M., Thompson, S. K., & Hussey, D. J. (2020). Serum outperforms plasma in small extracellular vesicle microRNA biomarker studies of adenocarcinoma of the esophagus. *World journal of gastroenterology*, *26*(20), 2570–2583. https://doi.org/10.3748/wjg.v26.i20.2570

Chiba, M., Kubota, S., Sato, K., & Monzen, S. (2018). Exosomes released from pancreatic cancer cells enhance angiogenic activities via dynamin-dependent endocytosis in endothelial cells in vitro. *Scientific reports*, *8*(1), 1-9.

Chinta, S. (2022). *Evaluation of small extracellular vesicular microRNAs as biomarkers for exposure of nicotine and E-liquids on human lung cells* [Unpublished Doctoral Thesis]. University of Salford.

Choe, C., Kim, H., Min, S., Park, S., Seo, J., & Roh, S. (2018). SOX2, a stemness gene, induces progression of NSCLC A549 cells toward anchorage-independent growth and chemoresistance to vinblastine. *OncoTargets and therapy*, 6197-6207.

Clinicaltrials.gov (2021) miRNA Biomarkers in Multiple Sclerosis. https://classic.clinicaltrials.gov/ct2/show/NCT04772495?term=NCT04772495&draw=2&rank=1

Clinicaltrials.gov (2024). MicroRNAs as Bile-based Biomarkers in Pancreaticobiliary Cancers (MIRABILE). https://classic.clinicaltrials.gov/ct2/show/NCT06258824?term=NCT06258824&draw=2&rank=1

Cooper, G.M. (2019). *The Cell: A Molecular Approach*. 8th Edition, New York: Sinauer Associates

Costa, E. C., Moreira, A. F., de Melo-Diogo, D., Gaspar, V. M., Carvalho, M. P., & Correia, I. J. (2016). 3D tumor spheroids: an overview on the tools and techniques used for their analysis. *Biotechnology advances*, *34*(8), 1427-1441.

Däster, S., Amatruda, N., Calabrese, D., Ivanek, R., Turrini, E., Droeser, R.A., Zajac, P., Fimognari, C., Spagnoli, G.C., Iezzi, G. & Mele, V. (2017). Induction of hypoxia and necrosis in multicellular tumor spheroids is associated with resistance to chemotherapy treatment. *Oncotarget, 8*(1), p.1725.

Datta, A., Kim, H., Lal, M., McGee, L., Johnson, A., Moustafa, A. A., ... & Abdel-Mageed, A. B. (2017). Manumycin A suppresses exosome biogenesis and secretion via targeted inhibition of Ras/Raf/ERK1/2 signaling and hnRNP H1 in castration-resistant prostate cancer cells. *Cancer letters*, *408*, 73-81.

Davis, J. D., & Wypych, T. P. (2021). Cellular and functional heterogeneity of the airway epithelium. *Mucosal immunology*, *14*(5), 978-990.

De Sousa, K. P., Rossi, I., Abdullahi, M., Ramirez, M. I., Stratton, D., & Inal, J. M. (2023). Isolation and characterization of extracellular vesicles and future directions in diagnosis and therapy. *Wiley Interdisciplinary Reviews: Nanomedicine and Nanobiotechnology*, *15*(1), e1835.

Djomehri, S. I., Burman, B., Gonzalez, M. E., Takayama, S., & Kleer, C. G. (2019). A reproducible scaffold-free 3D organoid model to study neoplastic progression in breast cancer. *Journal of cell communication and signaling*, *13*, 129-143.

Doll, R., & Hill, A. B. (1950). Smoking and carcinoma of the lung; preliminary report. *British medical journal*, *2*(4682), 739–748.https://doi.org/10.1136/bmj.2.4682.739

Doll, R., & Hill, A. B. (1952). A study of the aetiology of carcinoma of the lung. *British medical journal*, *2*(4797), 1271–1286. https://doi.org/10.1136/bmj.2.4797.1271

Dou, G., Tian, R., Liu, X., Yuan, P., Ye, Q., Liu, J., ... & Jin, Y. (2020). Chimeric apoptotic bodies functionalized with natural membrane and modular delivery system for inflammation modulation. *Science advances*, *6*(30), eaba2987.

Du, X., Qi, F., Lu, S., Li, Y., & Han, W. (2018). Nicotine upregulates FGFR3 and RB1 expression and promotes non-small cell lung cancer cell proliferation and epithelial-to-mesenchymal transition via downregulation of miR-99b and miR-192. *Biomedicine & Pharmacotherapy*, *101*, 656-662.

Duval, K., Grover, H., Han, L. H., Mou, Y., Pegoraro, A. F., Fredberg, J., & Chen, Z. (2017). Modeling physiological events in 2D vs. 3D cell culture. *Physiology*, *32*(4), 266-277.

Fatehullah, A., Tan, S. H., & Barker, N. (2016). Organoids as an in vitro model of human development and disease. *Nature cell biology*, *18*(3), 246-254.

Fathi, M., Martinez-Paniagua, M., Rezvan, A., Montalvo, M. J., Mohanty, V., Chen, K., Mani, S. A., & Varadarajan, N. (2023). Identifying signatures of EV secretion in metastatic breast cancer through functional single-cell profiling. *iScience*, *26*(4), 106482. https://doi.org/10.1016/j.isci.2023.106482

FDA-NIH Biomarker Working Group. (2016) BEST (Biomarkers, EndpointS, and other Tools) Resource. Silver Spring (MD): Food and Drug Administration (US); Bethesda (MD): National Institutes of Health (US), www.ncbi.nlm.nih.gov/books/NBK326791/

Foty, R. (2011). A simple hanging drop cell culture protocol for generation of 3D spheroids. *JoVE (Journal of Visualized Experiments)*, (51), e2720.

Foye, C., Yan, I. K., David, W., Shukla, N., Habboush, Y., Chase, L., Ryland, K., Kesari, V., & Patel, T. (2017). Comparison of miRNA quantitation by Nanostring in serum and plasma samples. *PloS one*, *12*(12), e0189165. https://doi.org/10.1371/journal.pone.0189165

Gao, Y., Qin, Y., Wan, C., Sun, Y., Meng, J., Huang, J., ... & Yang, K. (2021). Small extracellular vesicles: a novel avenue for cancer management. *Frontiers in Oncology*, *11*, 638357.

Garcia-Alegria, E., Potts, B., Menegatti, S., & Kouskoff, V. (2021). *In vitro* differentiation of human embryonic stem cells to hemogenic endothelium and blood progenitors via embryoid body formation. *STAR protocols*, *2*(1), 100367. https://doi.org/10.1016/j.xpro.2021.100367

Gareen, I. F., Duan, F., Greco, E. M., Snyder, B. S., Boiselle, P. M., Park, E. R., ... & Gatsonis, C. (2014). Impact of lung cancer screening results on participant health-related quality of life and state anxiety in the National Lung Screening Trial. *Cancer*, *120*(21), 3401-3409.

Gaurav, R. (2019). Vaping away epithelial integrity. *American Journal of Respiratory Cell and Molecular Biology*, *61*(2), 127-129.

Gealy, R., Zhang, L., Siegfried, J. M., Luketich, J. D., & Keohavong, P. (1999). Comparison of mutations in the p53 and K-ras genes in lung carcinomas from smoking and nonsmoking women. *Cancer Epidemiology Biomarkers & Prevention*, *8*(4), 297-302.

Giard, D. J., Aaronson, S. A., Todaro, G. J., Arnstein, P., Kersey, J. H., Dosik, H., & Parks, W. P. (1973). In vitro cultivation of human tumors: establishment of cell lines derived from a series of solid tumors. *Journal of the National Cancer Institute*, *51*(5), 1417–1423. https://doi.org/10.1093/jnci/51.5.1417

Goel, R., Bitzer, Z., Reilly, S., Trushin, N., Reinhart, L., Elias, R., & Richie, J. P. (2017). Tobacco smoke free radicals and related biomarkers of oxidative stress. *Free Radical Biology and Medicine*, *112*, 130-131.

Gong, Y., Fan, N., Yang, X., Peng, B., & Jiang, H. (2019). New advances in microfluidic flow cytometry. *Electrophoresis*, *40*(8), 1212-1229.

Gordon, T., Karey, E., Rebuli, M. E., Escobar, Y. N. H., Jaspers, I., & Chen, L. C. (2022). E-cigarette toxicology. *Annual review of pharmacology and toxicology*, *62*, 301-322.

Grasedieck, S., Schöler, N., Bommer, M., Niess, J. H., Tumani, H., Rouhi, A., ... & Kuchenbauer, F. (2012). Impact of serum storage conditions on microRNA stability. *Leukemia*, *26*(11), 2414-2416.

Greenberg, J. W., Kim, H., Ahn, M., Moustafa, A. A., Zhou, H., Barata, P. C., ... & Krane, L. S. (2022). Combination of tipifarnib and sunitinib overcomes renal cell carcinoma resistance to tyrosine kinase inhibitors via tumor-derived exosome and T cell modulation. *Cancers*, *14*(4), 903.

Groot, M., & Lee, H. (2020). Sorting mechanisms for MicroRNAs into extracellular vesicles and their associated diseases. *Cells*, *9*(4), 1044.

Habanjar, O., Diab-Assaf, M., Caldefie-Chezet, F., & Delort, L. (2021). 3D cell culture systems: tumor application, advantages, and disadvantages. *International journal of molecular sciences*, *22*(22), 12200.

Haisler, W. L., Timm, D. M., Gage, J. A., Tseng, H., Killian, T. C., & Souza, G. R. (2013). Three-dimensional cell culturing by magnetic levitation. *Nature protocols*, *8*(10), 1940-1949.

Handa, T., Kuroha, M., Nagai, H., Shimoyama, Y., Naito, T., Moroi, R., ... & Masamune, A. (2021). Liquid biopsy for colorectal adenoma: is the exosomal miRNA derived from organoid a potential diagnostic biomarker?. *Clinical and Translational Gastroenterology*, *12*(5).

Harkema, J. R., Nikula, K. J., & Haschek, W. M. (2018). Respiratory System. In M. A. Wallig, W. M. Haschek, C. G. Rousseaux, & B. Bolon (Eds.), *Fundamentals of Toxicologic Pathology* (3 ed., pp. 351-393). Academic Press. https://doi.org/10.1016/B978-0-12-809841-7.00014-9

Harrison, P., Gardiner, C., & Sargent, I. (Eds.) (2014). *Extracellular Vesicles in Health and Disease*. Pan Stanford Publishing.

Hartmann-Boyce, J., Begh, R., & Aveyard, P. (2018). Electronic cigarettes for smoking cessation. *Bmj*, *360*.

Hessvik, N. P., & Llorente, A. (2018). Current knowledge on exosome biogenesis and release. *Cellular and Molecular Life Sciences*, *75*, 193-208.

Hiddinga, B. I., Raskin, J., Janssens, A., Pauwels, P., & Van Meerbeeck, J. P. (2021). Recent developments in the treatment of small cell lung cancer. *European Respiratory Review*, *30*(161).

Hikita, T., Kuwahara, A., Watanabe, R., Miyata, M., & Oneyama, C. (2019). Src in endosomal membranes promotes exosome secretion and tumor progression. *Scientific Reports*, *9*(1), 1-14.

Hochreiter-Hufford, A. E., Lee, C. S., Kinchen, J. M., Sokolowski, J. D., Arandjelovic, S., Call, J. A., ... & Ravichandran, K. S. (2013). Phosphatidylserine receptor BAI1 and apoptotic cells as new promoters of myoblast fusion. *Nature*, *497*(7448), 263-267.

Hood, J. L., San, R. S., & Wickline, S. A. (2011). Exosomes released by melanoma cells prepare sentinel lymph nodes for tumor metastasis. *Cancer research*, *71*(11), 3792-3801.

Huang, J., Wu, J., Li, Y., Li, X., Yang, T., Yang, Q., & Jiang, Y. (2014). Deregulation of serum microRNA expression is associated with cigarette smoking and lung cancer. *BioMed research international*, *2014*.

Human Tissue Act. (2004). http://www.legislation. gov.uk/ukpga/2004/30/contents

Hutzler, C., Paschke, M., Kruschinski, S., Henkler, F., Hahn, J., & Luch, A. (2014). Chemical hazards present in liquids and vapors of electronic cigarettes. *Archives of toxicology*, *88*(7), 1295–1308. https://doi.org/10.1007/s00204-014-1294-7

Hwa Yun, B., Guo, J., Bellamri, M., & Turesky, R. J. (2020). DNA adducts: Formation, biological effects, and new biospecimens for mass spectrometric measurements in humans. *Mass spectrometry reviews, 39*(1-2), 55–82. https://doi.org/10.1002/mas.21570

IARC Working Group on the Evaluation of Carcinogenic Risks to Humans, World Health Organization, & International Agency for Research on Cancer. (2004). *Tobacco smoke and involuntary smoking* (Vol. 83).

Imamura, Y., Mukohara, T., Shimono, Y., Funakoshi, Y., Chayahara, N., Toyoda, M., ... & Minami, H. (2015). Comparison of 2D-and 3D-culture models as drug-testing platforms in breast cancer. *Oncology reports*, *33*(4), 1837-1843.

Iwakawa, H. O., & Tomari, Y. (2022). Life of RISC: Formation, action, and degradation of RNA-induced silencing complex. *Molecular cell*, *82*(1), 30–43. https://doi.org/10.1016/j.molcel.2021.11.026

Jenike, A. E., & Halushka, M. K. (2021). miR-21: a non-specific biomarker of all maladies. *Biomarker research*, *9*(1), 1-7.

Jenjaroenpun, P., Kremenska, Y., Nair, V. M., Kremenskoy, M., Joseph, B., & Kurochkin, I. V. (2013). Characterization of RNA in exosomes secreted by human breast cancer cell lines using next-generation sequencing. *PeerJ*, *1*, e201.

Jongpaiboonkit, L., King, W. J., Lyons, G. E., Paguirigan, A. L., Warrick, J. W., Beebe, D. J., & Murphy, W. L. (2008). An adaptable hydrogel array format for 3-dimensional cell culture and analysis. *Biomaterials*, *29*(23), 3346-3356.

Kapałczyńska, M., Kolenda, T., Przybyła, W., Zajączkowska, M., Teresiak, A., Filas, V., ... & Lamperska, K. (2018). 2D and 3D cell cultures–a comparison of different types of cancer cell cultures. *Archives of Medical Science*, *14*(4), 910-919.

Kaur, G., Pinkston, R., Mclemore, B., Dorsey, W. C., & Batra, S. (2018). Immunological and toxicological risk assessment of e-cigarettes. *European respiratory review : an official journal of the European Respiratory Society*, *27*(147), 170119.

Kilgore, J. A., Dolman, N. J., & Davidson, M. W. (2014). A review of reagents for fluorescence microscopy of cellular compartments and structures, Part III: reagents for actin, tubulin, cellular membranes, and whole cell and cytoplasm. *Current Protocols in Cytometry*, *67*(1), 12-32.

Kim, H., Sung, J. Y., Park, E. K., Kho, S., Koo, K. H., Park, S. Y., ... & Kim, Y. N. (2017). Regulation of anoikis resistance by NADPH oxidase 4 and epidermal growth factor receptor. *British journal of cancer*, *116*(3), 370-381.

Kinoshita, T., Yip, K. W., Spence, T., & Liu, F. F. (2017). MicroRNAs in extracellular vesicles: potential cancer biomarkers. *Journal of human genetics*, *62*(1), 67-74.

Kosaka, N., Iguchi, H., Hagiwara, K., Yoshioka, Y., Takeshita, F., & Ochiya, T. (2013). Neutral sphingomyelinase 2 (nSMase2)-dependent exosomal transfer of angiogenic microRNAs regulate cancer cell metastasis. *Journal of Biological Chemistry*, *288*(15), 10849-10859.

Kotrbová, A., Štěpka, K., Maška, M., Pálenik, J. J., Ilkovics, L., Klemová, D., ... & Pospíchalová, V. (2019). TEM ExosomeAnalyzer: a computer-assisted software tool for quantitative evaluation of extracellular vesicles in transmission electron microscopy images. *Journal of extracellular vesicles*, *8*(1), 1560808.

Kowal, J., Arras, G., Colombo, M., Jouve, M., Morath, J. P., Primdal-Bengtson, B., ... & Théry, C. (2016). Proteomic comparison defines novel markers to characterize heterogeneous populations of extracellular vesicle subtypes. *Proceedings of the National Academy of Sciences*, *113*(8), E968-E977.

Kozomara, A., Birgaoanu, M., & Griffiths-Jones, S. (2019). miRBase: from microRNA sequences to function. *Nucleic acids research*, *47*(D1), D155–D162. https://doi.org/10.1093/nar/gky1141

Kueltzo, L. A., Wang, W. E. I., Randolph, T. W., & Carpenter, J. F. (2008). Effects of solution conditions, processing parameters, and container materials on aggregation of a monoclonal antibody during freeze-thawing. *Journal of pharmaceutical sciences*, *97*(5), 1801-1812.

Lan, X., Ren, J., Du, X., Zhang, L., Wang, S., Yang, X., & Lu, S. (2023). lnc-HC ameliorates steatosis by promoting miR-130b-3p biogenesis and the assembly of an RNA-induced silencing complex. *Molecular and Cellular Endocrinology*, *578*, 112061.

Langhans, S. A. (2018). Three-dimensional in vitro cell culture models in drug discovery and drug repositioning. *Frontiers in pharmacology*, *9*, 6.

LeBleu, V. S., & Kalluri, R. (2020). Exosomes as a multicomponent biomarker platform in cancer. *Trends in cancer*, *6*(9), 767-774.

Lee, H., Han, S., Kwon, C. S., & Lee, D. (2016). Biogenesis and regulation of the let-7 miRNAs and their functional implications. *Protein & cell*, *7*(2), 100-113.

Lee, R. C., Feinbaum, R. L., & Ambros, V. (1993). The C. elegans heterochronic gene lin-4 encodes small RNAs with antisense complementarity to lin-14. *Cell*, *75*(5), 843–854. https://doi.org/10.1016/0092-8674(93)90529-y

Lerner, C. A., Sundar, I. K., Yao, H., Gerloff, J., Ossip, D. J., McIntosh, S., ... & Rahman, I. (2015). Vapors produced by electronic cigarettes and e-juices with flavorings induce toxicity, oxidative stress, and inflammatory response in lung epithelial cells and in mouse lung. *PloS one*, *10*(2), e0116732.

Levine, A. J., Momand, J., & Finlay, C. A. (1991). The p53 tumour suppressor gene. *Nature*, *351*(6326), 453–456.

Li, D., Yang, Y., Zhu, G., Liu, X., Zhao, M., Li, X., & Yang, Q. (2015). MicroRNA-410 promotes cell proliferation by targeting BRD7 in non-small cell lung cancer. *FEBS letters*, *589*(17), 2218-2223.

Li, Y., Zhang, Y., Qiu, F., & Qiu, Z. (2011). Proteomic identification of exosomal LRG1: a potential urinary biomarker for detecting NSCLC. *Electrophoresis*, *32*(15), 1976-1983.

Liu, Y., Nie, H., Zhang, K., Ma, D., Yang, G., Zheng, Z., ... & Yang, S. (2014). A feedback regulatory loop between HIF-1α and miR-21 in response to hypoxia in cardiomyocytes. *FEBS letters*, *588*(17), 3137-3146.

Livak, K. J., & Schmittgen, T. D. (2001). Analysis of relative gene expression data using real-time quantitative PCR and the 2− ΔΔCT method. *methods*, *25*(4), 402-408.

Loo, H. K., Mathen, P., Lee, J., & Camphausen, K. (2019). Circulating biomarkers for high-grade glioma. *Biomarkers in Medicine*, *13*(3), 161-165.

Lötvall, J., Hill, A. F., Hochberg, F., Buzás, E. I., Di Vizio, D., Gardiner, C., Gho, Y. S., Kurochkin, I. V., Mathivanan, S., Quesenberry, P., Sahoo, S., Tahara, H., Wauben, M. H., Witwer, K. W., & Théry, C. (2014). Minimal experimental requirements for definition of extracellular vesicles and their functions: a position statement from the International

Society for Extracellular Vesicles. *Journal of extracellular vesicles*, *3*, 26913. https://doi.org/10.3402/jev.v3.26913

Lu, T., Yang, X., Huang, Y., Zhao, M., Li, M., Ma, K., Yin, J., Zhan, C., & Wang, Q. (2019). Trends in the incidence, treatment, and survival of patients with lung cancer in the last four decades. *Cancer management and research*, *11*, 943–953. https://doi.org/10.2147/CMAR.S187317

Maia, J., Batista, S., Couto, N., Gregório, A. C., Bodo, C., Elzanowska, J., ... & Costa-Silva, B. (2020). Employing flow cytometry to extracellular vesicles sample microvolume analysis and quality control. *Frontiers in Cell and Developmental Biology*, *8*, 593750.

Malik, S., Zafar Paracha, R., Khalid, M., Nisar, M., Siddiqa, A., Hussain, Z., ... & Ahmad, J. (2019). MicroRNAs and their target mRNAs as potential biomarkers among smokers and non-smokers with lung adenocarcinoma. *IET Systems Biology*, *13*(2), 69-76.

Matias-Garcia, P. R., Wilson, R., Mussack, V., Reischl, E., Waldenberger, M., Gieger, C., ... & Kuehn-Steven, A. (2020). Impact of long-term storage and freeze-thawing on eight circulating microRNAs in plasma samples. *PloS one*, *15*(1), e0227648.

Matias-Garcia, P.R., Wilson, R., Mussack, V., Reischl, E., Waldenberger, M., Gieger, C., Anton, G., Peters, A. & Kuehn-Steven, A., 2020. Impact of long-term storage and freeze-thawing on eight circulating microRNAs in plasma samples. *PloS one*, *15*(1), p.e0227648.

Matsumoto, S., Fang, X., Traber, M. G., Jones, K. D., Langelier, C., Hayakawa Serpa, P., ... & Gotts, J. E. (2020). Dose-dependent pulmonary toxicity of aerosolized vitamin E acetate. *American journal of respiratory cell and molecular biology*, *63*(6), 748-757.

Matsuzaki, J., & Ochiya, T. (2017). Circulating microRNAs and extracellular vesicles as potential cancer biomarkers: a systematic review. *International journal of clinical oncology*, *22*, 413-420.

Mazzone, P. J., Sears, C. R., Arenberg, D. A., Gaga, M., Gould, M. K., Massion, P. P., ... & Wiener, R. S. (2017). Evaluating molecular biomarkers for the early detection of lung cancer: when is a biomarker ready for clinical use? An official American Thoracic Society policy statement. *American journal of respiratory and critical care medicine*, *196*(7), e15-e29.

McKelvey, K. J., Powell, K. L., Ashton, A. W., Morris, J. M., & McCracken, S. A. (2015). Exosomes: mechanisms of uptake. *Journal of circulating biomarkers*, *4*, 7.

Meister, G., Landthaler, M., Patkaniowska, A., Dorsett, Y., Teng, G., and Tuschl, T. (2004). Human Argonaute2 mediates RNA cleavage targeted by miRNAs and siRNAs. Mol. Cell 15, 185–197

Melo, S.A., Sugimoto, H., O'Connell, J.T., Kato, N., Villanueva, A., Vidal, A., Qiu, L., Vitkin, E., Perelman, L.T., Melo, C.A. & Lucci, A., 2014. Cancer exosomes perform cell-independent microRNA biogenesis and promote tumorigenesis. *Cancer cell*, *26*(5), pp.707-721.

Michlewski, G., & Cáceres, J. F. (2019). Post-transcriptional control of miRNA biogenesis. *RNA (New York, N.Y.)*, *25*(1), 1–16. https://doi.org/10.1261/rna.068692.118

Min, S., Choe, C., & Roh, S. (2021). AQP3 Increases Intercellular Cohesion in NSCLC A549 Cell Spheroids through Exploratory Cell Protrusions. *International journal of molecular sciences*, *22*(8), 4287. https://doi.org/10.3390/ijms22084287

Mitchell, P. S., Parkin, R. K., Kroh, E. M., Fritz, B. R., Wyman, S. K., Pogosova-Agadjanyan, E. L., ... & Tewari, M. (2008). Circulating microRNAs as stable blood-based markers for cancer detection. *Proceedings of the National Academy of Sciences*, *105*(30), 10513-10518.

Mobarrez, F., Antoniewicz, L., Hedman, L., Bosson, J. A., & Lundbäck, M. (2020). Electronic cigarettes containing nicotine increase endothelial and platelet derived extracellular vesicles in healthy volunteers. *Atherosclerosis*, *301*, 93-100.

Mompeón, A., Ortega-Paz, L., Vidal-Gómez, X., Costa, T. J., Pérez-Cremades, D., Garcia-Blas, S., ... & Hermenegildo, C. (2020). Disparate miRNA expression in serum and plasma of patients with acute myocardial infarction: a systematic and paired comparative analysis. *Scientific Reports*, *10*(1), 5373.

Morrison, E. J., Novotny, P. J., Sloan, J. A., Yang, P., Patten, C. A., Ruddy, K. J., & Clark, M. M. (2017). Emotional problems, quality of life, and symptom burden in patients with lung cancer. *Clinical Lung Cancer*, *18*(5), 497-503.

Muguruma, M., Teraoka, S., Miyahara, K., Ueda, A., Asaoka, M., Okazaki, M., ... & Ishikawa, T. (2020). Differences in drug sensitivity between two-dimensional and three-dimensional culture systems in triple-negative breast cancer cell lines. *Biochemical and Biophysical Research Communications*, *533*(3), 268-274.

Nederman, T., Norling, B., Glimelius, B., Carlsson, J., & Brunk, U. (1984). Demonstration of an extracellular matrix in multicellular tumor spheroids. *Cancer research*, *44*(7), 3090-3097.

NICE. (2023). Recommendations on treating tobacco dependence. https://www.nice.org.uk/guidance/ng209/chapter/recommendations-on-treating-tobacco-dependence

Oberg, C., Folch, E., & Santacruz, J. F. (2018). Management of malignant airway obstruction. *AME Med J*, *3*, 115.

Office for National Statistics (ONS) (2018). Adult drinking habits in Great Britain: 2017. https://www.ons.gov.uk/peoplepopulationandcommunity/healthandsocialcare/druguseal coholandsmoking/bulletins/opinionsandlifestylesurveyadultdrinkinghabitsingreatbritain/l atest

Office for National Statistics (ONS) (2020). Adult smoking habits in the UK: 2019. https://www.ons.gov.uk/peoplepopulationandcommunity/healthandsocialcare/healthan dlifeexpectancies/bulletins/adultsmokinghabitsingreatbritain/2019/pdf Accessed November 2022

Office for National Statistics (ONS) (2022). Adult smoking habits in the UK: 2021. https://www.ons.gov.uk/peoplepopulationandcommunity/healthandsocialcare/healthan dlifeexpectancies/bulletins/adultsmokinghabitsingreatbritain/2021

Panunzio, A., & Sartori, P. (2020). Lung cancer and radiological imaging. *Current radiopharmaceuticals*, *13*(3), 238-242.

Parimon, T., Brauer, R., Schlesinger, S.Y., Xie, T., Jiang, D., Ge, L., Huang, Y., Birkland, T.P., Parks, W.C., Habiel, D.M. & Hogaboam, C.M., 2018. Syndecan-1 controls lung tumorigenesis by regulating miRNAs packaged in exosomes. *The American journal of pathology*, *188*(4), pp.1094-1103.

Peto, R., Darby, S., Deo, H., Silcocks, P., Whitley, E., & Doll, R. (2000). Smoking, smoking cessation, and lung cancer in the UK since 1950: combination of national statistics with two case-control studies. *BMJ*, *321*(7257), 323-329.

Pizzino, G., Irrera, N., Cucinotta, M., Pallio, G., Mannino, F., Arcoraci, V., ... & Bitto, A. (2017). Oxidative stress: harms and benefits for human health. *Oxidative medicine and cellular longevity*, *2017*.

Porzycki, P., Ciszkowicz, E., Semik, M., & Tyrka, M. (2018). Combination of three miRNA (miR-141, miR-21, and miR-375) as potential diagnostic tool for prostate cancer recognition. *International urology and nephrology*, *50*, 1619-1626.

Reboul, E. (2017). Vitamin E bioavailability: mechanisms of intestinal absorption in the spotlight. *Antioxidants*, *6*(4), 95.

Reclusa, P., Taverna, S., Pucci, M., Durendez, E., Calabuig, S., Manca, P., ... & Rolfo, C. (2017). Exosomes as diagnostic and predictive biomarkers in lung cancer. *Journal of thoracic disease*, *9*(Suppl 13), S1373.

Roush, S., & Slack, F. J. (2008). The let-7 family of microRNAs. *Trends in cell biology*, *18*(10), 505–516. https://doi.org/10.1016/j.tcb.2008.07.007

Ruedinger, F., Lavrentieva, A., Blume, C., Pepelanova, I., & Scheper, T. (2015). Hydrogels for 3D mammalian cell culture: a starting guide for laboratory practice. *Applied microbiology and biotechnology*, *99*, 623-636.

Schraufnagel, D. E., Blasi, F., Drummond, M. B., Lam, D. C., Latif, E., Rosen, M. J., ... & Van Zyl-Smit, R. (2014). Electronic cigarettes. A position statement of the forum of international respiratory societies. *American journal of respiratory and critical care medicine*, *190*(6), 611-618.

Shaw, F. L., Harrison, H., Spence, K., Ablett, M. P., Simões, B. M., Farnie, G., & Clarke, R. B. (2012). A detailed mammosphere assay protocol for the quantification of breast stem cell activity. *Journal of mammary gland biology and neoplasia*, *17*(2), 111–117.

Shinbashi, M., & Rubin, B. K. (2020). Electronic cigarettes and e-cigarette/vaping product use associated lung injury (EVALI). *Paediatric respiratory reviews, 36*, 87–91.

Siegel, R. L., Miller, K. D., Wagle, N. S., & Jemal, A. (2023). Cancer statistics, 2023. *Ca Cancer J Clin*, *73*(1), 17-48.

Singh, K. P., Maremanda, K. P., Li, D., & Rahman, I. (2020). Exosomal microRNAs are novel circulating biomarkers in cigarette, waterpipe smokers, E-cigarette users and dual smokers. *BMC medical genomics*, *13*, 1-20.

Sivanantham, A., & Jin, Y. (2022). Impact of storage conditions on EV Integrity/Surface markers and cargos. *Life*, *12*(5), 697.

Solleti, S. K., Bhattacharya, S., Ahmad, A., Wang, Q., Mereness, J., Rangasamy, T., & Mariani, T. J. (2017). MicroRNA expression profiling defines the impact of electronic cigarettes on human airway epithelial cells. *Scientific reports*, *7*(1), 1081.

Stratton, M. R., Campbell, P. J., & Futreal, P. A. (2009). The cancer genome. *Nature*, *458*(7239), 719-724.

Sullivan, L., & Crotty Alexander, L. E. (2022). A Problem for Generations: Impact of E-Cigarette Type on Immune Homeostasis. *American Journal of Respiratory and Critical Care Medicine*, *206*(10), 1195-1197.

Sundar, I. K., Javed, F., Romanos, G. E., & Rahman, I. (2016). E-cigarettes and flavorings induce inflammatory and pro-senescence responses in oral epithelial cells and periodontal fibroblasts. *Oncotarget*, *7*(47), 77196–77204. https://doi.org/10.18632/oncotarget.12857

Sung, H., Ferlay, J., Siegel, R. L., Laversanne, M., Soerjomataram, I., Jemal, A., & Bray, F. (2021). Global cancer statistics 2020: GLOBOCAN estimates of incidence and mortality worldwide for 36 cancers in 185 countries. *CA: a cancer journal for clinicians*, *71*(3), 209-249.

Suryadinata, R. V., & Wirjatmadi, B. (2021). The Molecular Pathways of Lung Damage by E-Cigarettes in Male Wistar Rats. *Sultan Qaboos University medical journal*, *21*(3), 436–441. https://doi.org/10.18295/squmj.4.2021.003

Svoronos, A. A., Engelman, D. M., & Slack, F. J. (2016). OncomiR or tumor suppressor? The duplicity of microRNAs in cancer. *Cancer research*, *76*(13), 3666-3670.

Temple, J., Velliou, E., Shehata, M., Lévy, R., & Gupta, P. (2022). Current strategies with implementation of three-dimensional cell culture: the challenge of quantification. *Interface Focus*, *12*(5), 20220019.

Thermo Fisher. (2023). Useful Numbers for Cell Culture. https://www.thermofisher.com/uk/en/home/references/gibco-cell-culture-basics/cell-culture-protocols/cell-culture-useful-numbers.html

Théry, C., Witwer, K. W., Aikawa, E., Alcaraz, M. J., Anderson, J. D., Andriantsitohaina, R., ... & Jovanovic-Talisman, T. (2018). Minimal information for studies of extracellular vesicles 2018 (MISEV2018): a position statement of the International Society for Extracellular Vesicles and update of the MISEV2014 guidelines. *Journal of extracellular vesicles*, *7*(1), 1535750.

Thippabhotla, S., Zhong, C., & He, M. (2019). 3D cell culture stimulates the secretion of in vivo like extracellular vesicles. *Scientific reports*, *9*(1), 13012.

Tian, T., Zhu, Y. L., Zhou, Y. Y., Liang, G. F., Wang, Y. Y., Hu, F. H., & Xiao, Z. D. (2014). Exosome uptake through clathrin-mediated endocytosis and macropinocytosis and mediating miR-21 delivery. *Journal of Biological Chemistry*, *289*(32), 22258-22267.

Tindle, H. A., Stevenson Duncan, M., Greevy, R. A., Vasan, R. S., Kundu, S., Massion, P. P., & Freiberg, M. S. (2018). Lifetime smoking history and risk of lung cancer: results from the Framingham Heart Study. *JNCI: Journal of the National Cancer Institute*, *110*(11), 1201-1207.

Trang, P., Medina, P. P., Wiggins, J. F., Ruffino, L., Kelnar, K., Omotola, M., ... & Slack, F. J. (2010). Regression of murine lung tumors by the let-7 microRNA. *Oncogene*, *29*(11), 1580-1587.

Tseng, A. M., Chung, D. D., Pinson, M. R., Salem, N. A., Eaves, S. E., & Miranda, R. C. (2019). Ethanol exposure increases miR-140 in extracellular vesicles: implications for fetal neural stem cell proliferation and maturation. *Alcoholism: Clinical and Experimental Research*, *43*(7), 1414-1426.

Valdoz, J. C., Johnson, B. C., Jacobs, D. J., Franks, N. A., Dodson, E. L., Sanders, C., ... & Van Ry, P. M. (2021). The ECM: to scaffold, or not to scaffold, that is the question. *International Journal of Molecular Sciences*, *22*(23), 12690.

Volinia, S., Galasso, M., Costinean, S., Tagliavini, L., Gamberoni, G., Drusco, A., ... & Croce, C. M. (2010). Reprogramming of miRNA networks in cancer and leukemia. *Genome research*, *20*(5), 589-599.

Wang, G., Wang, R., Strulovici-Barel, Y., Salit, J., Staudt, M. R., Ahmed, J., ... & Crystal, R. G. (2015). Persistence of smoking-induced dysregulation of miRNA expression in the small airway epithelium despite smoking cessation. *PloS one*, *10*(4), e0120824.

Wang, H., Guo, M., Wei, H., & Chen, Y. (2023). Targeting p53 pathways: mechanisms, structures, and advances in therapy. *Signal transduction and targeted therapy*, *8*(1), 92.

Wang, J., Wuethrich, A., Lobb, R. J., Antaw, F., Sina, A. A., Lane, R. E., Zhou, Q., Zieschank, C., Bell, C., Bonazzi, V. F., Aoude, L. G., Everitt, S., Yeo, B., Barbour, A. P., Möller, A., & Trau, M. (2021). Characterizing the Heterogeneity of Small Extracellular Vesicle Populations in Multiple Cancer Types *via* an Ultrasensitive Chip. *ACS sensors*, *6*(9), 3182–3194.

Wang, J., Ye, H., Zhang, D., Hu, Y., Yu, X., Wang, L., ... & Liu, S. (2016). MicroRNA-410-5p as a potential serum biomarker for the diagnosis of prostate cancer. *Cancer cell international*, *16*, 1-6.

Wang, Y., Fang, Y.X., Dong, B., Du, X., Wang, J., Wang, X., Gao, W.Q. & Xue, W. (2021). Discovery of extracellular vesicles derived miR-181a-5p in patient's serum as an indicator for bone-metastatic prostate cancer. *Theranostics*, *11*(2), p.878.

Wieczorek, R., Phillips, G., Czekala, L., Trelles Sticken, E., O'Connell, G., Simms, L., Rudd, K., Stevenson, M., & Walele, T. (2020). A comparative in vitro toxicity assessment of electronic vaping product e-liquids and aerosols with tobacco cigarette smoke. *Toxicology in vitro: an international journal published in association with BIBRA, 66*.

Willms, E., Cabañas, C., Mäger, I., Wood, M. J., & Vader, P. (2018). Extracellular vesicle heterogeneity: subpopulations, isolation techniques, and diverse functions in cancer progression. *Frontiers in immunology*, *9*, 738.

Witwer, K. W., Goberdhan, D. C., O'Driscoll, L., Théry, C., Welsh, J. A., Blenkiron, C., ... & Zheng, L. (2021). Updating MISEV: Evolving the minimal requirements for studies of extracellular vesicles. *Journal of Extracellular Vesicles*, *10*(14), e12182.

Wozniak, M. B., Scelo, G., Muller, D. C., Mukeria, A., Zaridze, D., & Brennan, P. (2015). Circulating microRNAs as non-invasive biomarkers for early detection of non-small-cell lung cancer. *PloS one*, *10*(5), e0125026.

Wu, D., & O'Shea, D. F. (2020). Potential for release of pulmonary toxic ketene from vaping pyrolysis of vitamin E acetate. *Proceedings of the National Academy of Sciences*, *117*(12), 6349-6355.

Wu, H., Li, J., Luo, S., & Wang, G. (2018). MiR-410 acts as a tumor suppressor in estrogen receptor-positive breast cancer cells by directly targeting ERLIN2 via the ERS pathway. *Cellular Physiology and Biochemistry*, *48*(2), 461-474.

Yan, N., Guo, S., Zhang, H., Zhang, Z., Shen, S., & Li, X. (2022). BRAF-mutated non-small cell lung cancer: current treatment status and future perspective. *Frontiers in oncology*, *12*, 863043.

Yáñez-Mó, M., Siljander, P. R. M., Andreu, Z., Bedina Zavec, A., Borràs, F. E., Buzas, E. I., ... & De Wever, O. (2015). Biological properties of extracellular vesicles and their physiological functions. *Journal of extracellular vesicles*, *4*(1), 27066.

Yuan, Y., Liao, H., Pu, Q., Ke, X., Hu, X., Ma, Y., Luo, X., Jiang, Q., Gong, Y., Wu, M., Liu, L., & Zhu, W. (2020). miR-410 induces both epithelial-mesenchymal transition and radioresistance through activation of the PI3K/mTOR pathway in non-small cell lung cancer. *Signal transduction and targeted therapy*, *5*(1), 85. https://doi.org/10.1038/s41392-020-0182-2

Zahm, A. M., Thayu, M., Hand, N. J., Horner, A., Leonard, M. B., & Friedman, J. R. (2011). Circulating microRNA is a biomarker of pediatric Crohn disease. *Journal of pediatric gastroenterology and nutrition*, *53*(1).

Zhang, Q., Li, Y., Zhao, M., Lin, H., Wang, W., Li, D., Cui, W., Zhou, C., Zhong, J., & Huang, C. (2019). MiR-494 acts as a tumor promoter by targeting CASP2 in non-small cell lung cancer. *Scientific reports*, *9*(1), 3008.

Zheng, M. (2016). Classification and pathology of lung cancer. *Surgical Oncology Clinics*, *25*(3), 447-468.

Zhu, S. H., Sun, J. Y., Bonnevie, E., Cummins, S. E., Gamst, A., Yin, L., & Lee, M. (2014). Four hundred and sixty brands of e-cigarettes and counting: implications for product regulation. *Tobacco control*, *23 Suppl 3*(Suppl 3), iii3–iii9. https://doi.org/10.1136/tobaccocontrol-2014-051670

Zulfiqar, H., Sankari, A., & Rahman, O. (2022). Vaping-Associated Pulmonary Injury. In *StatPearls*. StatPearls Publishing.

Appendices

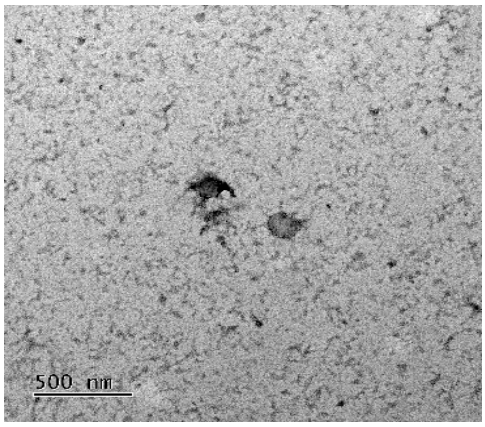

Figure A.1 TEM image of suspected sEVs from A549 3D cell culture, and additional unregular shaped particle.

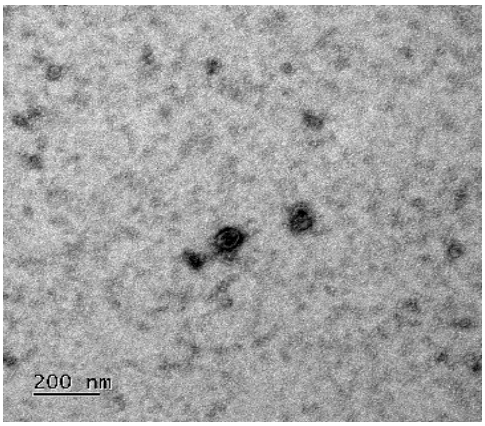

Figure A.2 TEM image of suspected sEVs from A549 3D cell culture, demonstrating cup-shaped morphology

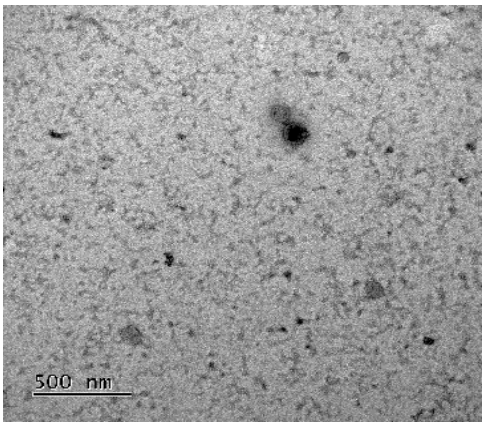

Figure A.3 TEM image of suspected sEVs from A549 3D cell culture

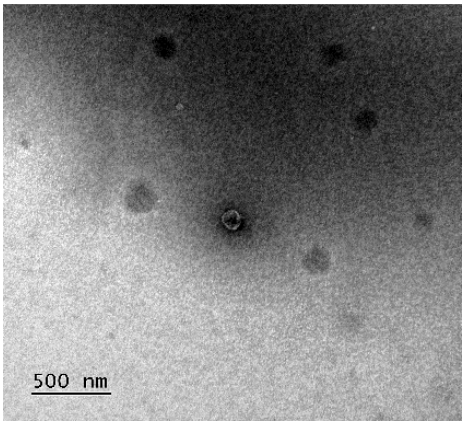

Figure A.4 TEM image of suspected sEVs from BEAS-2B 3D cell culture, demonstrating cup-shaped morphology with some shadowing on the images

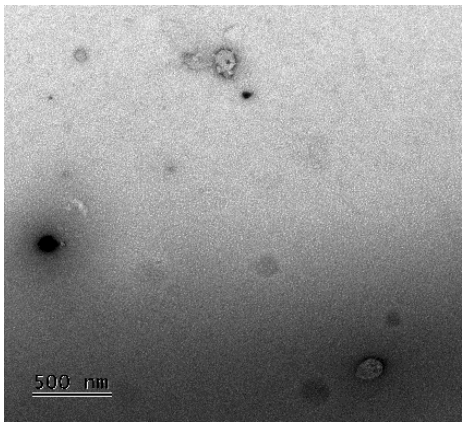

Figure A.5 TEM image of suspected sEVs from BEAS-2B 3D cell culture, demonstrating particles of the correct size with some shadowing on the images

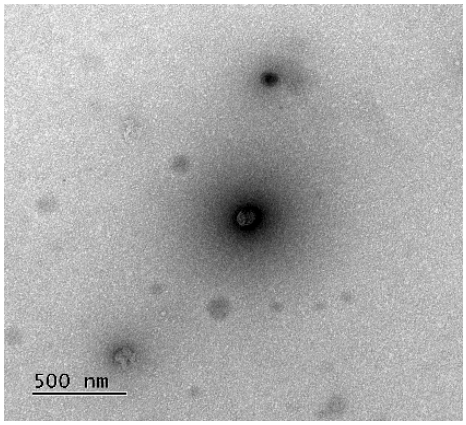

Figure A.6 TEM image of suspected sEVs from BEAS-2B 3D cell culture, particles appeared dark and not much detail was seen

Figure A.7 Full western blot membrane for 3D A549 tagged with CD9 primary antibody with protein marker in lane 1, untreated sEVs in lane 2, strawberry flavoured e-liquid with nicotine treated sEVs in lane 3, strawberry flavoured e-liquid without nicotine treated sEVs in lane 4, apple e-liquid with nicotine treated sEVs in lane 5, and App-Nic treated sEVs in lane 6. Cell lysate sample was added to lane 9. Due to differences in exposure required, protein marker, sample bands and cell lysate bands could not be imaged well together.

Figure A.8 Full western blot membrane for 3D A549 tagged with CD63 primary antibody with protein marker in lane 1, untreated sEVs in lane 2, strawberry flavoured e-liquid with nicotine treated sEVs in lane 3, strawberry flavoured e-liquid without nicotine treated sEVs in lane 4, apple e-liquid with nicotine treated sEVs in lane 5, and App-Nic treated sEVs in lane 6. Cell lysate sample was added to lane 9. Due to differences in exposure required, protein marker, sample bands and cell lysate bands could not be imaged well together.

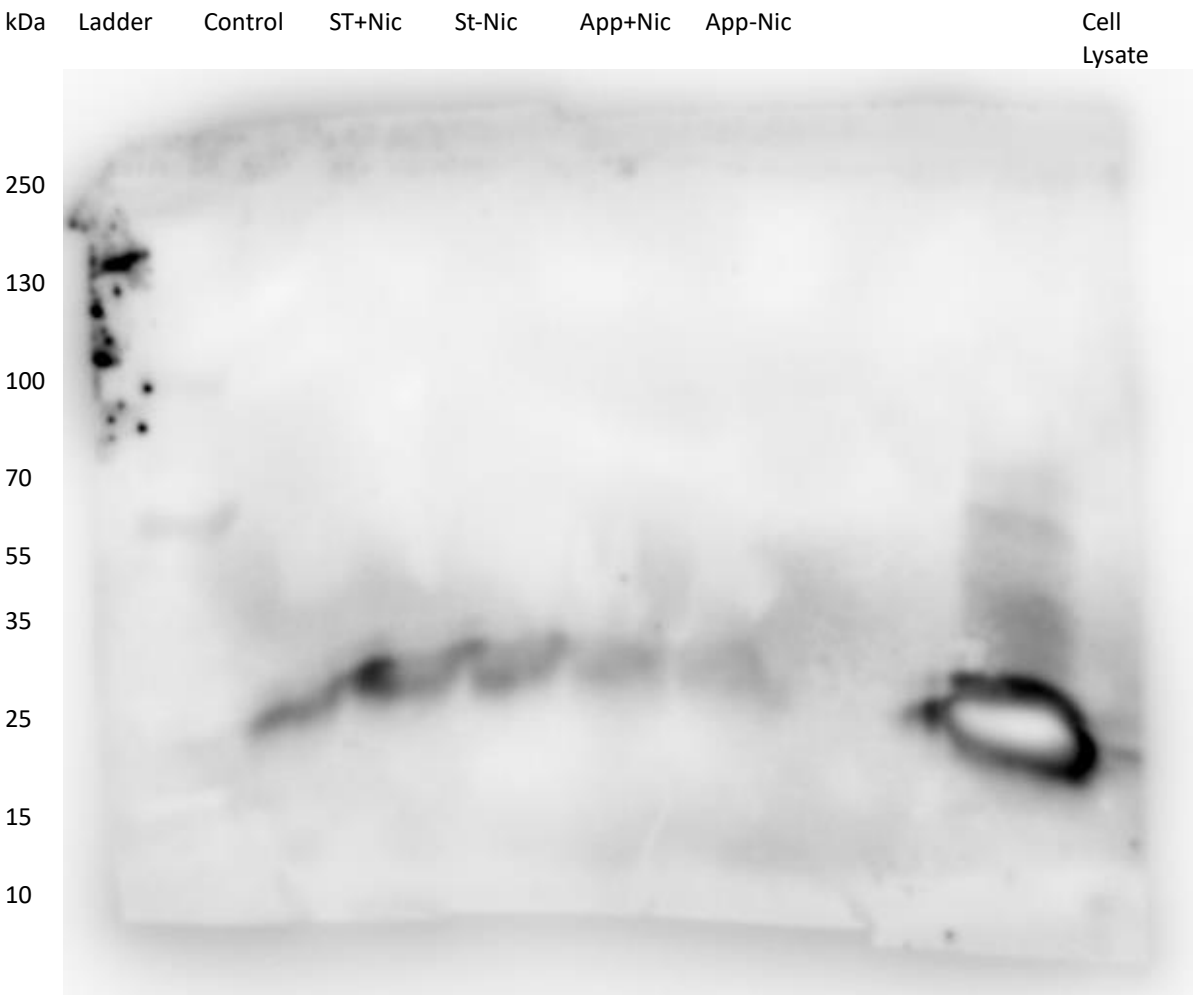

Figure A.9 Full western blot membrane for 3D BEAS-2B tagged with CD9 primary antibody with protein marker in lane 1, untreated sEVs in lane 2, strawberry flavoured e-liquid with nicotine treated sEVs in lane 3, strawberry flavoured e-liquid without nicotine treated sEVs in lane 4, apple e-liquid with nicotine treated sEVs in lane 5, and apple e-liquid without nicotine treated sEVs in lane 6. Cell lysate sample was added to lane 9. Due to differences in exposure required, protein marker, sample bands and cell lysate bands could not be imaged well together**.**

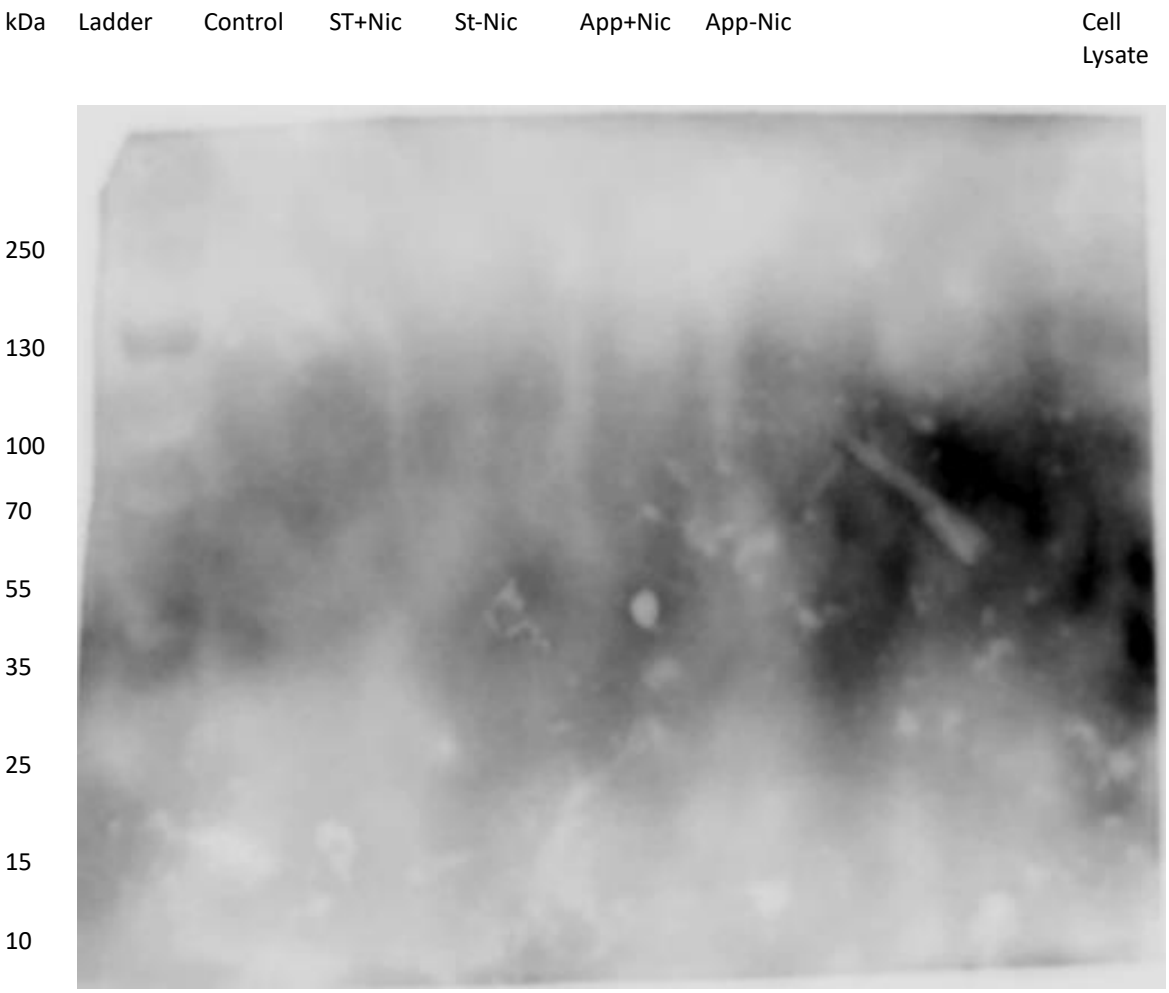

Figure A.10 Full western blot membrane for 3D BEAS-2B tagged with CD63 primary antibody with protein marker in lane 1, untreated sEVs in lane 2, strawberry flavoured e-liquid with nicotine treated sEVs in lane 3, strawberry flavoured e-liquid without nicotine treated sEVs in lane 4, apple e-liquid with nicotine treated sEVs in lane 5, and apple e-liquid without nicotine treated sEVs in lane 6. Cell lysate sample was added to lane 9. Due to differences in exposure required, protein marker, sample bands and cell lysate bands could not be imaged well together. Cell lysate appeared to leak into other lanes.

Figure A.11 Full western blot membrane for 3D A549 tagged with Calnexin primary antibody with protein marker in lane 1, untreated sEVs in lane 2, strawberry flavoured e-liquid with nicotine treated sEVs in lane 3, strawberry flavoured e-liquid without nicotine treated sEVs in lane 4, apple e-liquid with nicotine treated sEVs in lane 5, and apple e-liquid without nicotine treated sEVs in lane 6. Cell lysate sample was added to lane 9. Calnexin bands did not appear in the sEV sample lanes, indicating relative purity in the sample. Degradation of cell lysate sample appeared to cause additional bands outside of the expected 67 KDa band.

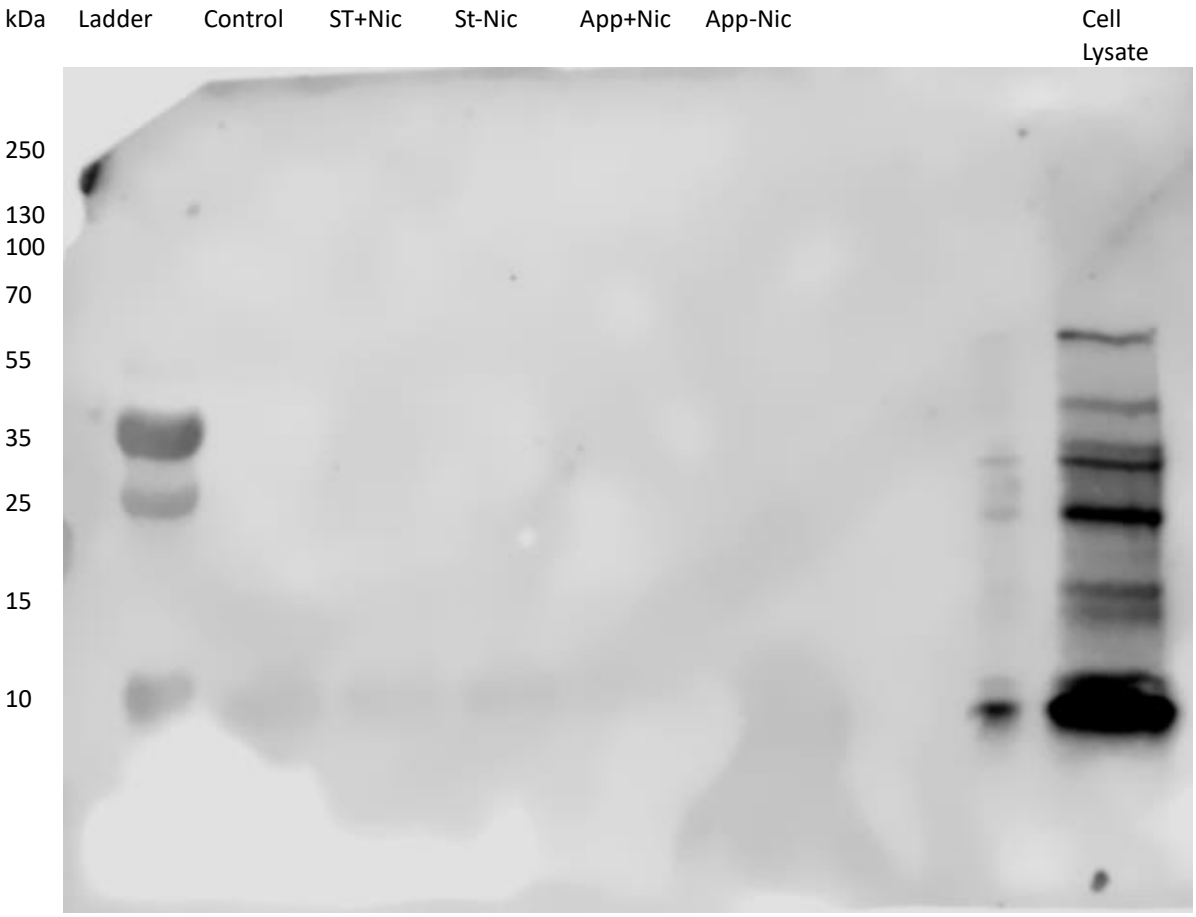

Figure A.12 Full western blot membrane for 3D BEAS-2B tagged with calnexin primary antibody with protein marker in lane 1, untreated sEVs in lane 2, strawberry flavoured e-liquid with nicotine treated sEVs in lane 3, strawberry flavoured e-liquid without nicotine treated sEVs in lane 4, apple e-liquid with nicotine treated sEVs in lane 5, and apple e-liquid without nicotine treated sEVs in lane 6. Cell lysate sample was added to lane 9. Calnexin bands did not appear in the sEV sample lanes, indicating relative purity in the sample. Degradation of cell lysate sample appeared to cause additional bands outside of the expected 67 kDa band.

Table A.1 MiRNA showing expression in various samples isolated from A549 3D Cultures

	A549 Derived sEV Small RNA				
	Untreated	St+Nic	St-Nic	App+Nic	App-Nic
MiR-410-5p	Yes	Yes	Yes	Yes	Yes
MiR-21-5p	Yes	No	No	No	Yes
MiR-382-5p	Yes	Yes	Yes	Yes	Yes
MiR-541-5p	Yes	Yes	Yes	No	Yes